PRODUCTIVITY INFLUENCES ON OXYGENATION OF THE SANTA BARBARA BASIN, CALIFORNIA, DURING THE LATE QUATERNARY

By

Tara S. Ivanochko

B.Sc. The University of British Columbia 1996

A THESIS IN PARTIAL FULFILLMENT OF THE REQUIREMENTS FOR THE DEGREE

MASTER OF SCIENCE

In

THE FACULTY OF GRADUATE STUDIES

(Department of Earth and Ocean Sciences)

We accept this thesis as conforming to the required standard

THE UNIVERSITY OF BRITISH COLUMBIA

August, 2001

Abstract

Short-term fluctuations in the bottom water oxygen content of Santa Barbara Basin have been previously recognized from variations in a sedimentary bioturbation index (Behl and Kennett, 1996). A correlation between such anoxic events in the basin and Dansgaard-Oeschger interstadials, as measured from $\delta^{18}O_{ice}$ in Greenland ice cores, was then used by the same authors to relate variations in bottom water oxygenation to high-frequency changes in the ventilation of the Santa Barbara Basin, driven by pan-hemispheric changes in climate transmitted through the atmosphere. An additional control on the oxygen content at depth is the local settling flux of metabolizable organic matter. Trace metal measurements from closely-spaced sediment samples are used here to distinguish oxygen depletion resulting from local increases in export production from oxygen depletion introduced by the importation of O_2-poor water. Molybdenum, Re, U, Cd, and Ag and interelement ratios are used in conjunction with organic carbon concentrations, opal fluxes, and $\delta^{15}N$ measurements to deduce into past redox conditions of the basin, variations in the depth of the redox boundary and the flux of organic material to the basin floor. Comparisons between ODP Holes 893A (Santa Barbara Basin), 1019 and 1017 (both California margin) allows one to distinguish of regional signals dominated by ventilation changes from local signals dominated by vertical organic flux. During the Holocene, variations in productivity appear indeed to have impacted the oxygen content of the Santa Barbara Basin bottom waters. However, anoxic events concurrent with the Bølling-Ållerød and during the last glacial interval are regional events associated with intermediate water mass characteristics.

Table of Contents

List of Figures

List of Tables

Acknowledgements

I would sincerely like to thank Tom Pedersen for his support, wisdom and encouragement throughout my entire stay at UBC, but especially for his supervision of this research. Ironically, in a year when I supported, and looked forward to, the counting and re-counting that was happening below the 49th, I was grateful when Tom finally stopped reading and re-reading. I would also like to acknowledge Maureen, Kathy and Bert for their assistance in the lab and on the instruments used for this work. The technical expertise of these individuals added to my education and made my life much easier than it otherwise would have been. Thanks as well to the geochemistry group for the continual contact and seminars that broadened my interest in paleoceanography. During my time away, it was this communication that I missed the most.

The Keeling's became both my family and my scientific community while I was down in San Diego and I would like to express my pleasure in having the opportunity to be accepted in such a fine family.

Recognition must be given to my mother and father for continually encouraging me in my studies, supporting me in my frustrations and not questioning me too much even when my decisions were unconventional. From my parents I have learned the need to balance good hard work with commitment to personal relationships. I hope I will do as well with both as they have done.

Finally I would like to dedicate this work to Jack who first introduced me to the beauty and mystery of the sea.

1. Introduction

Both the degree of oxygen depletion and thickness of the Eastern Subtropical Pacific oxygen minimum zone (OMZ) have varied on a geologic timescale. In the deep waters of the Santa Barbara Basin (SBB), the degree of oxygenation has similarly changed with time. The Santa Barbara Basin is located in the California Borderland region, slightly removed from the large pool of oxygen-depleted water that bathes the adjacent continental slope. The partial isolation of this basin and the high sedimentation rate make the SBB an ideal setting in which to study high-resolution variations in bottom water oxygen content on a continental margin.

In 1992, drilling at Ocean Drilling Program Site 893, Hole 893A, in the SBB recovered a 196 m long sedimentary section (Figure 1). This section is now providing an opportunity to study historic fluctuations in sedimentary chemistry that will add to an understanding of the mechanisms that control the oxygen content in the SBB bottom waters through time.

Within SBB the bottom waters have alternated between oxic and anoxic states over the last 50,000 years. Behl and Kennett (1996) developed a system for recording bottom water oxygen variations using a correlation between the occurrence of laminated sediments and the inferred absence of oxygen in the bottom waters. Laminated sediments were interpreted as indicating anoxic conditions in bottom waters. Whereas bioturbated sediments were interpreted as reflecting accumulation under bottom waters containing enough oxygen to support a

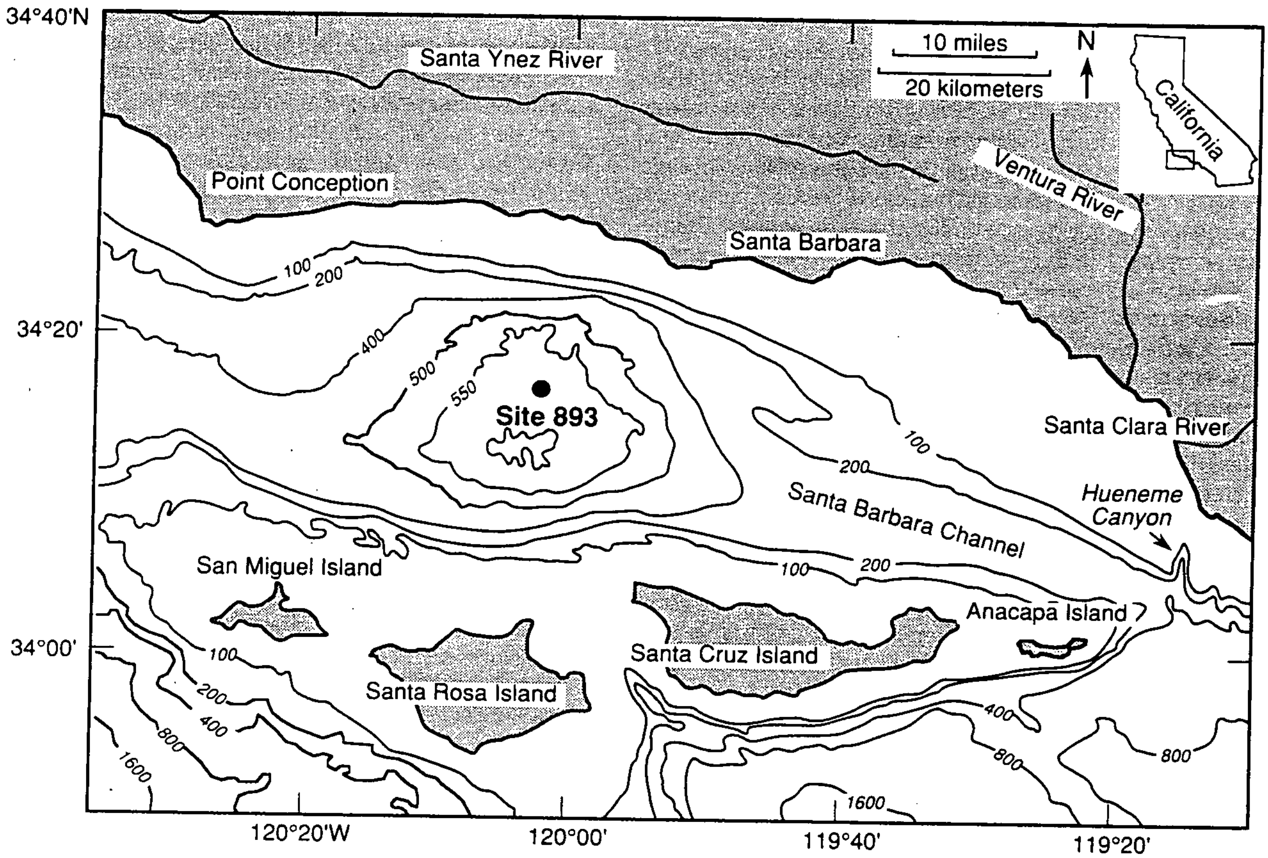

Figure 1. Location of Site 893 in the Santa Barbara Basin showing the present day physiography including rivers flowing into the surrounding area. From Ingram and Kennett (1995).

benthic fauna. This "bioturbation index" was then compared to the $\delta^{18}O$ of ice recovered from the GISP (Greenland) ice core and the laminated intervals were correlated with the stage 2-3 interstadials. Behl and Kennett (1996) used this inferred correlation to propose that variations in SBB bottom water oxygenation resulted from millennial-scale changes in the rate of ventilation of the basin. This required an external mechanism driven by pan-hemispheric changes in climate that must have been transmitted through the atmosphere, thereby affecting both Greenland and the California margin approximately synchronously. However, the bottom water oxygen content is influenced not only by the renewal rate of deep waters but also by the local settling flux of metabolizable organic matter. A principal focus of this thesis is to explore the history of the flux of organic matter to SBB sediments.

Trace metal determinations from closely-spaced sediment samples are used in this work to distinguish between oxygen depletion resulting from local increases in export production and oxygen depletion introduced by the importation of O_2-poor water from a remote source. Sedimentary Mo, Re, U, Cd and Ag concentrations were measured and inter-element ratios were determined. These data were then compared to organic carbon concentrations, opal fluxes, and $\delta^{15}N$ values provided by other researchers. Three questions guided the comparisons. First, can past changes in the ventilation of SBB be differentiated from historical variations in the vertical organic flux? Second, did changes in the vertical flux of organic matter affect the bottom water oxygen content of SBB? Finally, can the temporal variability in the organic flux to the sediment be used to explain the oxygenation history of SBB?

Trace metal concentration data obtained through analysis of marine sediment cores provide insight into past redox conditions at a given depositional site and can be used to infer variations in the depth of the sedimentary redox boundary (Irino et al., 2000). Organic proxies can variously indicate changes in the flux of organic material to the basin floor (Dymond, Suess et al. 1992; McManus, Hammond et al. 1995; Gardner, Dean et al. 1997). This thesis will demonstrate that by comparing the trace metal, organic proxy and $\delta^{15}N$ measurements of Hole 893A to similar data from other sites on the California margin, it is possible to discern local (basin-scale) changes from geographically broader (regional) variations. New data from ODP Hole 1017E, drilled in 900 m of water on the continental slope west northwest of the SBB and from Site 1019, drilled in the Eel River Basin in 980 metres of water off northern California, will be used in this comparison.

This thesis comprises six chapters including the introduction, an overview of the sample site and the methods practiced to measure the multiple proxies used in this study. A geochemical summary of the five redox sensitive trace metals chosen to investigate the Santa Barbara Basin bottom water oxygenation is offered in Chapter 3. Chapters 4 and 5 examine the results of this study and employ research from the international community to shed light on the local and regional trends of the SBB and the California Current System in the past 50,000 years. In the concluding chapter, the three questions that spurred this research are addressed.

1.2. Site and Sample Collection

Santa Barbara basin has been the site of extensive studies of local, regional and global climate variations over time. Located 20 km south of the central California coastline within the California borderland region, it is separated from the continental slope by an east-west trending group of islands. At present, the western and eastern sills of the basin are 475 m and 230 m below sea surface, respectively. This isolation allows the rapid accumulation of hemipelagic sediments making SBB an ideal setting to focus on questions requiring high-resolution sampling and multi-proxy analyses.

A principal consequence of the isolation is the development of oxygen depletion in the bottom waters of the basin and anoxic pore waters in the sediments. The early diagenetic decomposition of organic matter within the SBB sediments at present drives an intense oxidant demand and this promotes the reduction of dissolved sulphate to sulphide in the pore waters at very shallow sub-bottom depths.

The deep waters in SBB are periodically anoxic, with "spillover events" refreshing the oxygen content of the basin annually (Reimers et al., 1990; Sholkovitz et al., 1971). During these events, the depth at which dissolved hydrogen sulphide is present in pore waters also varies. During the 1986-1989 spring oxygen renewals, dissolved H_2S was present 2-4 cm below the sediment water interface. As bottom waters became depleted in oxygen, the depth of pore water H_2S shoaled to 0.25 cm (Reimers et al., 1990). Despite periodic oxygen injections, suboxic to anoxic conditions are maintained in the sediment by the large flux of organic material to the basin floor. During periods of anoxia, benthic organisms are present in very low abundance and bioturbation is limited. Under these conditions, varves (annual layers) result from preservation of the original laminated texture of the deposits that derives from seasonal variations in sedimentation (Thunell et al., 1995).

Sediments in SBB are dominated by lithogenic material (50-80%) which is delivered to the basin floor primarily during periods of high winter rains and river discharges (Thunell, 1998). The Santa Clara River is the main source of sediments (~ 50%), although some material is also supplied from the Ventura River, local island and coastal drainage, and southward longshore drift (Fleischer, 1972). The mineralogy of SBB sediment reflects arid to semi-arid weathering products (Fleischer, 1972). Periodic historic flood events associated with the Santa Clara River have resulted in multiple "grey beds" which are intercalated with the typical Holocene organic-rich sediment.

Recent studies indicate that opaline silica dominates the biogenic flux and comprises up to 35% of the total flux to the basin floor at the present time. Though the spring bloom is mainly composed of the diatom *Skeletonema costatum* (Reimers et al., 1990), progressive dissolution leaves sparse evidence of this species below a few metres in the sediment (Hemphill-Haley et al., 1995). In contrast, calcium carbonate comprises approximately 5-10% of the total flux (Thunell, 1998). The bulk of the carbonate component consists of calcareous detritus derived from nannofossils. Today, productivity is highest from spring through early autumn, due to seasonal wind-driven upwelling.

The samples used in this study were collected in 1992 on Ocean Drilling Program Leg 146 from Hole 893A at 34° 17.25'N, 120° 02.19'W, in 576.5 m water depth. Twenty-one cores were recovered using the advanced hydraulic piston coring system. In total, 196.5 m of sediment was raised spanning some 150,000 years. The upper Quaternary sequence comprises olive grey silt and clay. Surface sediments consist of anoxic mud containing hydrogen sulphide and are rich in organic carbon and microbially generated methane. At the time of coring (late fall), waters deeper than sill depth of 475 m contained oxygen concentrations below 5 μM.

1.3. Hydrography of the Santa Barbara Basin and the California Current System

The surface waters of the modern Santa Barbara Basin are composed of a mixture of two separate water masses. Warm, saline water from the Southern California Bight enters the basin over the eastern sill at a modern water depth of ~230 m. Flow at this eastern entrance, driven by the intensity of the coastal Davidson Current, displays seasonal variations: poleward movement from July through January and equatorward flow from February through June (Hendershott et al., 1996). Shorter period variations in current direction lasting days to weeks are also seen, which may episodically reverse the subtidal flow.

The south-flowing California Current brings cooler, fresher waters into the basin from upwelling sites near Point Conception and Point Arguello. Sinking particulate matter derived from upwelling- driven primary productivity is degraded, increasing the nutrient content of the intermediate water and decreasing the oxygen content. Water entering the basin over the western sill is therefore nutrient rich and oxygen poor. Upwelling-favourable winds off the coast north of SBB occur year round; however summer winds are steadier and stronger than those in winter months (Hendershott and Winant, 1996). The upwelled water flows over the western sill of SBB (475 m) and hugs the northern coast of the island chain. The result is the formation of a counterclockwise gyre, which is strongest in the summer months, mixing these two water masses (Figure 2).

Along the eastern arm of the Pacific gyre, the California Current system collectively describes the southward surface current (0-300 m), seasonal inshore counter current, and northward flowing California undercurrent (~250 m) (Lynn et al., 1987). The balance between the flow of these currents is dictated by seasonal wind patterns. The differential heat capacity of the North American continent and the North Pacific Ocean drive the atmospheric flow patterns of this region. In summer, the greater warming of air masses over the land generates an atmospheric pressure gradient and the resultant predictable strong northerly, upwelling inducing, winds.

Atmospheric variations in wind strength and position, such as the El Niño-Southern Oscillation (ENSO), affect the waters flowing into the SBB, enhancing or suppressing the formation of a seasonal thermocline and basin stratification. Upwelling off Point Conception is dampened during El Niño years and enhanced when conditions abate and the Southern Oscillation is positive. Nutrient concentrations in the California Current are affected both by ENSO events and seasonal variations in upwelling. Water column profiles of Cd, P and Si obtained off the California coast indicate that nutrient concentrations in these waters vary in response to regional wind forcing, not changes in source water masses (van Geen, 1996). Though the remineralization depths vary among these three elements, during upwelling events they all show conservative mixing with P and Si concentrations

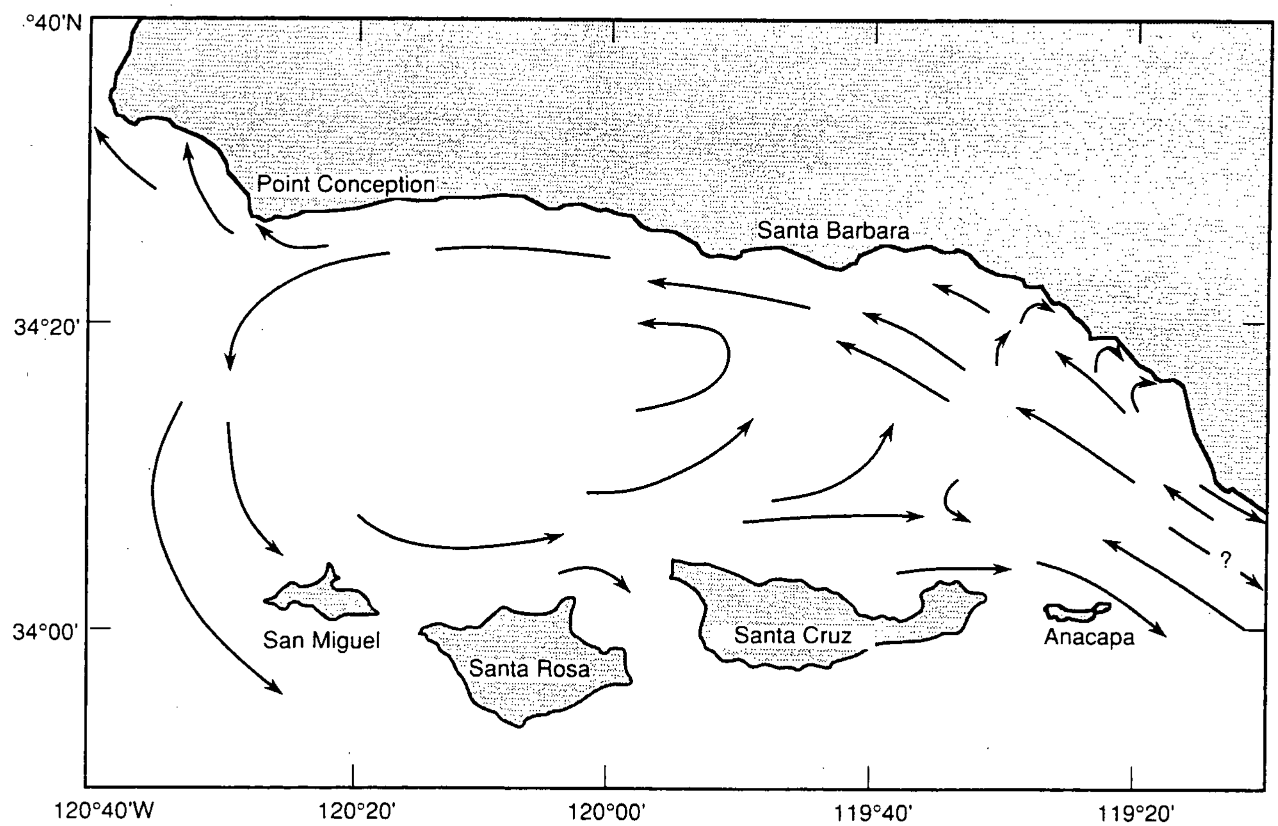

Figure 2. Map illustrating the cyclonic gyre surface circulation in Santa Barbara Basin. The strength of this gyre varies seasonally with the northward flowing Davidson current being strongest in the winter. From Kennett and Baldauf (1994).

predictable from the Cd concentrations. "Nearshore" concentrations of dissolved Cd reached >0.6 nmol/kg during summer upwelling events and dropped to ~0.2 nmol/kg during the winter (van Geen, 1996). Similarly Si concentrations were high (>30 μmol/kg) in the summer and lower (~14 μmol/kg) in the winter. Within Santa Barbara Basin, fluxes of planktonic foraminifera and diatoms indicate annual changes in species composition and abundance in response to these variations of the surface water nutrient concentrations and temperatures (Kincaid et al., 2000).

Today, North Pacific Intermediate Water (NPIW) flows from the Sea of Okhotsk and intercepts the California margin at approximately 300 - 700 m water depth (Talley, 1993). This intermediate water forms from intense cooling in the north Pacific but is identified by its relatively low salinity. Oxygen concentrations in this water mass are highest (~220 μM) near the source and decrease to ~90 μM near the eastern reach (Talley, 1993). Within the coastal region beneath the surface-confined California Current system, the oxygen and salinity signals of the NPIW are significantly altered (Talley, 1993). Coastal productivity lowers the oxygen content of this water. As well, only sporadic low salinity areas are detected proximal to the coast.

It has been suggested that the source of intermediate waters entering Santa Barbara Basin has changed on a glacial-interglacial timescale. High-resolution planktonic foram assemblages have varied with time suggesting contrasting influences from the subpolar Pacific during stadials and the subtropical Pacific during interstadials (Hendy et al., 2000). The balance between the strength of the California Current and the California Undercurrent as well as the areal extent of the

NPIW may also influence the oxygen content of the SBB (Behl et al., 1996; Cannariato et al., 1999a).

2. Methods

2.1. Determination of Trace Metal Concentrations

2.1.1. Overview of Methodology

Analyses of Mo, U, Re, Ag and Cd were performed by isotope dilution using a Plasmaquad II+ inductively-coupled plasma mass spectrometer (ICP-MS) in peak jumping mode.

Freeze-dried, powdered sediment samples (approximately 15 mg) were spiked with known weights of isotopically labeled Re, Mo, U, Ag, and Cd stock solutions. Samples were microwave digested in an acid cocktail containing HF, HNO_3 and HCl. This solution was then evaporated to dryness. HCl was added to the residue and redigested in the microwave. Aliquots of the sample were isolated for Mo and U measurements. The remaining sample was run through an anion exchange column using Dowex 1-X8 resin to remove potential polyatomic interferences of Nb, Zr and Mo with Ag and Cd isotopes and to concentrate Re in the sample. Blanks were run using the same procedure, averaged and then subtracted during the concentration calculations for each element individually. Samples were also corrected for instrument mass bias.

2.1.2. Isotope Dilution and Calculation of Trace Metal Concentrations

Isotope dilution has been developed as a method of obtaining high precision values for trace elemental analysis. Used in conjunction with the ICP-MS, high sensitivity can be achieved. This procedure is performed using a known quantity of a "spike isotope" that is added to the sample in question. The spike isotope usually has a low natural abundance and is not subject to mass interferences when being measured on the ICP-MS (Heumann, 1988). Within the sample a "reference isotope" with a high natural abundance is selected. Again isobaric and polyatomic interferences must be considered. Once the spike has been added and complete mixing takes place, the known ratios of the spike and reference isotopes in nature, in the spike solution, and the measured ratio of the these isotopes in the spiked sample are used to determine the concentration of the element in question in the original sediment sample (Montaser, 1998):

$$N = C \bullet Wt \bullet \frac{A^{b}_{Spike}}{A^{b}_{Natural}} \bullet \frac{(R_{Sample} - R_{Spike})}{(R_{Natural} - R_{Sample})}$$

Where:
N = Concentration of trace metal in sample
C = Concentration of spike (mol/g)
Wt = Weight of spike added (g)
A = Abundance of reference isotope (b) in the isotope pair (a/b)
R = Ratio of the spike isotope (a) to the reference isotope (b).

Note that all Mo, Cd and U data in this thesis have been converted to ppm (mg kg^{-1}). Ag and Re data are expressed as ppb ($\mu g\ kg^{-1}$).

Molybdenum, Cd, Ag, and Re measurements are corrected for the mass bias of the instrument using a standard solution of known natural isotopic abundances. The mass bias = [solution(natural) isotopic ratio/ measured isotopic ratio] and is measured during each session with the ICP-MS to determine any variations in the sensitivity of the instrument. For U mass bias corrections a solution with a ratio of

^{235}U:^{238}U=1 was used. As well, all samples are corrected by averaging and subtracting the values obtained by running blanks through the same digestion and anion exchange procedure as the samples:

$$\text{Isotopic ratio of the sample} = \frac{(\text{Isotope}_b - \text{blank avg. of Isotope}_b)}{(\text{isotope}_a - \text{blank avg. of isotope}_a)} \times \text{Mass Bias}$$

Molybdenum:

For molybdenum analysis, isotopes ^{95}Mo and ^{98}Mo were used as the spike and reference isotopes respectively. Although ^{95}Mo has a higher natural abundance (Table 1) and experiences a polyatomic interference by BrO^+ at this mass, this interference is reduced as Br- is oxidized to volatile Br_2 in the digestion procedure (Zheng, 1999). The alternative isotope, ^{94}Mo, although less abundant in nature, is affected by Zr which is present in SBB sediment at concentrations ranging from 90-250 ppm (Appendix i) and is therefore unacceptable as a spike isotope. Using two standards, SCO-1 and Saanich Inlet bulk sediments, Mo concentrations were reproducible to better than 8% (1σ, relative standard deviation) over two years of repeated measurements (Table 2).

Uranium:

99% of natural uranium exists as ^{238}U. This isotope was therefore used as the reference isotope. The spike was prepared using ^{235}U (Table 1). The method yielded results reproducible to less than 7% (1σ, relative standard deviation) as determined from standards measured over two years (Table 2).

Mo	Natural Abundance%	Spike Abundance %
92	14.80	0.26
94	9.30	0.63
95	15.90	96.47
96	16.70	1.45
97	9.60	0.46
98	24.10	0.63
100	9.60	0.15
Ratio 95:98	**0.66**	**153.13**

Cd	Natural Abundance%	Spike Abundance %
106	1.25	<0.05
108	0.90	<0.05
110	12.50	0.63
111	12.80	96.50 +/- 0.10%
112	24.10	1.84
113	12.20	0.44
114	28.70	0.59
116	7.55	0.05
Ratio 111:113	**1.05**	**219.32**

Ag	Natural Abundance%	Spike Abundance %
107	51.80	0.30
109	48.20	99.70
Ratio 109:107	**0.93**	**332.33**

Re	Natural Abundance%	Spike Abundance %
185	37.40	96.66
187	62.60	3.34
Ratio 185:187	**0.60**	**28.94**

U	Natural Abundance%	Spike Abundance %
233	0.00	0.00
234	0.01	0.52
235	0.72	49.70
236	0.00	0.08
238	99.28	49.71
Ratio 235:238	**0.01**	**1.00**

Table 1. Natural and spike abundances of trace metal isotopes

Standard Reference Material	Element	Measured Value +/- 1sigma (no.of measurements)
Saanich Inlet bulk sediment	Mo ppm	58.0 +/- 4.5 (8)
Saanich Inlet bulk sediment	Cd ppm	5.1 +/- 0.3 (16)
Saanich Inlet bulk sediment	Re ppb	6 +/- 0.33 (12)
Saanich Inlet bulk sediment	Ag ppb	161 +/- 8 (12)
Saanich Inlet bulk sediment	U ppm	4.5 +/- 0.3 (9)
SCO-1	Mo ppm	1.1 +/- 0.1 (10)
SCO-1	Cd ppm	0.2+/- 0.01 (12)
SCO-1	Ag ppb	135 +/- 9 (12)
SCO-1	U ppm	2.2 +/- 0.2 (10)

Table 2. Measured values of trace metal concentrations in standard reference materials.

Silver, Cadmium and Rhenium:

The spike (a) and reference (b) isotope pairs (a:b) used for these three elements were ^{109}Ag:^{107}Ag, ^{111}Cd :^{113}Cd and ^{185}Re:^{187}Re. Ag and Re only occur as the listed isotopes. Cd has eight isotopes, and isobaric interferences arise at all masses except ^{111}Cd. The measurement of ^{111}Cd is affected by a polyatomic interference with MoO^-. The presence of ZrO (Beary et al., 1993), ZrOH and NbO result in polyatomic interferences with Ag isotopes ^{107}Ag and ^{109}Ag (Gordon, 1997). To reduce the effect of these compounds, an ion-exchange column was used to remove Zr, Nb and Mo from the digested sample solution on which Ag and Cd measurements were to be made.

Silver, Cd and Re all exhibit a high affinity to the Dowex 1-X8 resin in low molarity HCl and low affinity in HNO_3 solutions > 6 N. Therefore, the column was originally prepared by rinsing the resin with 8N HNO_3 for half an hour to remove contamination. Zr , Nb and Mo are removed from the resin at low HCl molarities (Gordon, 1997; Walton, 1976). Consequently, the column was rinsed with 0.5 N HCl after sample uptake for 4 min to remove these elements. The sample was then eluted with 8N HNO_3. Rinsing with 2 N HNO_3 for 1min completed the process and the column was prepared for the next sample by flushing the lines with 0.5 N HCl. The eluted sample was then measured for Ag, Cd and Re on the ICP-MS. Ag, Re and Cd measurements were reproducible to less than 7, 7 and 5% respectively (1σ, relative standard deviation) over the duration of this study (Table 2).

2.2. Major and Minor Element Analysis

The concentrations of major (Al, K, Fe, Ca, Mg, Mn, Na, Ti, P, Si) and minor (V, Cr, Co, Ni, Cu, Zn, Rb, Sr, Y, Zr, Ba, Pb, Nb, I, Br) elements were determined using X-ray fluorescence spectrometry on a Philips PW 2400 wavelength-dispersive sequential automatic spectrometer (Calvert et al., 1985). International rock standards were used to calibrate the instrument and to monitor accuracy and precision during analysis (Table 3).

Major elements were prepared by adding Spectroflux 105, a combination of 47.0% $Li_2Ba_4O_7$, 36.6% La_2O_3 and 16.3% Li_2CO_3, to the sample in a 9:1 dilution. Individual samples in platinum crucibles were then melted at 1100°C in a muffle furnace for 30 minutes. Upon cooling, Spectroflux 100 (100% $Li_2Ba_4O_7$) was added to compensate for the weight lost from volatized material. This mixture was re-melted in a flame and cast as a glass disc for XRF analysis.

Samples for minor element analysis were prepared as pressed pellets using powdered sediment (4 g) backed with borax and solidified under ~10 tons hydraulic pressure.

	Reported Value				Measured Value			
	BIR-1	JA-2	JB-2	JB-3	BIR-1 (n=5)	JA-2 (n=4)	JB-2 (n=4)	JB-3 (n=4)
Al	8.221	8.152	7.745	9.004	7.96±0.08	8.07±0.08	7.32±0.07	8.66±0.12
Ca	9.527	4.495	7.018	6.997	9.21± 0.01	4.40±0.01	6.75±0.01	6.76±0.01
Fe	7.899	4.341	9.961	8.262	7.76± 0.01	4.26±<0.01	9.67±<0.005	9.67±0.02
K	0.025	1.502	0.349	0.647	0.02±<0.005	1.46±<0.005	0.32±0.02	0.62±0.03
Si	22.416	26.348	24.868	23.798	21.49±0.03	25.78±0.01	23.47±0.03	22.64±0.03
Ti	0.575	0.395	0.713	0.863	0.56±<0.005	0.39±<0.005	0.67±<0.005	0.82±<0.005
	JA-2	JA-3	JG-1A	QLO-1	JA-2 (n=6)	JA-3 (n=4)	JG-1A (n=6)	QLO-1 (n=6)
Mn	850	820	464	720	1038.9±10	856.08±13.17	569.47±8.76	771.77±8.34
Sr	252	294	185	336	248.7±0.94	289.15±1.33	182.15±0.65	335.00±2.48
Zr	119	123	115	185	110.03±0.07	118.98±0.41	109.32±1.11	194.37±1.54
Ba	317	318	458	1370	251.72±4.69	304.43±4.88	448.70±9.41	1440.58±22.01

Table 3. Major and minor element error analysis

2.3. Determination of Carbon, Nitrogen and Sulphur

Approximately 30 mg of dried, homogenized sample were weighed into a tin cup for measurement by flash combustion gas chromatography on a Carlo Erba NA-1500 analyzer. For every carousel of fifty samples, five samples of sulphanilamide, with known %C, %N, %S and a weight range from 0.05 -2.00 mg were measured to create a sulphur regression line. Generic marine sediment standards MESS-1 and BCSS-1 were used for carbon and nitrogen regressions. For every carousel, two blanks were included and used as a zero standard for carbon regressions.

Plots of N versus organic C showed a Y-intercept of -0.18. This was assumed to represent residual inorganic N, and the value was subtracted from all N measurements prior to calculating the C_{org}:N ratio (Figure 3).

2.4. Carbonate Carbon ($CaCO_3$)

Weight %carbonate carbon was determined on a Coulometrics 5010 coulometer. Weighed sediment samples (~25 mg) were flushed for two minutes with CO_2 free air to remove atmospheric carbon dioxide contamination before dissolution in warm 10% HCl. The CO_2 produced in this reaction was carried by CO_2 free air and bubbled through a beaker of blue ethanolamine solution. A clear solution results . The transmittance of this solution is monitored by a photo-detector, which then generates OH^- ions electrolytically by reducing H_2O at a silver electrode. The %$CaCO_3$ in the sample is directly proportional to the current required to restore the original transmittance of the solution.

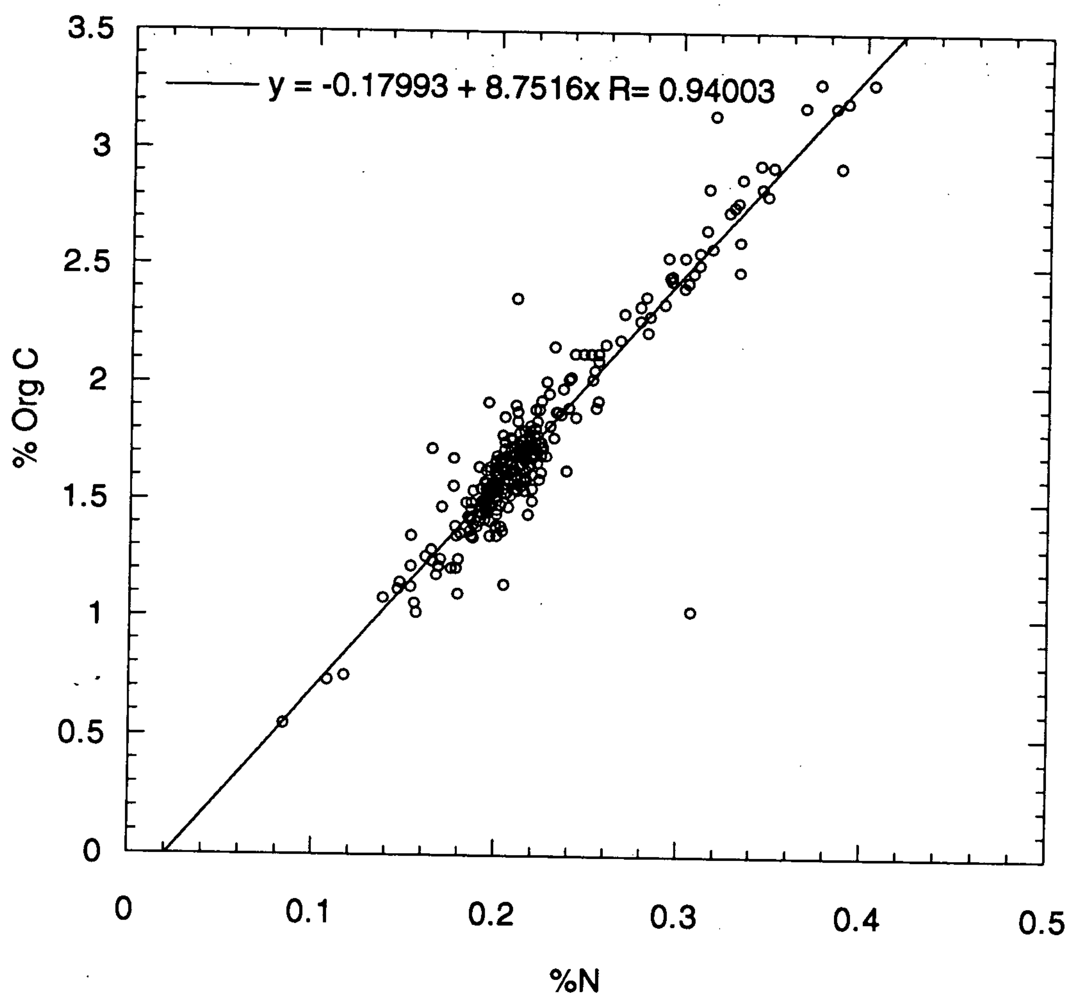

Figure 3.%C versus %N. All 893a data presented in this thesis have been corrected for the inorganic nitrogen present in these samples. Inorganic N is evident by the non-zero y-intercept in this graph.

Reagent grade $CaCO_3$ (12% C) was used to monitor the performance of the instrument. The one sigma precision of the method was $\pm 0.01\%$ based on replicate measurements of this standard (n=43).

2.5. Nitrogen Isotope Ratios

Stable isotope ratios of nitrogen (^{15}N:^{14}N) were determined by Continuous Flow - Isotope Ratio Mass Spectrometry (CF-IRMS) using a Fisons NC-2500 CNS analyzer coupled directly to a VG Isotech Prism mass spectrometer. The samples were prepared for analysis by weighing powdered sediment into tin cups. Following flash combustion, the N_2 gas released from the sample was separated chromatigraphically. Using helium as a carrier gas, the N_2 from each sample was transferred to the mass spectrometer on which masses 28, 29 and 30 were monitored. The ratio of ^{15}N to ^{14}N was calculated and converted to $\delta^{15}N$ using atmospheric N_2 (one pulse per sample) as the reference ratio. Analytical precision of the instrument based on multiple analyses of a splits of a laboratory bulk sediment standard is $\pm$ 0.2 ‰ (1 sigma).

2.6. Determination of Salt Content

Upon drying of sediment samples, trapped pore water evaporates leaving behind ions previously in solution. The addition of salts from this process contributes to the weight of the powdered sediment measured for all analysis conducted for this study. The effect of dilution on each sample was corrected by measuring the salt content of each sample and applying the corrections described below. Based on the assumptions that the salinity of interstitial water is 35‰ and that the Cl content in pore waters is entirely present as NaCl, all data have been corrected for sea salt dilution and are presented as "Salt Free".

The salt content of the individual samples was determined by measuring chlorinity volumetrically and applying a conversion based on the chloride to total salt ratio in seawater. The method was adapted from Strickland and Parsons, 1968. The salt contained in 100-200 mg of dried, ground samples was dissolved in 5 ml of distilled water using a vortex stirrer. After centrifugation, the supernatant was titrated using silver nitrate ($AgNO_3$) with potassium dichromate (K_2CrO_4) as the indicator. Sea salt corrections for specific elements were applied using the equation:

$$[\text{Element}] = [\text{Element}]_{\text{sediment+salt}} - \frac{[\text{Element}]_{\text{seawater}}}{[\text{Cl-}]_{\text{seawater}}} \times [\text{Cl-}]_{\text{sediment+salt}}.$$

% Major and minor elements as well as CNS measurements were corrected for dilution by sea salt using the formula:

$$[\text{Element}]_{\text{salt free}} = [\text{Element}] \times \frac{100}{100 - 1.82[\text{Cl}^-]_{\text{sediment+salt}}}.$$

2.7. Correcting for Dilution Effects and Terrestrial Input

Major, minor and trace metals are delivered to the seafloor by different mechanisms. Specifically, metals can be supplied to marine sediments from both terrestrial and marine sources, including post-depositional (diagenetic) precipitation reactions. Terrestrial inputs, such as the accumulation of pelagic clay, may compromise interpretation of the strictly marine signal provided by sinking organic matter, which may adsorb some metals, and authigenic mineral precipitation. To distinguish the non-terrestrial input from continental sources, metals are normalized to the average aluminosilicate content (assuming Al is supplied solely from clay particles) (Calvert et al., 1993). Element to aluminum ratios are thus used for all major and minor elements discussed in this thesis to reduce variability introduced by changes in dilution by fluctuating rates of input of non-aluminosilicate components through time.

3. Review of Trace Metal Geochemistry

3.1. Molybdenum

Dissolved Molybdenum (Mo) has a concentration of approximately 107 ± 2.5 nM in the water column of the open ocean (Collier, 1985). It is regularly described as having the profile (concentration versus water depth) of an entirely conservative element, though recently this has come into question. Within Santa Barbara Basin, "particulate non-lithogenic" Mo has been identified in a sediment trap suspended at 590m water depth (Zheng, 1999). This component of particulate Mo, calculated from sediment trap data, appears to have contributions from both labile and non-labile fractions. Zheng (1999) submits that the first of these fractions is associated with Mn-oxides. The source of the latter is still unknown due to an inconclusive correlation between the non-labile fraction and the organic carbon flux.

Molybdenum is known to be involved in biological processes and used by plankton in nitrogenase and nitrate reductase complexes (Burgess, 1990; Collier, 1985). Recently, a small deficit in dissolved Mo has been detected in the surface waters of the Eastern Tropical Pacific and ascribed to biological removal by heterotrophic bacteria (Tuit et al., 2000). However, no removal is apparent in the Arabian Sea where primary productivity is as high as it is in the ETP. Surface removal in the Pacific, however, is minor and the non-reactive nature of Mo in oxic waters implied by this observation is reflected by its calculated residence time of 800,000 years. Water column profiles from other areas indicate no noticeable input or removal from either hydrothermal activity or as a function of proximity to ocean margin environments (Collier, 1985). Indeed, although the main sources of Mo to the ocean are rivers and continental margin sediments, water column profiles from continental margin settings show no significant deviations from the conservative nature of the open ocean (Collier, 1985).

Molybdenum (VI) is the stable oxidation state in oxic seawater, and the metal occurs as molybdate ion (MoO_4^{2-}), which displays little affinity for adsorption onto clay minerals, $CaCO_3$ or Fe oxyhydroxides at marine pH (Helz et al., 1996). Molybdate does adsorb to Mn-oxyhydroxides, however, and concentrations of the element are known to be elevated in MnO_2 rich sediments. Studies of oxic marine sediments and ferromanganese nodules show that Mo is associated with Mn in such deposits with a constant Mo/Mn weight ratio of 0.002 (Shimmield et al., 1986). During diagenesis, MnO_2 is reduced and the associated Mo is released. Multicores collected from beneath the oxic waters of the Japan Sea contain Mo with concentrations of up 20 ppm associated with the abundant Mn-oxyhydroxides in the surface sediments (Crusius et al., 1996). Under well oxygenated bottom waters, both Mn and Mo diffuse up from reducing sediments, along the concentration gradient, and form an oxide "cap" at the depth of oxygen penetration (Shimmield and Price, 1986). Through this process of Mn recycling between oxidizing and reducing environments, Mn and Mo are largely trapped and not released from the sediments.

Mo is strongly enriched in ocean sediments that have accumulated under anoxic conditions (Emerson et al., 1991). The exact mechanism of Mo enrichment in sulphidic environments is still unresolved. Concentrations on the order of 100 ppm have been observed and these far exceed both background levels and detection limits. Molybdenum has been identified as having a high affinity for pyrite, being more enriched in the pyrite phase relative to bulk sediments taken from various depositional environments in the Gulf of Mexico (Huerta-Diaz et al., 1992). Irrespective of sedimentary environment (i.e. anoxic- sulphidic, anoxic-nonsulphidic), Mo showed rapid and essentially complete incorporation into the pyrite fraction even when the "Degree of Pyritization" (%DoP = [Pyrite-Fe / Pyrite-Fe+ Reactive-Fe] * 100) was relatively low (Huerta-Diaz and Morse, 1992). Extended X-ray absorption fine structure analysis (EXAFS) conducted by Helz *et al* (1996) indicates scavenging of Mo by Fe or organic matter (as an Fe carrier) which in the presence of sulphides produces Fe-Mo-S clusters that appear to persist over geological time.

Recently, the scavenging and co-precipitation of Mo-sulphides with Fe-sulphides has been acknowledged as an initial stage of Mo accumulation in reducing sediments (Zheng et al., 2000a). Diffusion across the sediment water interface, reduction of Mo (VI) under anoxic conditions to Mo (IV), and sequestration of the reduced species have also been identified (Adelson et al., 2001; Helz et al., 1996; Zheng, 1999).

Though MoO_4^{2-} is non-reactive in seawater, the oxygen atoms are susceptible to replacement by "soft ligands" such as sulphur. Thus, in the presence of H_2S, sulphur replaces the oxygen in MoO_4^{2-}, one sulphur molecule at a time in a stepwise fashion, leading to tetrathiomolybdate (MoS_4^{2-}) (Helz et al., 1996). The progressive replacement of oxygen by sulphur in MoO_4^{2-} facilitates Mo complexation with humic compounds or iron sulphides. Each step in this reaction, the sulphidation of molybdate to tetrathiomolybdate, becomes successively slower but are all first order with respect to both H_2S and $MoO_xS_{4-x}^{2-}$ within the concentration range studied (pH 8.4;NaCl 0.7 M; $H_2S_{(aq)}/HS^-$ 63; ΣNH4 0.51 M; ΣMo 1mM; T=25°C) (Helz et al., 1996). Calculations using published Black Sea values for pH, sulphide and Mo concentrations (without temperature and pressure corrections), predict that the transformation from MoO_4^{2-} to MoS_4^{2}, through intermediates MoO_3S^{2-}, $MoO_2S_2^{2-}$, and $MoOS_3^{2-}$, occurs almost concurrently at 400 m water depth (Erickson et al., 2000). This de-emphasizes Mo (VI) reduction as the initial step of precipitation and suggests that a threshold level of HS^- is necessary for Mo sequestration.

The equation:

$$MoO_4^{2-} + 4H_2S \leftrightarrow MoS_4^{2-} + 4H_2O,\ \ K_{O4}= [MoS_4^{2-}]/[MoO_4^{2-}][H_2S]^4,$$

has been used to describe the reaction. Due to the $[H_2S]^4$ dependence in the denominator, Erickson and Helz (2000) argued for the existence of an extremely sharp transition or "geochemical switch", which is dependent on a sufficient concentration of HS^-. In laboratory-based studies that simulate seawater conditions (25°C, I= 0.8-2.2M), $[H_2S] = K_{O4}^{-1/4} = 11 \pm 3$ μM was identified as the threshold concentration required to transform inert MoO_4^{2-} to particle reactive MoS_4^{2-} (Erickson and Helz, 2000).

In seawater (pH ≅ 8), thermodynamics suggest MoS_4^{2-} would remain in solution. However, at low pH MoS_4^{2-} can react with a proton to precipitate as $MoS_3(s)$:

$$MoS_4^{2-} + H^+ \leftrightarrow MoS_3(s) + HS^-,\ \ K=10^{2.4}.$$

In the ocean, when HS^- concentrations exceed μM levels, this equilibrium favors MoS_4^{2-}. Therefore, for precipitation of Mo-compounds in anoxic sediments, a scavenging agent is required, as MoS_4^{2-} requires a threshold level of H_2S to exist and $MoS_{3(s)}$ will not endure in sulphidic bottom waters (Helz et al., 1996).

The rapid transition of MoO_4^{2-} to MoS_4^{2-} within the water column is supported by profiles of dissolved Mo from the Cariaco Trench, Saanich Inlet, Lake Nitinat, the Black Sea and Framvaren Fjord (Emerson and Huested, 1991). These five basins all display anoxic conditions below various depths in the water column. Measurements of H_2S and Mo indicate that dissolved Mo decreases across the O_2 - H_2S boundary (Emerson and Huested, 1991). However, the adsorption of Mo onto scavenging particles above the sediment-water interface is not evident in data from Saanich Inlet (Francois, 1988) and the Black Sea (Crusius et al., 1996). Sediment trap studies in Saanich Inlet reveal that the Mo concentration in the settling particulate matter is less than in the bottom sediments (Francois, 1988). Similarly, a flux-weighted annual averaged sediment trap sample in the Black Sea produced Mo values of 3.1 ppm. Compared to the surficial fluff values of 33 ppm at the same site, this indicates that authigenic Mo-rich mineral formation occurs at or below the sediment water interface (Crusius et al., 1996).

Recent studies in Santa Barbara Basin confirm that a threshold value of dissolved sulphide is necessary for authigenic MoS_4 formation. However, Zheng *et al* (2000) detected not one, but two critical stages of Mo precipitation in the sediments. A primary threshold of $H_2S \approx 0.1$ μM was associated with Fe reduction. Over a sub-bottom depth range of 0-7 cm, pore water concentrations of Mo steadily decreased and sedimentary Mo increased, while H_2S remained below 1 μM. With $H_2S \approx 0.1$ μM, removal of Mo from solution coincided with Fe-sulphide formation suggesting the possibility of Mo-Fe-sulphide co-precipitation. Zheng et al (2000) identified a second threshold value of H_2S appears to be approximately 100 μM. When sulphide concentrations reach this critical level, Mo-sulphide complex formation is maintained even after Fe has been completely removed from pore waters. Though this field determined threshold is higher than that proposed by lab studies, the second threshold is consistent with that proposed by Helz (2000).

Adelson *et al* (2001) developed a model of the Mo fixation process within Chesapeake Bay sediments based on multiple cores from this seasonally anoxic estuary as well as laboratory studies. This model uses manganese cycling as a means of concentrating Mo at the sediment-water interface. When Mn oxides dissolve upon burial, MoO_4^{2-} then diffuses into the sediments where precipitation of authigenic Mo-bearing minerals occurs after encountering organic thiols or H_2S at concentrations sufficient to convert MoO_4^{2-} to a scavengable form.

The depth of the H_2S =11 μM isopleth in Chesapeake Bay varies seasonally with the intensity of overlying anoxia in the water column (Adelson et al., 2001). Calculations of the contribution of molecular diffusion of MoO_4^{2-} to authigenic Mo accumulation in this environment are only reasonably compared to the data when the isopleth is located at a very shallow depth within the sediment (not water) column. This virtually eliminates diffusive resistance, creating a very steep gradient of Mo in the pore waters near the sediment-water interface. Maintaining the threshold value of H_2S = 11 μM at such a shallow depth in the sediments requires anoxia in the very bottom waters of the basin. Adelson *et al* (2001) concluded there should be a temporal linkage between Mo fixation and oxygen depletion in the water column. Their conclusion is borne out when it is realized that reducing sediments with high Mo concentrations indicating sedimentary Mo enrichment occur only when bottom waters are anoxic (Black Sea, Saanich Inlet, Cariaco Trench and Framvaren Fjord). Furthermore, Mo can be enriched when the bottom waters have both oxygen levels <10 µM and receive a very high flux of organic matter, as is true for the Santa Barbara Basin and the Mexican Margin (Zheng et al., 2000a).

3.2. Uranium

Uranium (U) and its daughter products are widely used in marine chemistry as sediment geochronometers and for assessing rates of hydrothermal processes. Uranium has also been used as a redox sensitive metal to describe the oxygenation history of anoxic marine sediments (Morford et al., 1999; Zheng, 1999). Uranium is stable in oxygenated waters as U (VI) and in anoxic settings occurs as uraninite (UO_2) (Cochran et al., 1986). In seawater, U (VI) complexes with CO_3^- to form $[UO_2(CO_3)]^{4-}$. Uranium displays nearly conservative behavior in the open ocean, with a residence time of 500,000 years (Colodner et al., 1995).

The source of authigenic U in sediments can be attributed to both a particulate non-lithogenic flux, associated with organic material, and a diffusive input from the water column. The relative proportion attributed to these two fractions is dependent on the surface productivity, the flux of the carrier delivering organic matter to the seafloor (Tyson, 2001), and the remobilization of U at the sediment water interface. In sediments underlying an oxic water column, only 20% or less of the accumulating U is from the labile organic fraction (Thomson et al., 1998). There is, however, evidence that the concentration of U in the sediments is proportional to the organic flux. Sediment trap studies from SBB show the same trend: under high organic flux, non-lithogenic U is high; under low organic flux, non-lithogenic U is low (Anderson et al., 1989; Zheng, 1999). The proportion of non-lithogenic U in sediments appears to increase when the oxygen content of the water column is low (Zheng et al., 2000a).

Klinkhammer *et al* (1991) suggested that the mechanism for sedimentary authigenic formation of U-bearing compounds is directly related to organic flux in another way. During the decomposition of labile organic matter the release of associated U creates a concentration gradient that facilitates diffusion of dissolved U into the sediments from the water column. The intensity of this gradient, caused by the magnitude of the labile organic flux and by the consumption of dissolved U at depth, determines the overall concentration of authigenic U found in the sediments.

In sulphide rich waters, U (VI) is not scavenged or reduced to U (IV) (Anderson et al., 1989). Instead $[UO_2(CO_3)]^{4-}$ diffuses into the sediments where precipitation occurs at or below the depth of Fe remobilization. It has been suggested that the formation of authigenic U minerals is bacterially mediated. U reduction could be coupled to the oxidation of organic matter with U acting as the electron acceptor via (Cochran et al., 1986):

$$CH_2O + 2UO_2(CO_3)_3^{4-} + H_2O + 2H^+ = 2UO_2 + 6HCO_3^- + CO_2.$$

The energy yield from this process, $\Delta G^\circ = -63.3$, falls between that for the reduction of Mn and Fe, $\Delta G^\circ = -83.4$ and $\Delta G^\circ = -27.2$ respectively (Cochran et al., 1986). Zheng (1999) provides evidence that U reduction occurs in conjunction with Fe(III) reduction. Pore water data from SBB, San Clemente Basin, the Northern California margin and the Mid-Atlantic Bight all show dissolved U depletion is accomplished above the depth of the dissolved Fe maximum. However, Zheng (1999) does not dismiss the potential of further U reduction in more reducing conditions with sulfate reduction.

Similar studies from samples collected in central California, south of the Monterey fan, provide contrasting results (Klinkhammer et al., 1991). Microbial facilitation of authigenic U formation is contraindicated by pore water profiles that indicate U precipitation occurs below the Fe maximum where SO_4^{2-} reduction is occurring. Klinkhammer et al cite Langmuir (1978):

$$4[UO_2(CO_3)]^{4-} + HS^- + 15H^+ = 4UO_2(c) + SO_4^{2-} + 12CO_2(g) + 8H_2O$$

and suggest that U precipitation may not be bacterially mediated.

3.3. Rhenium

Rhenium (Re) is thought to be present in seawater as the perrhenate ion, ReO_4^-, which has an oxidation state Re (VII) in oxygenated seawater and is reduced to Re (IV) in suboxic conditions. ReO_4^- is an unreactive ion and by analogy with molybdate it was predicted that Re would act conservatively in the ocean. In 1993 this was confirmed by Anbar et al (1992). Rhenium concentrations measured in both the North Atlantic and North Pacific, normalized to salinity of 35‰, are approximately 44.6 and 43.9 pmol/kg, respectively, and its residence time has been estimated at 750,000 years (Colodner et al., 1993). Re is greatly enrichment in reducing sediments. In crustal samples, Re is present at 0.5 ppb; however, concentrations up to 300 times greater are found in sediments below suboxic and anoxic bottom waters (Colodner et al., 1993).

The conservative behavior of Re in oxygenated seawater suggests that authigenic sedimentation occurs below the sediment water interface. Re diffuses down a concentration gradient and precipitates under lower redox conditions. Oxic pore water data from cores off Point Conception, California show little variation in the concentrations of Re with depth (Colodner et al., 1993). Although evidence for Mo release from Mn-oxides exists, no synchronous increase in Re is seen (Colodner et al., 1993). Unlike Mo, Re is not associated with Mn-oxides and is not present above crustal levels in manganese nodules (Koide et al., 1986). This suggests that cycling of Re is not associated with Mn during sedimentary diagenesis.

Depletion of Re occurs within the upper 2-5 cm of the anoxic pore waters in Chesapeake Bay sediments (Colodner et al., 1993). Although Re does not correlate with sulphide concentrations in the pore solutions, slightly elevated concentrations are seen when H_2S is present. Colodner *et al* (1993) postulate that sulphides may indirectly stabilize Re in solution by incorporation onto colloidal sulphides (particles less than 0.2 μm). In the Black Sea, the water column profile shows a decrease of Re with depth. Though the Re-salinity relationship remains linear, the complex hydrography of the Black Sea makes the conservative nature of Re difficult to determine (Colodner et al., 1995). Once again the competing roles of scavenging particles versus diffusion into reducing sediments are ambiguous.

Within the actively denitrifying sediments (suboxic) of the Pakistan margin, solid-phase Re measurements from within the OMZ ($[O_2] < 2$ μM) reach 25 ppb . In this same area, but in sediments above the OMZ ([O2>10 μM]), Re contents are <2 ppb (Crusius et al., 1996). Crusius *et al* (1996) challenge the results of Colodner *et al* (1993) by suggesting that suboxic sediments, rather than anoxic deposits, are the largest sink of Re in the global mass balance. With contributions from hydrothermal processes still poorly constrained, Re removal in the ocean appears to be driven by the areal extent of suboxic sediments, currently some 3% of the ocean floor.

Exposure to oxygenated waters can cause the remobilization of authigenic Re. This is thought to compromise sedimentary Re concentrations as a proxy for past redox conditions in areas with low sedimentation rates (< 10 cm/kyr) and high exposure to oxygenated bottom waters where "burndown" may result (Crusius et al., 1996). In the Santa Barbara Basin, the sustained high sedimentation rate of > 100 cm/kyr quells any doubts that may arise – "burndown" under such conditions cannot be significant.

In reducing marine sediments, Re enrichment occurs slightly later in the redox sequence than U and prior to Mo. It is exactly this small variation in redox sensitivity that makes these three trace elements useful for they can be used as indicators of the paleo-environment, specifically oxic, suboxic and anoxic conditions.

3.4. Cadmium

Cadmium (Cd) exists in the marine environment only as Cd (II). Deep water Cd concentrations in the ocean vary from 170- 900 pM with maximum values associated with the Oxygen Minimum Zone. Dissolved Cd in the water column displays a "nutrient- like" profile, and is correlated strongly with HPO_4^{2-} (Boyle, 1988).

Within the California Current system a linear relationship between Cd and PO_4^{3-} has also been established (van Geen, 1996). Cd has a residence time of 30-150 kyr, once again indicating biologically reactive chemistry. The Cd - PO_4^{3-} relationship can be used to estimate the amount of Cd delivered to the sediments with the flux of organic matter.

Using a Redfield ratio for C:P between 106-175 and a Cd:PO_4 ratio of 4×10^{-6}, sediments with 1% organic carbon content add ≅ 0.03 μg/g Cd to the seafloor (Rosenthal et al., 1995). Though this amount appears to be negligible, pore water data from both the California borderlands and the Laurentian Trough suggest Cd is released upon the degradation of organic matter (Rosenthal et al., 1995) (Gendron et al., 1986). In oxic waters, a sharp increase in dissolved Cd is evident just below the sediment water interface. Cadmium added to the pore waters may be lost to the water column by diffusion out of the sediments, or be sequestered by precipitation under reducing sedimentary conditions.

Cd values in suboxic marine sediments can reach > 8 ppm (Morford and Emerson, 1999; Pedersen et al., 1989), a significant enrichment over crustal levels of ≈0.8 ppm. Again however, there is controversy over the mechanism of Cd removal from the pore waters to the sediments. Evidence exists for authigenic precipitation of Cd occurring as CdS under suboxic conditions even when H_2S is present in concentrations ≤ 4 μmol/kg (Gobeil et al., 1997; Rosenthal et al., 1995; van Geen et al., 1995). However, scavenging by Fe-oxyhydroxides has also been proposed as a possible means for Cd containment within the sediments (McCorkle et al., 1991). When comparing sediment profiles from reducing environments, Cd appears to be precipitated in sequence after Mn and Fe reduction occurs (Rosenthal et al., 1995). This allows Cd to be used in addition to U and Mo to identify variations in the redox conditions

When considering Cd as an indicator of paleo-environmental conditions, post-depositional remobilization must be considered. Cd is sensitive to the oxygenation state of the sediments and is sequestered in sediments only below the depth of solid phase Mn enrichment under oxic bottom waters (Gobeil et al., 1997). If the depth of the redox boundary changes, solid phase Cd may be oxidized and lost to the water column (Gendron et al., 1986) or diffuse downward and form a peak at the new redox boundary (Gobeil et al., 1997; Rosenthal et al., 1995).

The amount of Cd transported to the sediments is proportional to the flux of organic matter reaching the sediments. Consequently, a high carbon flux will produce a sharp Cd concentration gradient and a shallow redox boundary. A change in the carbon flux will affect the depth of the redox boundary. If the rain rate of organic matter decreases and oxygen penetration within the sediments increases, post-depositional remobilization of redox sensitive metals such as Cd will occur.

3.5. Silver

Studies of the marine geochemical cycle of silver (Ag) have so far been limited. Although studies in the Pacific Ocean yielded a water column profile of Ag in 1983 (Martin et al., 1983), it was not until 1995 that the first Atlantic profiles were measured (Flegal et al., 1995), while North Atlantic measurements were conducted in 1999 (Rivera-Duarte et al., 1999). In contrast, there has been considerable work on the toxic effects of Ag due to increasing pollution and waste products introduced to both freshwater and marine systems (Berry et al., 1999; Karen et al., 1999; Ratte, 1999). Implicit in these studies are questions that focus on the reactivity of the Ag^+ ion and the ability for Ag^+ to bind to organic carbon and reduced sulphur compounds (Andren et al., 1999).

In the open ocean a relationship between dissolved Ag and particulate organic carbon has been identified (Martin et al., 1983). Off the coasts of California and central Mexico, surface water Ag concentrations were 1.1-1.5 pmol/kg. These dropped to a distinct minimum of 0.04 pmol/kg at 60 m corresponding to the depth of the chlorophyll maximum (Martin et al., 1983). Temperature and salinity plots showed no structure other than the conservative mixing of merging water masses (Subtropical Surface Water, Subtropical Subsurface Water and Antarctic Intermediate Water). However, the Ag profile distinctly mirrored that of particulate organic carbon in this area (Martin et al., 1983).

In the Eastern Pacific (Zhang et al., 2001), North Pacific and eastern Atlantic oceans (Flegal et al., 1995) the Ag profile is tightly correlated to that of H_4SiO_4:

$$Ag(pM)= 0.685+0.107 \times H_4SiO_4\ (\mu M) \qquad (R=0.916)$$

The implication of this observation is that particulate Ag is associated with particulate opal, $SiO_2{\cdot}nH2O$. SiO_2 is a biological "hard part" constituent and has a deeper regeneration depth in the ocean than other nutrients (PO_4^{3-}, NO_3^-), reflecting the gradual dissolution of sinking diatom frustules.

Silver has been found to be bound to the structural components of diatoms (Fisher et al., 1993) and released from a cell upon dissolution of the frustule (Lee et al., 1994). Sediment traps deployed at various water depths in the California Current indicate that organic material is a likely vector that delivers Ag to the sediments (Martin et al., 1983). In this region , the Ag flux was highest at surface, 510 pmol/m^2 at 120 m, and decreased with depth to 60 pmol/m^2 at 1950 m, closely resembling the removal of organic carbon. From these data a surface residence time for Ag of >1year and an ocean residence time of 5000 years was calculated.

The acknowledged relationships between Ag:H_4SiO_4 and Cd:PO_4^{3-} and the varying depths of regeneration between "hard part" and "soft part" processes may provide insight into ocean dynamics as documented by the distribution of Ag and Cd in the sediments. This hypothesis requires that Ag and Cd are both captured geochemically by the sediments in proportions that reflect their respective concentrations in both bottom and pore waters.

Authigenic Ag formation in marine sediments appears to occur rapidly in the presence of Fe-sulphides, resulting in the precipitation of acanthite (Ag_2S) (Adams et al., 1998). Accordingly, silver enrichment in coastal anoxic sediments has been identified worldwide. Crustal values of 70 ppb are far exceeded in anoxic sediment cores from the Baltic Sea (300 ppb), in sediments off the coast of Chile (1.12 ppm) and Peru (540 ppb), in Saanich Inlet (220 ppb) and San Clemente Basin (250 ppb) sediments, and in the Santa Barbara basin deposits (290 ppb) (Koide et al., 1986). Extreme enrichment such as seen in surface sediments from Whites Point, Los Angeles (13 ppm) (Koide et al., 1986) suggests a local pollution source. In contrast, Ag concentrations cluster around the expected crustal value in pelagic sediments.

4. Results and Discussion

4.1. Chronology of ODP Site 893A

The age model used in this work was provided by Behl and Kennett (1996). The first 10,000 years of this core were dated by varve counting . All voids larger than 0.5 cm, turbidites and "instantaneous" deposits in the core were removed. Core catcher sediments were included. 17 AMS ^{14}C ages were determined on forams in the portion of the core used in this study (50 ka). A reservoir age of 825 years was used to correct for the basin residence time. Using a curve fit (r^2=0.998), an age-depth correlation was used to assign ages to undated sample depths. Behl and Kennett's age model has been used for all data presented in this work. This has changed both the sub-bottom depths and dates assigned to $\delta^{15}N$ and opal accumulation rate data that were provided by R. Thunell (written communication, 1999).

4.2. Downhole Variations in Major and Minor Elements

4.2.1. Indicators of Grain Size and Mineralogy

Downcore fluctuations of major and minor element concentrations can be used to glean information about variations in the depositional environment of an area. In addition to changes in sedimentation rate, departures from background elemental concentrations, whether episodic or persistent , provide information that is helpful in the historical interpretation of sedimentation and diagenesis in a given region. Concentrations of selected major elements can be used to illustrate changes in such factors as grain size (Zr, Si) and regional productivity (Ca, Sr, Ba) (Berger et al., 1975; Calvert et al., 2001).

In Santa Barbara Basin, there is no visible difference in lithology from the Holocene to the last glacial maximum (LGM), including the glacial termination (Figure 4). A near constant sedimentation rate, consistently remaining near 120 cm/kyr (Behl, 1995), prevailed for the past 50,000 years. Similarly, the bulk composition has been essentially constant. No dramatic changes in the Si/Al, Ti/Al, K/Al, Zr/Al, and Fe/Al ratios occur with depth. This indicates that there have been no apparent large-scale shifts in the relative concentrations of quartz, Ti-bearing minerals, K-feldspars, zircon and/or pyrite, respectively, over 50,000 years, as shown in Figure 4.

Consistent with Stein (1995), sand layers have been identified at approximately 57 and 63 mbsf (39.2 and 43 ka). These layers represent two turbidity-current events that have been previously documented (Stein, 1995). Samples from these layers are lighter in colour and exhibit a coarser texture than other samples from this core. Geochemically, the textural change is evident from peaks in Si/Al, Zr/Al (Figure 4) and Ba/Al (Figure 5) ratios. The element zirconium occurs predominantly in zircon, a resistate heavy mineral that is usually associated with the fine-sand to coarse-silt fraction of marine sediments (Calvert and Fontugne 2001) because it has a relatively high density (~ 4.6), fostering its hydrodynamic association with coarser sediments. High Si/Al ratios may also reflect increases in the coarse-grained fraction, owing to increases in the relative proportions of quartz to clay (Calvert and Fontugne 2001).

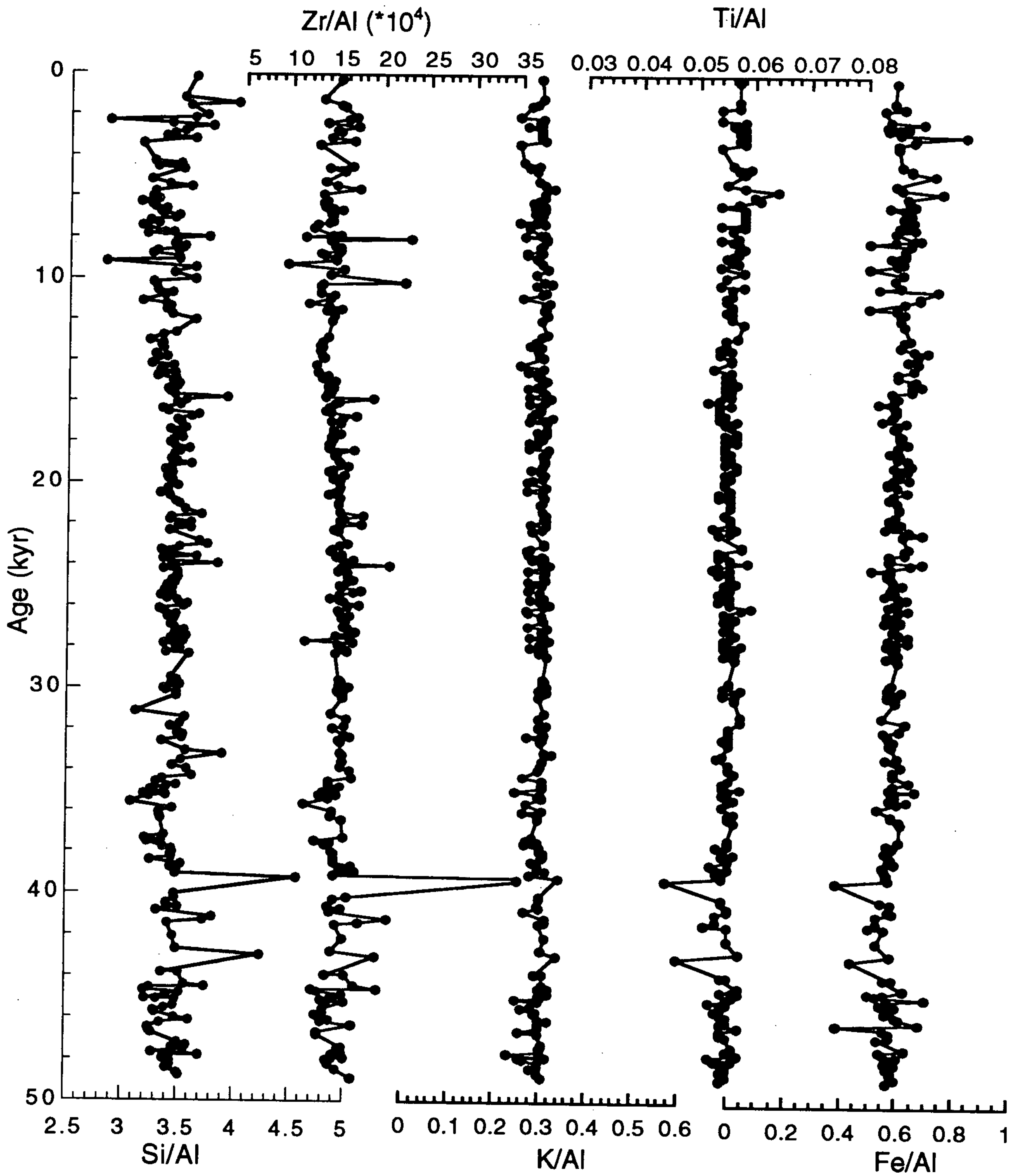

Figure 4. Downhole variations in major and minor elements. The Si/Al ratio represents the ratio of quartz/clay. Zr/Al is indicative of the coarse grained fraction of the sediment. K/Al reflects input from potassium feldspars. Ti/Al and Fe/Al are proxies of titanium bearing heavy minerals and pyrite, respectively. Iron is also a major constituent of aluminosilicate minerals.

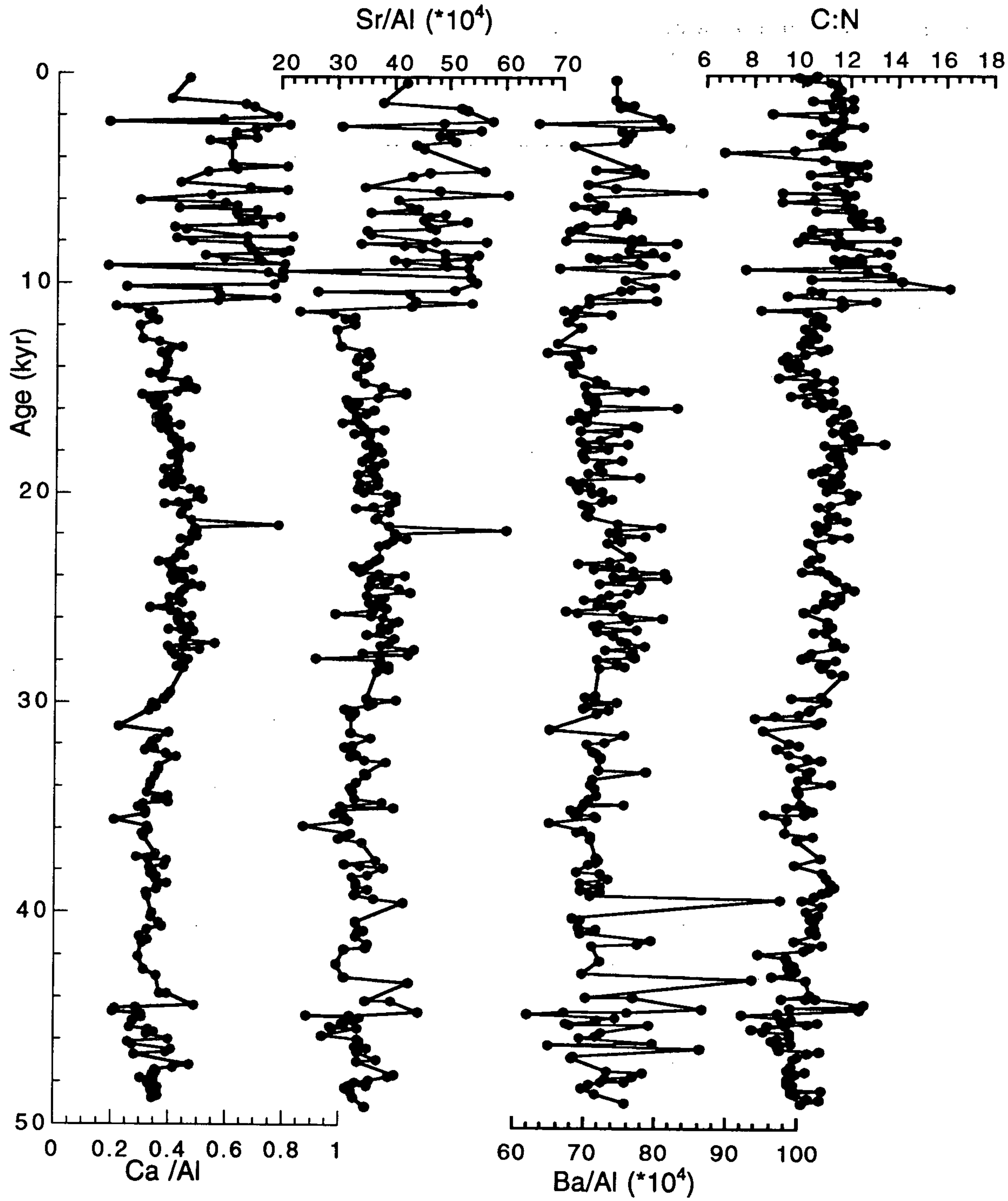

Figure 5.Downhole variation of organic proxies. Both Ca/Al and Sr/Al vary with $CaCO_3$. Ba/Al has both organic and inorganic sources. The ratio of C_{org}:N suggests little variation in the input of marine vs. terrestrial organic matter.

In addition to its occurrence in the lithogenous fraction of sediments, barium is also associated with organic carbon fluxes in the ocean and can be used as a paleoproductivity proxy (Brumsack et al., 1983; Dean et al., 1997; Dymond et al., 1996; Dymond et al., 1992). Ba is thought to precipitate as barite ($BaSO_4$) within the microenvironment of decaying biological debris (Bishop, 1988; McManus et al., 1994). Within these confined spaces Ba^{2+} and SO_4^{2-} may reach high enough concentrations for barite precipitation even when the surrounding water column is undersaturated in $BaSO_4$ (Dymond and Collier, 1996). Once at the seafloor, sulphate reduction may cause the dissolution of $BaSO_4$. Post-depositional mobilization of bio-Ba in anoxic sediments therefore attenuates the organic signal, diminishing the value of Ba as a productivity proxy in reducing sediments (Dymond et al., 1992).

Detrital aluminosilicates also contain Ba, and concentrations in such phases may range from 300-1000 ppm (Dymond et al., 1992). With the expected loss of bio-barium under anoxic conditions, the increase in the Ba/Al ratio seen in the two sand layers is most likely a result of increases in associated aluminosilicates in which the Ba is lattice bound and preserved more readily. As well, Ba substitution for K into K-feldspars may occur for barium has a similar ionic radius to that of potassium. This can explain a small portion of the Ba/Al spike. However, the increase in the K/Al ratio during these episodes (Figure 4) varies only slightly and does not account for the magnitude of the Ba/Al spike. Therefore, the increase in the Ba/Al ratio seen in the sand layers is almost certainly a result of additional coarse aluminosilicate content (Dymond et al., 1992) (excluding increased orthoclase input) rather than a reflection of enhanced production. Based on the visual and compositional observations, it is concluded that the sandy layers indeed represent turbidites that were deposited essentially instantly. Apart from these two depositional events, the lithological consistency downhole suggests that neither the mineralogy nor the grain size of the sediments have changed significantly over the past 50,000 years.

4.2.2. Indicators of Organic Flux

In addition to being influenced by the presence of detrital quartz, the Si/Al ratio is affected by the biological flux of opal from diatom production in the overlying waters (Kamatani et al., 2000). Diatom productivity is high in the waters off southern California, with most production occurring in the spring and summer seasons. Sediment trap studies and box cores taken from SBB indicate an increase in diatom frustules settling to the basin floor in June, post-spring bloom. The spring assemblage of diatoms appeared to be smaller and more weakly silicified than the autumn assemblage (Reimers et al., 1990). Despite the present-day knowledge of diatom production in SBB, relating measurements of sedimentary biogenic silica content to diatom production in the overlying waters is difficult because the sedimentary Si/Al ratio does not appear to reflect this biological flux. Throughout the core, Si/Al generally varies in coherence with the detrital Zr/Al ratio. Post-depositional dissolution of opal may be largely responsible for the lack of an obvious biogenic silica contribution to the buried sediments. The relationship between opal flux to the sea floor and preservation within the sediments is often compromised by the dissolution of opal (Archer et al., 1993; McManus et al., 1995), both in the water column and at the sediment-water interface (Pilskaln et al., 2001; Ragueneau et al., 2000), and only where the opal settling flux is exceptionally high is the sedimentary opal content significant (Archer et al., 1993). The Santa Barbara Basin deposits do not appear to fall into this category.

Opal is undersaturated in seawater throughout the water column and therefore has the thermodynamic tendency to dissolve in the ocean. Nevertheless, opal is also one of the major constituents of marine sediments in specific geographic areas. Primarily, the balance between the diatom flux and the rate of burial at the seafloor controls the preservation of sedimentary biogenic opal in any specific setting. Having reached the sediments, opal dissolution will occur until pore waters become supersaturated or chemical inhibition occurs. As well, the water column depth, surface layer temperature, diatom species composition, frustule morphology, grazer characteristics, aggregate particle formation and trace metal chemistry all have some effect on the relationship between surface production and sedimentary concentrations of silica (Nelson et al., 1995).

Preservation of siliceous shells in SBB does not appear to vary between the aerobic sediments above the sill depth (475 m) and the anaerobic sediments below (Berger and Soutar, 1975). Variation in oxygenation of the bottom waters over time at this site therefore has little potential to significantly affect the preservation of biogenic opal in the sediments. If differential preservation occurs, it is more likely due to the speed with which a frustule reaches the sediment-water interface and the time spent in the "fluff" layer (Pilskaln and Pike, 2001; Ragueneau et al., 2000). The former is a function of fecal pellet production and/or the formation of aggregates such as "marine snow". The latter affects the organic flux to the sea floor and bacterial activity within the surface sediments (Pilskaln and Pike, 2001).

Much more significant than the nearly invariant and low biogenic opal content in Hole 893A is the change in the Ca/Al and Sr/Al ratios at the onset of the Holocene (Figure 5). These data indicate that the abundance of $CaCO_3$ at this site increased dramatically at the beginning of the Holocene (direct measurements of $CaCO_3$ are shown in Figure 13). The amount of calcium in marine sediments is predominantly controlled by the flux and preservation of foraminiferal and coccolithophorid calcium carbonate "shells". Strontium (Sr^{2+}) and calcium (Ca^{2+}) have similar ionic radii and chemical behaviours. Therefore, Sr^{2+} readily replaces Ca^{2+} in the $CaCO_3$ lattice of these tests, and the fluctuation of the Sr/Al ratio with depth consequently mimics that of Ca/Al. Both proxies therefore indicate changes in the biological carbonate concentration in the sediments. Similar results have been published in the Scientific Results for ODP Leg 146, Site 893A (Gardner et al., 1995). Additionally, the Southern Californian coastline shows a corresponding trend, with elevated sedimentary $CaCO_3$ during the past 10,000 years (Gardner et al., 1997). This suggests that the abrupt increase in carbonate content at the beginning of the Holocene is at least a regional feature.

Within Santa Barbara Basin surface sediments, the number of foraminiferal tests present in anoxic sediments (below the sill) is almost ten times that found in oxic sediments (above the sill) (Berger and Soutar, 1975). Aragonitic shells are not present at all in shallow aerated sediments, but are relatively abundant below the sill depth in suboxic and anoxic sediments (Berger and Soutar, 1975). Under oxic conditions the degradation of organic matter (simplified to CH_2O) releases CO_2:

$$CH_2O + O_2 \longleftrightarrow CO_2 + H_2O.$$

The addition of carbon dioxide to the water column increases the total carbon content but not the alkalinity as the hydrolysis of CO_2:

$$H_2O + CO_2 \longleftrightarrow H^+ + HCO_3^-,$$

produces an equal amount of positive and negative charges. The protons released by the dissociation of carbonic acid react with carbonate ions to produce bicarbonate. This does not change the carbonate alkalinity (CA), defined as:

$$[CA] = [HCO_3^-] + 2[CO_3^{2-}] \text{ (= constant in this case)}$$

but it does decrease the carbonate ion concentration which pushes the equilibrium between calcium carbonate and pore solution ($CaCO_3 = Ca^{2+} + CO_3^{2-}$) toward undersaturation. Thus, the addition of enough carbonic acid will cause dissolution of $CaCO_3$.

The oxidation of organic matter by sulphate, however, increases both the total carbon and the carbonate alkalinity through the reduction of the SO_4^{2-} ion, which has a double negative charge, to HS^-, which has a single charge:

$$SO_4^{2-} + 2CH_2O + 2H^+ \longleftrightarrow HS^- + H^+ + 2CO_2 + 2H_2O.$$

To compensate for this loss of negative charge, HCO_3^- is converted to CO_3^{2-}. This drives the pore solution toward supersaturation with $CaCO_{3(s)}$. As a result, calcareous components of the sediment have a tendency to be disproportionately preserved under anoxic conditions. Therefore, the variation seen in the downcore

Ca/Al and Sr/Al ratios here, as well as the %$CaCO_3$ measurements may have been influenced by differential preservation under varying oxygen conditions.

The sharp increase in sedimentary $CaCO_3$, seen at the onset of the Holocene is not repeated during the Bølling-Allerød, however, nor elsewhere downcore. Transitions from oxic to anoxic sediments (section 4.3) are not all accompanied by a resultant increase in $CaCO_3$ concentrations. The almost perpetual shallow redox boundary in this basin (section 4.3.3) maintains sedimentary suboxic conditions very near the sea floor surface. This may dampen the effects of $CaCO_3$ dissolution seen in samples collected from shallower areas that underlie oxic bottom waters and that have a much deeper redox boundary in the sediments. Given the relatively constant sedimentation rate in SBB throughout the last 50,000 years and the perpetually shallow redox boundary during this time (section 4.3.3), it is concluded that the higher ratios of Ca/Al and Sr/Al and enhanced concentrations of $CaCO_3$ seen in the post-glacial deposits reflect an increase in the biogenic carbonate flux.

Terrestrial input may also include organic matter. The proximity of Site 893A to land changed with the fluctuations in sea level on the glacial/ interglacial timescale. However, Santa Barbara Basin sits within a region of active tectonic uplift. The annual uplift of > 5 mm/yr at the southern sill suggests the local sealevel minimum during eustatic low lowstand of the LGM was moderated and potentially not more than 80 m lower than today (Hendy and Kennett, 2000). Nevertheless, the exposed shelf during lowstand could have affected the terrestrial carbon flux to the deep basin.

The character of the terrestrial vegetation surrounding SBB has also changed in response to global climate fluctuations (Heusser et al., 1997). Dramatic differences in the local pollen record show transitions from conifer (*Pinus*) dominated to broadleaf (*Quercus*) ecosystems on glacial/interglacial timescales as well as rapid fluctuations on millennial timescales (Heusser and Sirocko, 1997). Despite variations in both the vegetation cover and relative sea level, there appears to have been little change in the proportions of organic material of marine and terrestrial origins deposited in Santa Barbara Basin sediments. Evidence for this suggestion is provided by the Corg:Ntotal ratio in basin sediments (Figure 5).

The ratio of carbon/nitrogen (C:N) offers a crude and qualitative means of determining the potential impact of terrestrial organic carbon fluctuations with time. Sediments containing marine-derived organic carbon typically exhibit low C:N ratios, whereas terrestrial organic matter typically although not always shows higher C:N values. By adopting representative ratios for these two end members, terrestrial and marine contributions to the organic matter pool in the sediments might be defined if there has been a significant change from marine to terrestrial inputs. The C:N ratio observed at this site shows little deviation from the mean value of approximately 11, though the range of values seen in the Holocene is greater. These measurements are consistent with those of Stein and Rack (1995) who report a general range of C:N values for SBB of 6-12. Thin flood and turbidite deposits with predominantly terrestrial organic material are common in this core throughout the Holocene (Rack et al., 1995) and add to the fluctuations in the C:N ratio during this time. The constancy of the C:N ratio from 10-50 ka in SBB suggests that the organic component has not been affected by the terrestrial organic flux to the basin floor due to a variable sea level and/or regional precipitation .

The analysis of major and minor elements from Site 893A in the Santa Barbara Basin thus suggests that there has been no significant change in the mineralogy or grain size of the accumulating sediments over the last 50,000 years. This, in conjunction with a near constant and very high sedimentation rate, provides a relatively stable setting within which trace metals can be used to determine the oxygenation history of the area. The Si/Al ratio shows very little downcore variation, indicating either no change in the quartz input to the area, a non-varying flux of diatoms to the seafloor or almost complete dissolution of biogenic opal at this site over the past 50,000 years. On the other hand, there has been an inferred increase in the flux of biogenic carbonate to the sediments over the past 10,000 years suggesting that oceanographic conditions in the Holocene have been somewhat different than in the late Pleistocene. As discussed below, this change may reflect a switch in the character and/or intensity of primary production in the basin.

4.3. Determining The Oxygenation History Of Santa Barbara Basin

In 1996, Richard Behl and Jim Kennett provided a description of the oxygenation history of Santa Barbara Basin by documenting both the presence and absence of laminated sediments. It was concluded that within this basin the Holocene has been a period of prolonged anoxia, while the last glacial maximum and glacial termination was mainly oxic with distinct, relatively short-lived anoxic events. Behl and Kennett (1996) used a four-tiered scale, from clearly laminated (anoxic: <0.1 ml/l O_2) to clearly bioturbated (oxic: >0.3 ml/l O_2), to "quantify" the paleo-oxygen content of Santa Barbara Basin sediments.

Although laminated sediments have commonly been used as a proxy for anoxic bottom waters (Behl, 1995; Cannariato et al., 1999b; Kennett et al., 1995), conditions may exist that facilitate deposition of laminated sediments beneath an oxygenated water column (Pike et al., 1999). Conversely, if there is little seasonal change in the composition of sedimentary material supplied to the sea floor, sediments lacking laminations may accumulate despite the absence of bioturbating organisms (Brodie et al., 1994; Grimm et al., 1996). Direct correlation between laminated sediments and anoxic bottom waters must therefore be supplemented with data pertaining to the depositional and preservational environment.

Downcore variations in biota, including assemblages of forams capable of flourishing in oxic or dysoxic sediments (Cannariato and Kennett, 1999a; Cannariato et al., 1999b; Hendy and Kennett, 2000) are consistent with the bioturbation index and provide a picture of Santa Barbara Basin through time, intimating that anoxic interstadials and oxic stadials correspond to $\delta^{18}O_{(ice)}$ values measured on the GRIP ice-core. Furthermore, the Holocene sediments are dominated by *Bolivina*, *Buliminella* and *Globobulimina spp.*, all dysoxic taxa (Cannariato et al., 1999b).

As opposed to the "on" and "off" depiction provided by laminations, trace metal data provide a more detailed representation of the variations in oxic and anoxic conditions in the basin. The trace metal/aluminum ratios shown in Figures 6a and 6b indicate that sedimentary trace metal concentrations have varied at this site over time. Downcore variations in trace metal concentrations as a result of

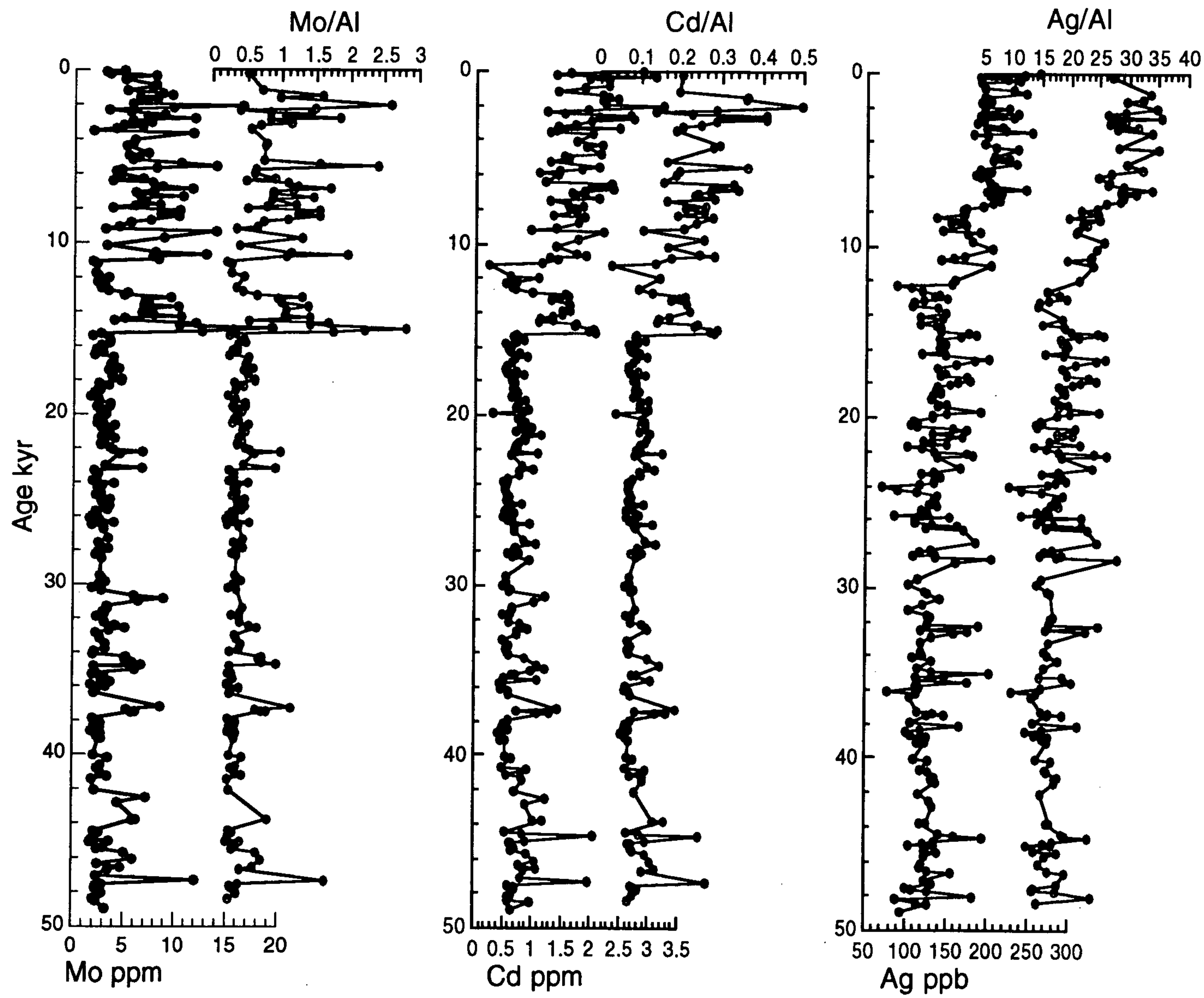

Figure 6a. Total trace metal concentrations of Mo (ppm), Cd (ppm) and Ag (ppb) in the downcore profile compared to the same data normalized to Al.

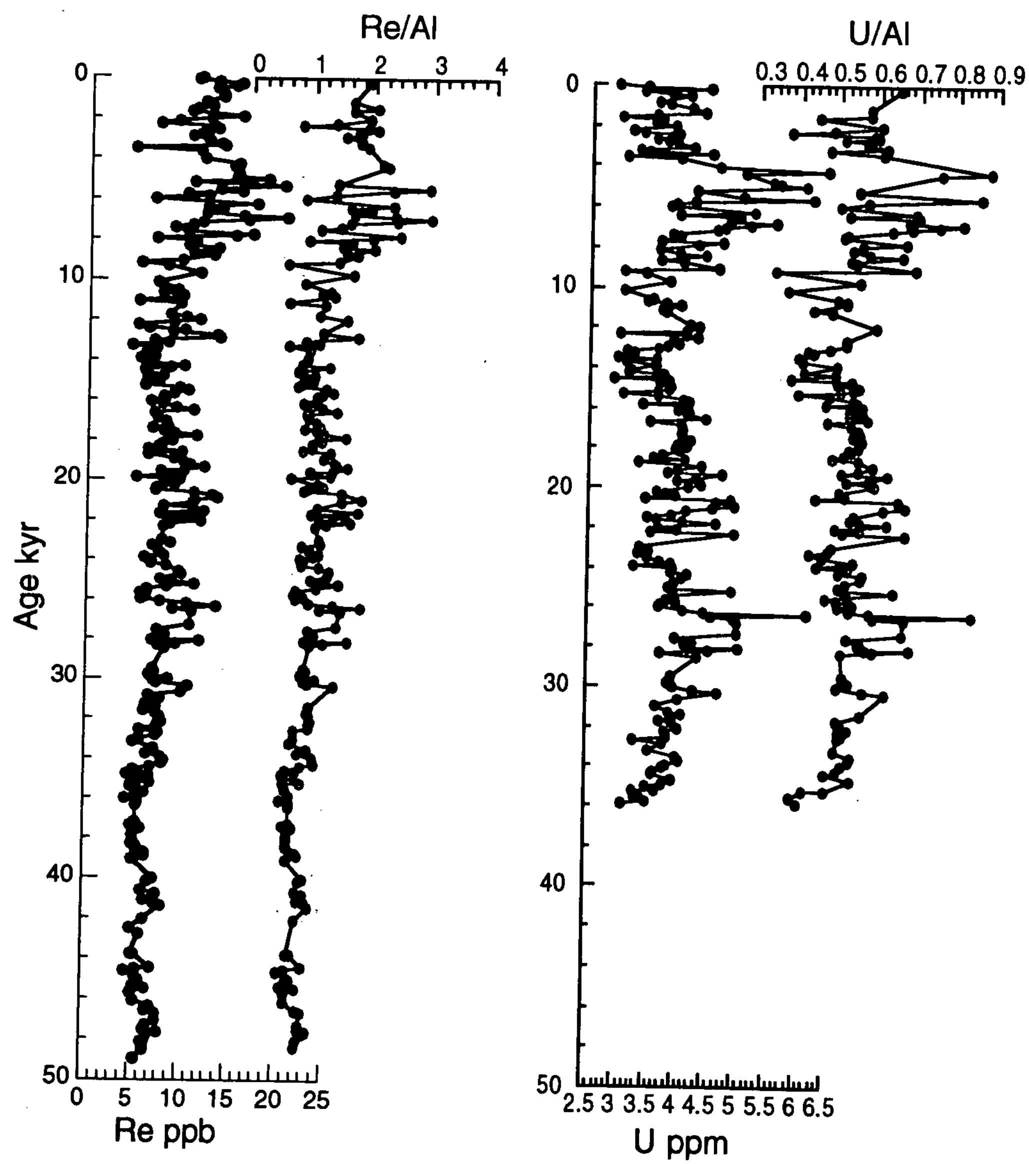

Figure 6b. Total trace metal concentrations of Re (ppb) and U (ppm) in the downcore profile compared to the same data normalized to Al.

authigenic mineral formation is also evident in the profiles of total Mo, Cd, Re, Ag and U. Thus, if the trace metal/ aluminum ratios are compared to the total trace metal profiles, the variations and the magnitudes of the downcore fluctuations are very similar. Figure 6 shows that the trace metal profiles have higher resolution than the metal/aluminum ratios because Al data are lacking where sample sizes prevented major element (Al) determinations. In order to maximize the resolution of this core, the Mo, Re, Cd, Ag and U data will be presented as "total" concentrations, rather than normalized to aluminum.

As discussed in Chapter 1, information on the amount of oxygen present in the bottom waters of the basin can most effectively be extracted by applying a multitracer approach. Such multiple element analyses yield details that, when considered as a suite, provide insight into the oxygenation history of the basin. The various tracers applied in this study, including molybdenum, rhenium and manganese, place limitations on the potential amount of oxygen present in the bottom waters and/or pore waters at the time of precipitation. Thus, downcore profiles of Mn, Mo, Cd, Re and U along with the distributions of other parameters are used here to reconstruct the oxygenation history of Santa Barbara Basin through time.

4.3.1 Manganese

The range of manganese (Mn) concentrations in Hole 893A is 300-500 ppm (Figure 7). This is less than average crustal values, which tend to be on the order of 600 ppm (Shimmield and Price, 1986). Thus, there is no indication in the data of any enrichment of Mn relative to the average terrigenous concentration in SBB over the

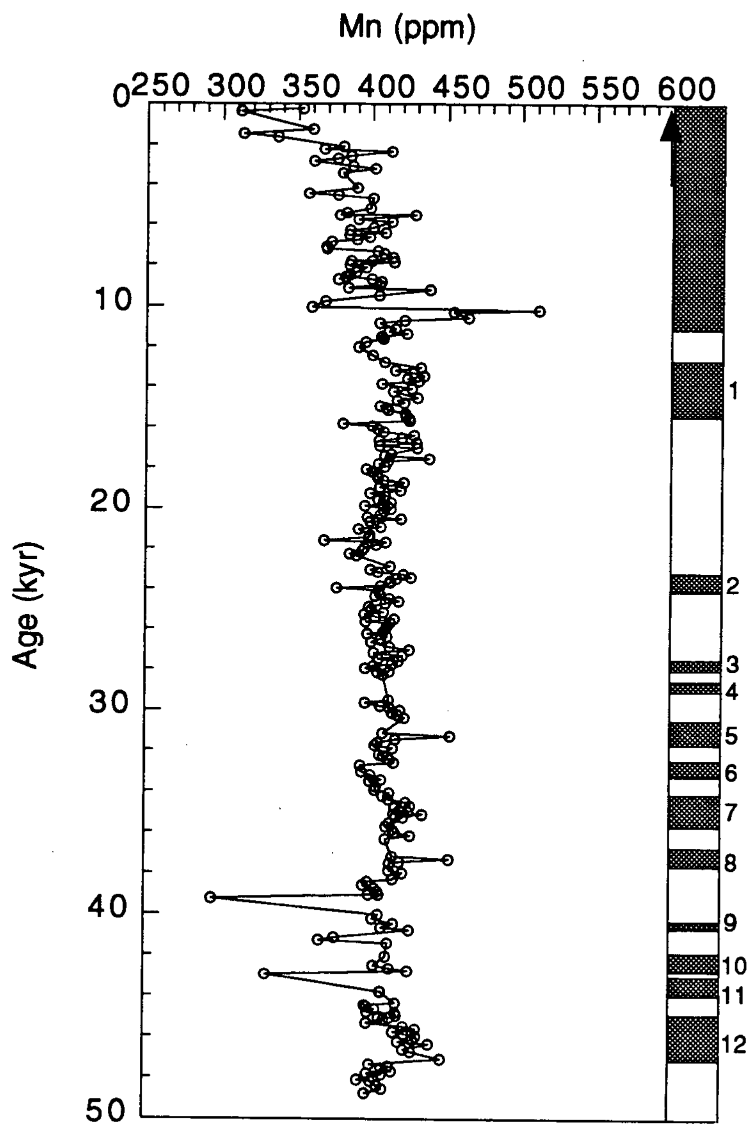

Figure 7. Downhole Mn profile. The black arrow indicates the crustal concentration. The shaded areas indicate sections with laminated sediments, while unshaded areas indicate "massive " sediments that included visible bioturbation and burrows.

last 50,000 years. This indicates that during this entire period very low oxygen concentrations prevailed in the bottom waters and the sedimentary redox boundary must have remained very close to the sediment-water interface. Even during episodes of visible bioturbation within the core, reducing conditions in very shallow depths in the sediment impeded the accumulation of Mn in this core (Figure 7).

The lack of Mn enrichment also indicates Mn-carbonate accumulation is absent in this core. Mn-carbonates form at subsurface anoxic horizons in areas bathed with oxic bottom waters, due to the recycling of Mn between solid oxide form and reduced dissolved form (Calvert et al., 1996). Under these conditions, the reduction of Mn-oxyhydroxides produces dissolved Mn concentrations high enough to facilitate $MnCO_3$ precipitation (Calvert and Pedersen, 1996). The lack of Mn-carbonates in this core suggests that the concentration of dissolved Mn remained low. Therefore, bottom water dysoxia and/or the organic flux to the sediments were in combination powerful enough to keep the redox boundary so shallow that a Mn-rich aerobic zone could not have formed.

4.3.2. Molybdenum and Cadmium

Molybdenum and cadmium accumulate in marine sediments in the presence of reduced sulphur species, with Mo requiring a threshold concentration of H_2S for precipitation to occur (Sections 3.1 and 3.4). Cadmium, however, does not require more than minimal amounts of H_2S in order to be fixed during early diagenesis, and will precipitate when ΣH_2S concentrations are at or below detection limits (Rosenthal et al., 1995). During diagenesis, bacteria use SO_4^{2-} as an oxidant after the sequential depletion of O_2, NO_3^-, MnO_2 and Fe_2O_3 in the sediments. The production of H_2S therefore indicates sedimentary anoxic conditions, which are evident by elevated amounts of authigenic Mo and Cd. The difference between the profiles of these two trace metals largely reflects the variations in the concentration of H_2S present at the time of deposition.

The frequent enrichments of sedimentary Mo and Cd in Santa Barbara Basin over the last 50,000 years correspond to the laminated sediment sections (Figure 8). Molybdenum and Cd are enriched in 8 out of 12 of the anoxic periods identified by the Bioturbation Index described by Behl and Kennett (1996). Events 2, 3, 4 and 9 are all ≥2.5 on the bioturbation scale indicating diffuse, discontinuous or irregular laminations. The oxygen content associated with level 2 of the Bioturbation Index is 0.1 ml/l O_2. This oxygen concentration is expected to allow micro- and meiofaunal bioturbation (millimetre-scale), which may disrupt but not destroy laminations in the sediment (Behl and Kennett, 1996). During these "intermediate" stages with disturbed laminations, the trace metal data thus suggest that the sediments did not contain sufficient H_2S to allow the precipitation of authigenic molybdenum-rich compounds; in other words, the threshold level of sulphide in the sediment required for authigenic Mo formation was not reached.

The positive correlation between Mo and Cd concentrations and the Bioturbation Index reaffirms the recent history of anoxia in SBB, as well as the transition from predominantly oxic conditions present during the last glacial maximum. During periods of "oxic" bottom waters as characterized by Behl and Kennett (1996), Mo drops to a constant background level of approximately 2 ppm.

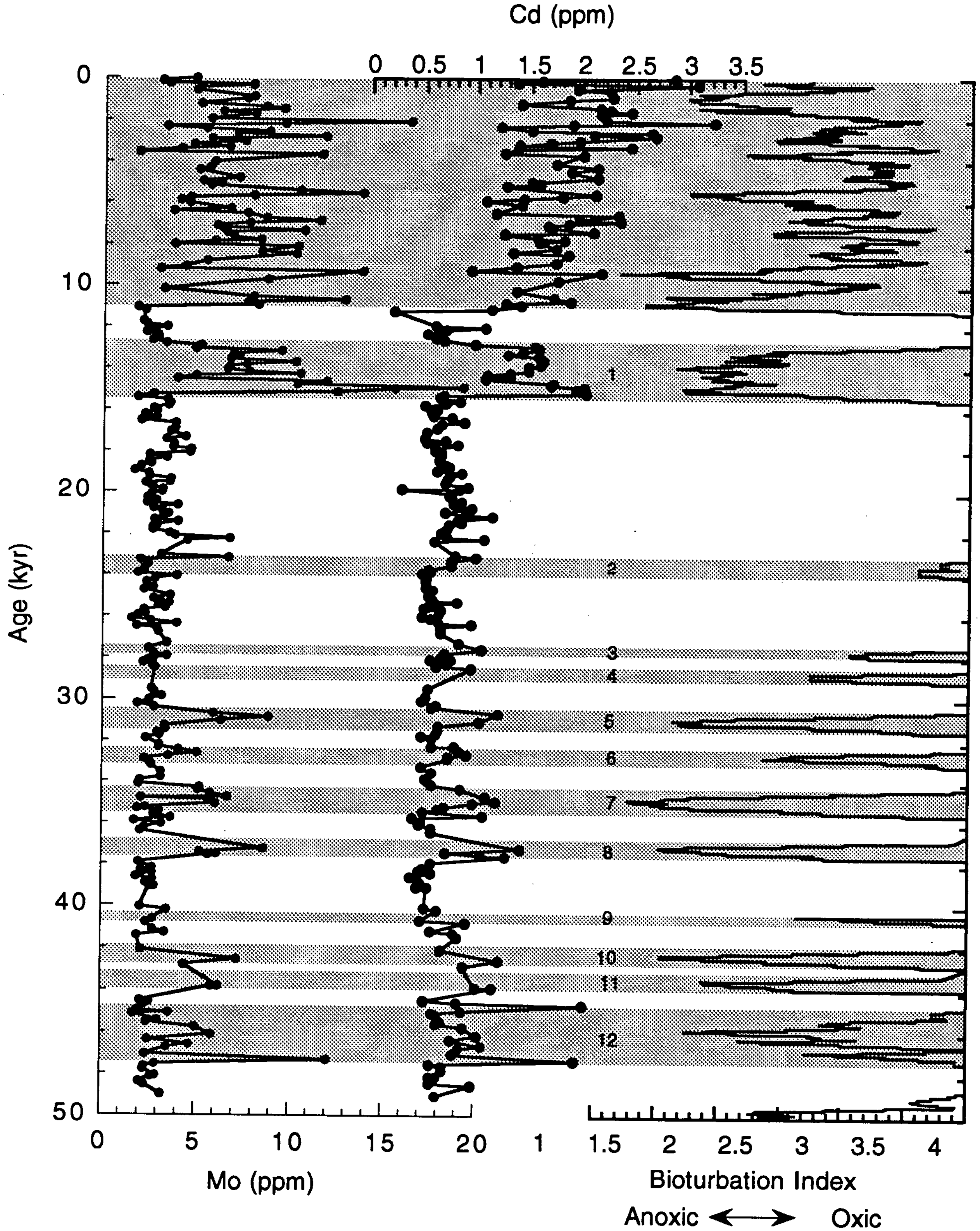

Figure 8. Mo and Cd concentrations compared to the Behl and Kennett (1996) "Bioturbation Index" where low numbers represent low oxygen concentrations. Shaded areas imply laminated sediments. The associated numbers are used in the text to indicate "anoxic events" identified by Behl and Kennett (1996).

This low concentration suggests a lack of H_2S in the sediments, but it does not indicate the presence of oxygen.

Under oxic conditions, Mo is readily sequestered in the sediments with Mn-oxides (Section 3.1) When the Mo and Mn data from this core are considered together, no such enrichment is seen. For the last 50,000 years, the Mo/Mn ratio ranges from 0.005 – 0.04, this low value being above the constant ratio of 0.002 that is representative of oxic sediments and manganese nodules (Shimmield and Price, 1986) (Figure 9). In conjunction with the lack of a Mn-rich aerobic zone at the sediment-water interface, implied by the lack of $MnCO_3$ in the SBB deposits, the Mo and Mn relationship suggests that the "oxic" conditions associated with bioturbated sediments were limited to, at most, a thin surface-sediment veneer.

4.3.3. Rhenium and Uranium

Rhenium and uranium accumulate in reducing sediments but do not necessarily require the presence of H_2S for sequestration (Sections 3.3 and 3.2). Rhenium concentrations in the sediments of Hole 893A are elevated 10 to 40-fold above crustal levels of 0.5 ppb throughout the entire core section (Figure 10). Though spikes of lower Re concentrations found during the Holocene may be a result of partial burndown or sharp changes in the depth of the redox boundary, the overall enrichment in Re suggests that there has been no extensive remobilization or oxidative burndown (Colodner et al., 1992; Crusius et al., 2000). The high Re values in this core and the accompanying elevated U concentrations suggest SBB sediments have been suboxic, if not anoxic, for the past 50,000 years. However,

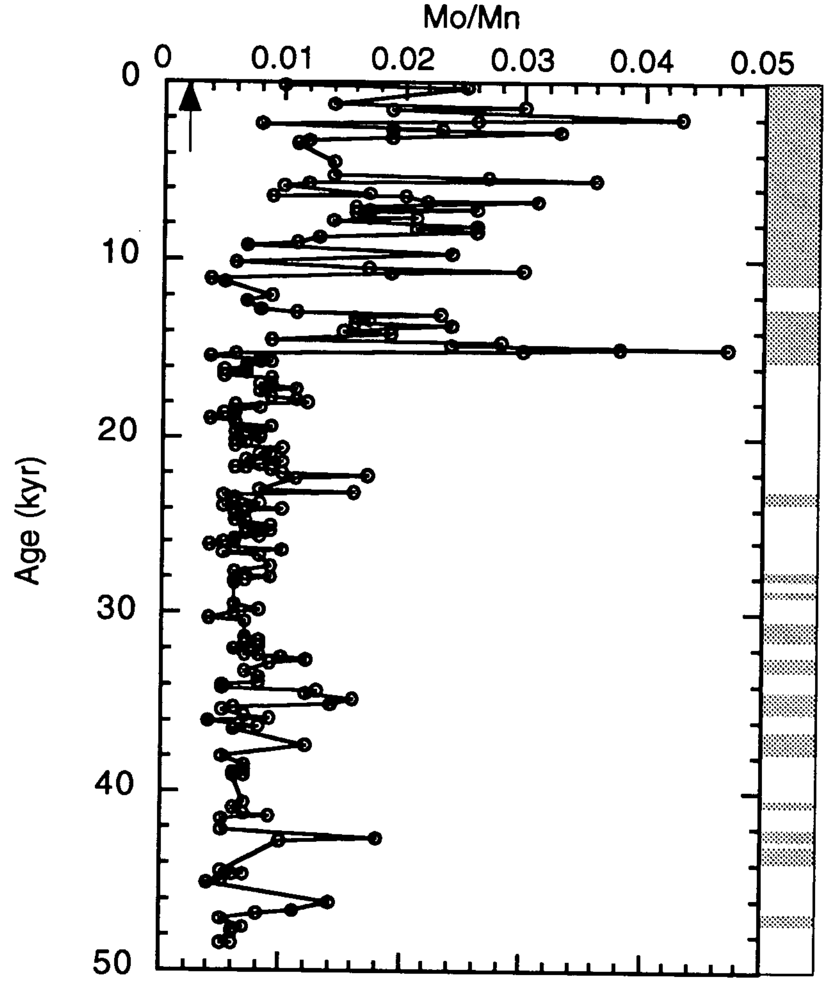

Figure 9. The ratio of Mo/Mn. The black arrow indicates the ratio of Mo/Mn in oxic sediments and Mn nodules. Shaded areas indicate laminated sediments.

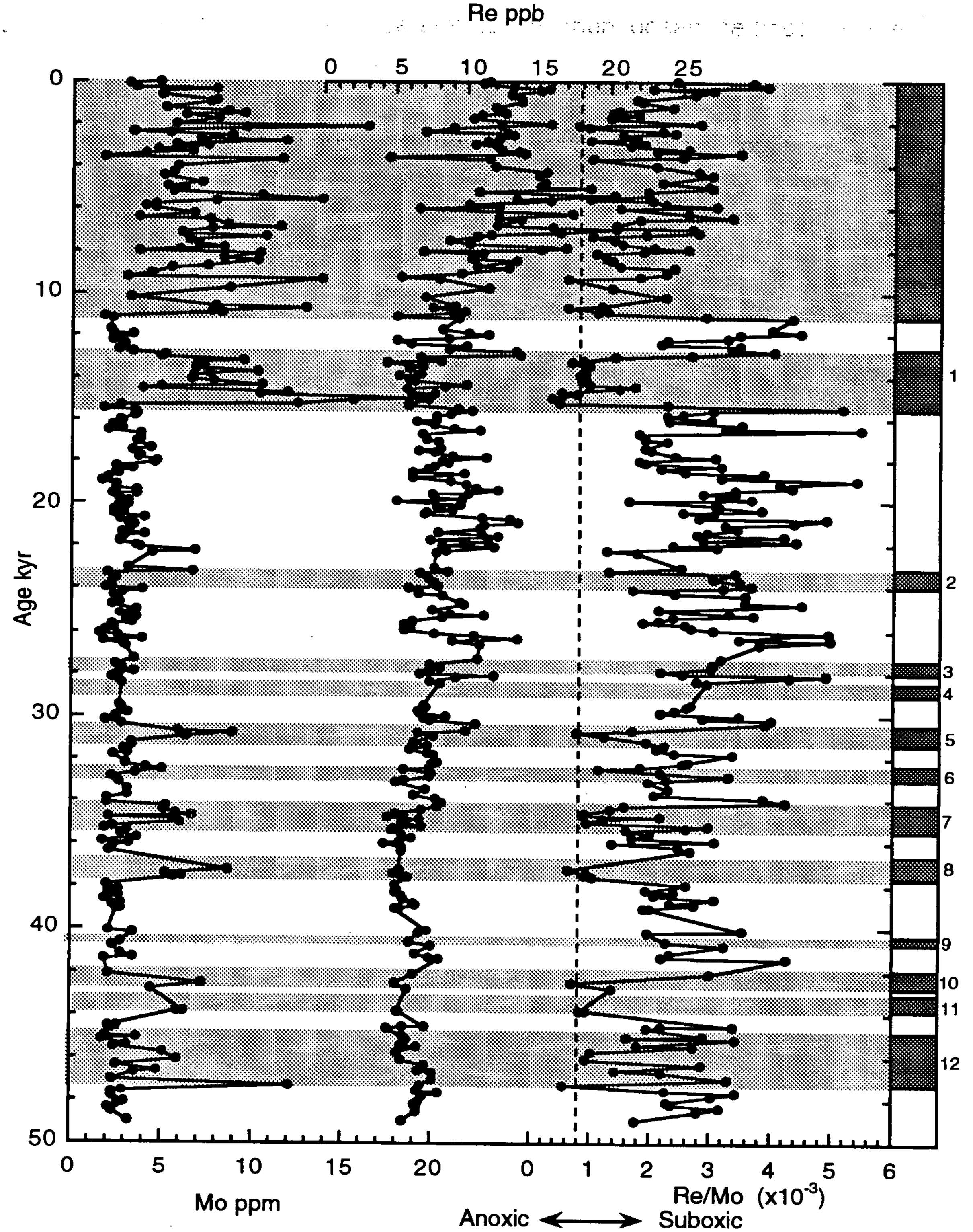

Figure 10. Downcore Re (ppb) and U (ppm) concentrations and the Re/Mo ratio in core 893A. The black arrows indicate the background crustal concentrations. The dashed line indicates the seawater Re/Mo ratio. The shaded, numbered areas indicate sections with laminated sediments.

both the Bioturbation Index and the foraminiferal assemblages constructed for SBB indicate periodic oxic conditions, either from evidence of bioturbation (Behl and Kennett, 1996) or oxic taxa (Cannariato et al., 1999b; Kennett and Ingram, 1995), in the bottom waters of the basin. Nevertheless, even during sections of bioturbated sediments, Re and U concentrations remain elevated.

This apparent conflict between the biological signals and the geochemistry can be reconciled if a very shallow redox boundary was maintained during the entire course of deposition of the sampled section. In this view, the high sedimentation rate in SBB and the large flux of organic carbon to the sediments (Gardner et al., 1997) potentially have perpetuated suboxic conditions near the sediment-water interface mutually allowing accumulation of rhenium and the presence of "oxic" foraminiferal taxa.

4.3.4 Analysis of the Re/Mo Ratio

The Re/Mo ratio has been identified as a potential means to differentiate between anoxic and suboxic sedimentary conditions (Crusius 1996). The significant differences in Re and Mo geochemistry (Sections 3.3 and 3.1) suggest this ratio can be exploited as a tool to understand fluctuations of the oxygenation state of the depositional environment. Both Mo and Re behave almost conservatively in the water column. When the sediment pore water becomes suboxic, Re precipitates and enriches the solid-phase. Molybdenum, however, does not accumulate in marine sediments until anoxia occurs and dissolved sulphide reaches a threshold value

(Helz et al., 1996). The ratio of Re/Mo can therefore provide evidence of transitions from suboxia to anoxia that occur within the sediments.

Under suboxic conditions, accumulation of solid-phase Re, but not Mo, will cause the ratio to increase above the Re/Mo ratio of the bottom waters (~0.8×10^{-3}). However, when H_2S produced during diagenesis reaches high enough concentrations, the authigenic precipitation of Mo will cause the Re/Mo ratio to return to the seawater value. A Re/Mo ratio equal to or lower than that of the bottom water ratio thus suggests Mo accumulation and anoxic conditions.

In Santa Barbara Basin, the Re/Mo ratio approaches the seawater ratio (0.8 $\times 10^{-3}$) during events 1, 5, 7, 8, 10, 11,and 12. The lack of Mo enrichment during events 2, 3 and 4 is evident again in the Re/Mo ratio, indicating that severely anoxic circumstances did not dominate during these periods. The Holocene is punctuated by numerous approaches of the sedimentary Re/Mo ratio toward the seawater value. The periodic high ratios of the last 10,000 years are typically associated with terrestrial flood deposits (section 4.4.1). Therefore, the Holocene period in SBB has been dominated by anoxia but "instantaneous" injections of low-organic-content detrital material appear to have affected the Re/Mo ratio.

Although the resolution of the %TOC and trace metal data are not identical, within the grey beds sampled for the organic carbon data (Stein et al., 1995) Mo concentrations plunge to values ranging from 1.8-4.5 ppm where TOC is also low (Figures 11 and 12). Multiple factors may be responsible for the decrease in Mo during these episodes. These beds may not contain enough organic material to maintain H_2S at concentrations high enough to trigger authigenic formation of Mo-

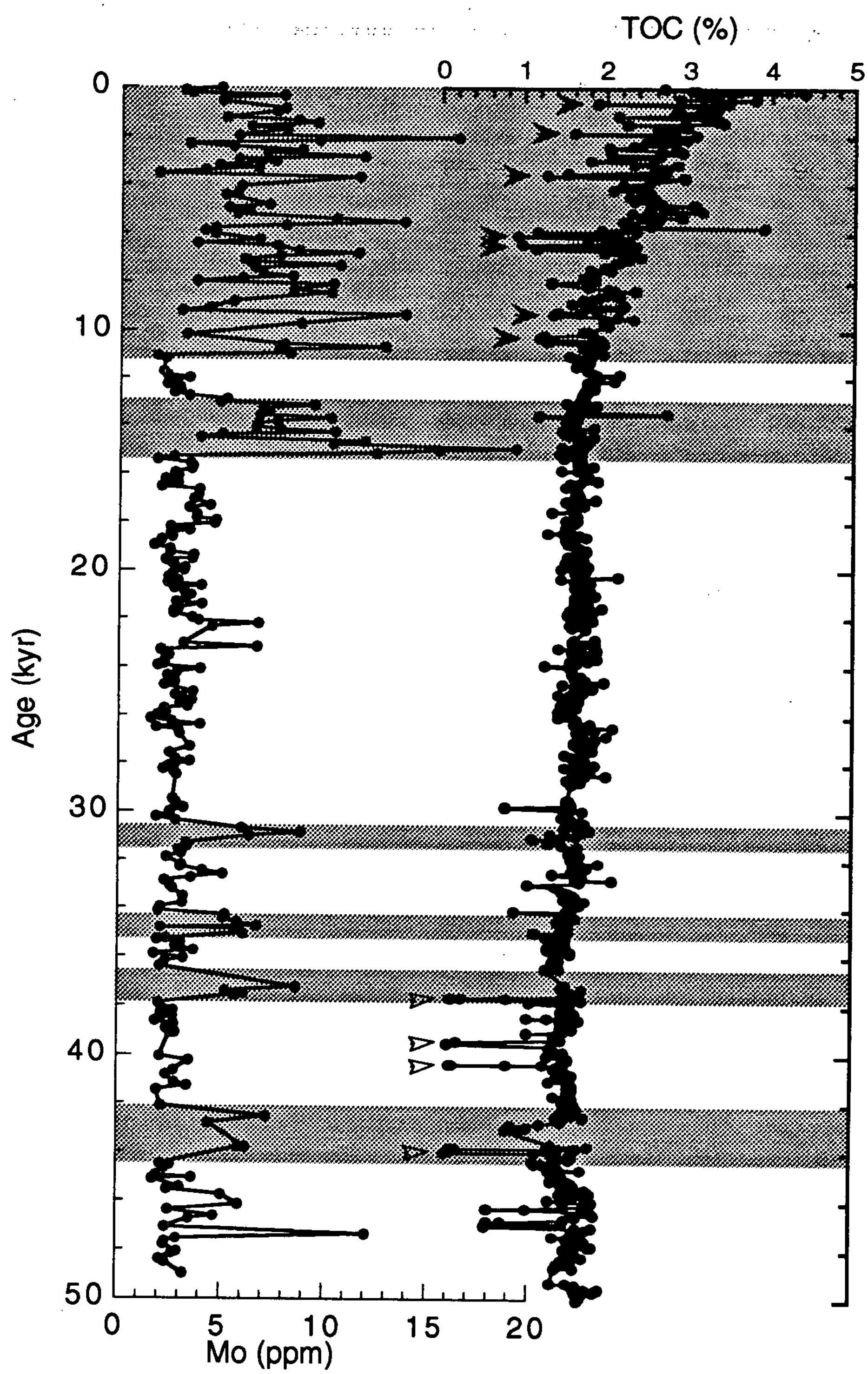

Figure 11. Downhole profiles of Mo (ppm) and % organic carbon in Hole 893A combined from Stein and Rack, 1995 and Gardner and Dartnell, 1995. Solid arrows indicate samples taken from terrestrial flood deposits labeled "grey beds". Open arrows indicate samples taken from sand layers. The shaded areas indicate sections with laminated sediments.

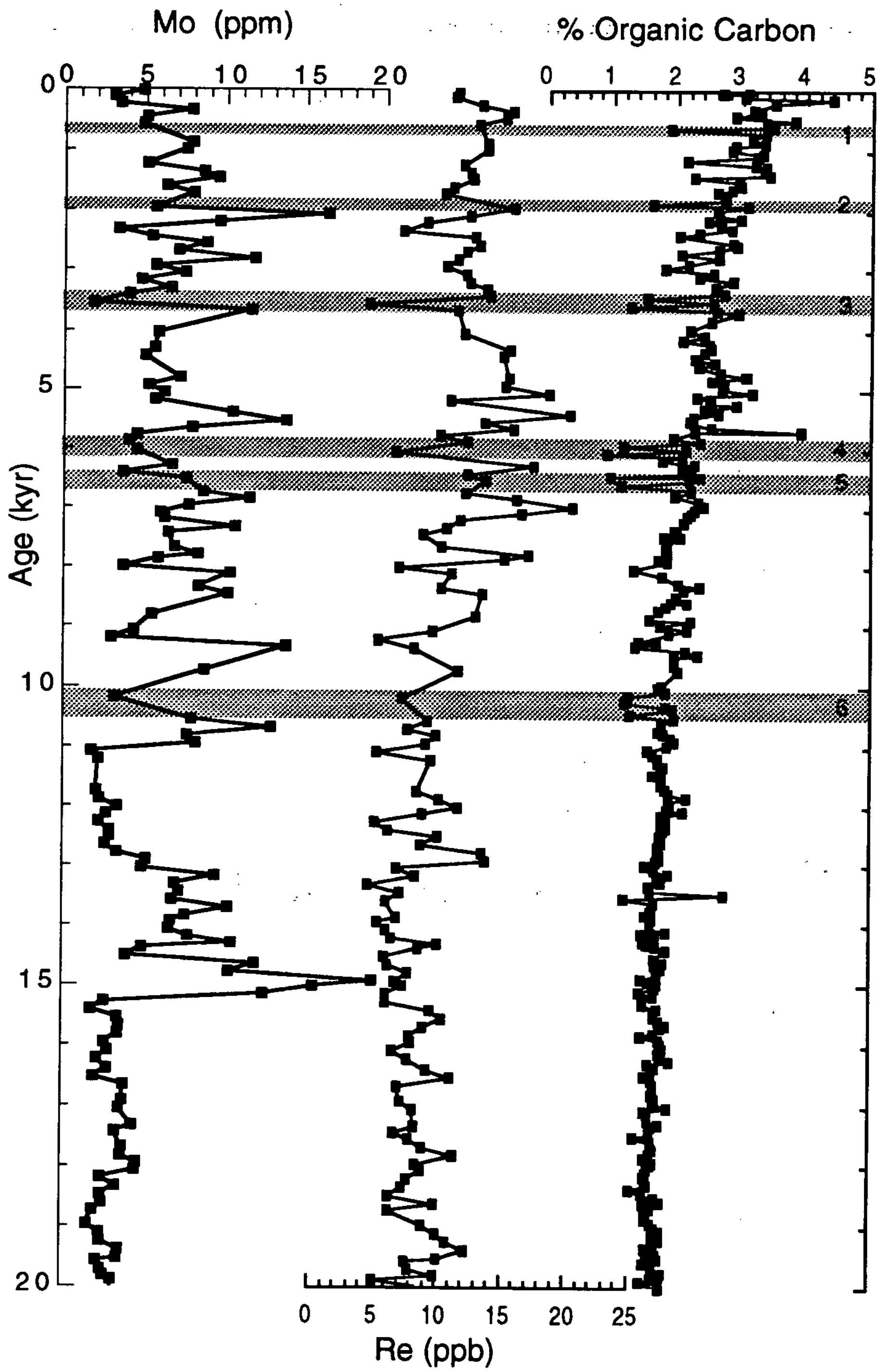

Figure 12. Downhole Mo (ppm) and Re (ppb) profiles compared to the Holocene grey beds deposits. Grey beds are indicated by the numbered, shaded areas.

bearing compounds (section 3.1.). Therefore, this decrease in Mo may reflect H_2S concentrations that fell below the threshold necessary for Mo precipitation. Re accumulation is not affected by the concentration of H_2S (section 3.2.), and within grey beds 1, 2, 5, and 6, Re concentrations do not decrease (Figure 12). The Mo and Re data together suggest a switch from anoxic to suboxic conditions during these episodes.

4.4. The Impact Of Local Productivity On The Oxygen Record

Santa Barbara Basin is situated within the California Current system, an area where seasonal, wind-driven upwelling replenishes the surface waters with the nutrients necessary for plankton growth, thereby fueling high surface productivity (Dean et al., 1998; Premuzic et al., 1982). The flux of organic carbon to the floor of Santa Barbara Basin is a crucial variable affecting the amount of oxygen present, both in the bottom waters and in the sediment. As organic material is degraded (respiration) oxygen is consumed and CO_2 and nutrients are re-released into the environment. If the "rain rate" of organic material is large enough, total consumption of oxygen can result in water column anoxia. Once the stock of oxygen is consumed, remineralization of organic material continues using NO_3^- as the oxidant. Much of this remineralization occurs in the surface and intermediate waters, recycling nutrients and carbon before organic matter reaches the sediments.

Only a small portion (≤4%) of the overlying production of organic matter is transported to the sediment-water interface (Muller et al., 1979) where only a fraction again is preserved. The factors controlling the preservation of organic carbon over geologic time are difficult to determine. In open ocean settings, oxygen may penetrate metres into the sediment. The combination of low sedimentation rate, low organic content and continual bioturbation, allows the nearly complete degradation of organic carbon in abyssal areas within 1000 years (Emerson et al., 1988). However, in continental margin settings, beneath upwelling zones, the flux of organic carbon to the sediment can be high enough to significantly affect the sedimentary and bottom water oxygen concentrations. Preservation of organic carbon is not necessarily a consequence of the resulting low oxygen conditions (Ganeshram, 1996; Thunell et al., 2000). The rate at which the degradation of organic matter occurs under oxic and anoxic conditions in such settings is essentially the same (Emerson and Hedges, 1988). As well, enhanced preservation of organic carbon is not systematically seen in sediments within modern oxygen minima (Calvert et al., 1992; Pedersen et al., 1992; Thunell et al., 2000).

The enhanced "rain rate" of particulate organic carbon in upwelling regions may itself lead to enhanced preservation in these areas: the larger the flux of carbon to the sediment, the more carbon is preserved (Muller and Suess, 1979). If the flux is high enough and burial occurs quickly, organic material may be removed from the surface sediments and the zone of active diagenesis before it is degraded. Conversely, once the entire pool of oxidants is completely consumed, preservation of organic matter is enhanced (Pedersen et al., 1992). Consequently, it is the balance between the flux of particulate organic carbon and the consumption of oxidants, including oxygen replenished through bioturbation and diffusion, that dictates the proportion of the organic flux that is preserved in the sediment (Emerson and Hedges, 1988). This balance changes with time as environmental conditions vary.

Today, in Santa Barbara Basin, degradation continues within the sediments, consuming all available oxygen and proceeding with less energetic but still efficient oxidizers: NO_3^-, MnO_2, Fe_2O_3 and SO_4^{2-}, respectively. This results in the modern basin having anoxic sediments and seasonally anoxic bottom waters (Reimers et al., 1990). Multiple organic proxies can be used to determine the effects of sedimentary biological oxygen demand on the oxygen content of the deep basin over the past 50,000 years. For this purpose sedimentary % organic carbon, %$CaCO_3$ and nitrogen isotope ratios, as well as Ag/Cd ratios, can provide insight into the impact of the local organic settling flux on the historic oxygen content of Santa Barbara Basin.

4.4.1. % Organic Carbon

Two groups previously measured the % organic carbon and % CaCO3 for Site 893A: Ruediger Stein and Frank Rack; and James Gardner and Peter Dartnell. The results were published separately in the ODP Leg 146 Scientific Results (Part 2). In this thesis, the % organic carbon measurements from both papers have been combined to give a sampling resolution of 30-125 years (Figure 11). Total organic carbon (TOC) concentrations throughout this core vary from % 1 - % 4, with values increasing upcore into the Holocene. This trend is consistent with higher organic carbon percentages occurring in the last interglacial (Stein and Rack, 1995). The sources of sedimentary organic carbon include surface plankton, macroalgae, bacterial biomass, terrigenous biomass and re-deposited fossil organic carbon (Stein and Rack, 1995). Marine sources appear to dominate the sediment record in SBB except within the intermittent flood and turbidite deposits (Stein and Rack, 1995). Periodic minima in %TOC are seen in the Holocene grey flood/turbidity deposits and in sandy turbidites between 37-44 ka. with total organic carbon contents dropping as low as 0.9 and 0.1%, respectively.

During the Holocene, the terrigenous deposits (labeled "grey beds" from the visible difference from the more common olive-green organic-rich sediments (Hulsemann et al., 1961)) have low concentrations of molybdenum (Figure 12). These intermittent deposits are well sorted with an average grain size of 2 μm and are associated with riverine discharge (Fleischer, 1972). The existence of a grey bed was reported to have "exerted no influence on the sequence of sedimentation" (Hulsemann and Emery, 1961). Thus they occur above both laminated and massive sediment sections and do not appear to affect the general oxygen content of the sediment.

The low molybdenum concentrations associated with these terrigenous deposits may be a result of an injection of oxygen associated with the transport of aerobic sediments from above the sill into the basin. The large peaks of Mo below beds 2, 3 and 6 (Figure 12) suggest potential remobilization of Mo once short lived oxic conditions were succeeded by reducing conditions. However, consideration of the Re data does not indicate an influx of oxygen. In addition, there is no evidence for burndown events in the Re data because no large Re remobilization peaks are associated with increases in Mo.

Finally, the lower Re concentrations associated with beds 3 and 4 may be a result of the "instantaneous" deposits increasing the depth of the redox boundary. The rate of diffusion, and therefore Re accumulation, is affected by the intensity of the chemical gradient between the water column and the sediments. The increase in sedimentation during these deposits may have changed the intensity of the gradient, resulting in lower accumulation of both Re and Mo.

Hence, the diminished concentration of authigenic Mo in the Holocene grey deposits can be explained by the combination of a) a small oxygen demand due to a low organic content during these episodes, and b) a deepening of the redox boundary as a result of the deposit. A more complete understanding of the Mo and Re responses to the grey bed deposits requires trace metal data with a higher resolution than is described here.

Large variations of the molybdenum concentrations prior to the Holocene do not appear to coincide with fluctuations in % TOC (Figure 11). During the Bølling-Allerød (13-15.5 ka), no increase in the % TOC is seen. As well, other "anoxic events" signified by both laminated sediments and increased Mo concentrations do not appear to be associated with increases in % organic carbon.

4.4.2. Nitrogen isotopes

The $\delta^{15}N$ data used in this study were supplied by Ed Emmer and Robert Thunell (Emmer et al., 2000). However, the chronology has been updated from the original ODP timescale to conform to that of Behl and Kennett, 1996. The comparison of $\delta^{15}N$ and the bioturbation index (Figure 3 from (Emmer and Thunell, 2000) has been altered as a result of the new timescale. Agreement between these two parameters in the 50,000 year record appears better than was reported by Emmer and Thunell (1999).

Variations in the standardized nitrogen isotope ratio:

$$\delta^{15}N\ (‰) = \frac{(^{15}N/^{14}N_{\,sample} - {}^{15}N/^{14}N_{\,atm.\,N2})}{(^{15}N/^{14}N_{\,atm.\,N2})} \times 1000,$$

have been interpreted as a reflection of nutrient availability and utilization (Altabet et al., 1994; Farrell et al., 1995) or denitrification in the water column (Emmer and Thunell, 2000; Ganeshram et al., 1998). Plankton fractionate the two nitrogen isotopes during growth and preferentially assimilate the light isotope, ^{14}N (Altabet, 2001). In the open ocean deep waters, the $\delta^{15}N$ of dissolved NO_3^- is 5-6 ‰. But, in waters where the flux of organic rich material is high and/or the oxygen content is very low, NO_3^- is consumed as the oxidant during degradation of organic matter. Bacteria mediate this remineralization of organic matter, also fractionating these two nitrogen isotopes, preferentially removing the "light" isotope, leaving residual nitrate that is enriched in ^{15}N. In oxygen-deplete upwelling areas, the heavy $\delta^{15}N$ signal caused by denitrification in the intermediate waters may be brought to the surface. If the surface waters are NO_3^- limited and total utilization of this nutrient occurs, the $\delta^{15}N$ of the sediments will reflect the $\delta^{15}N$ of the surface waters (Altabet, 2001).

The relationship between the $\delta^{15}NO_3^-$ of the water column and the sedimentary record has been established in a number of studies (Altabet et al., 1999; Ganeshram and Pedersen, 1998; Pride et al., 1999). Sediments below the oxygen depleted waters of the Eastern Tropical North Pacific (ENTP) have $\delta^{15}N$

values of 9-10‰, reflecting the intense denitrification occurring in this area (Ganeshram et al., 1995), Within the California Current system, Monterey Bay and San Pedro Basin were found to have modern sedimentary $\delta^{15}N$ values of 7.1‰ and 8.5‰, respectively. The sub-euphotic zone $\delta^{15}NO_3^-$ was 8.0 ‰ for both sites (Altabet et al., 1999). The northward flow of the California Undercurrent supplies the California margin with isotopically heavy NO_3^- from the ETNP, which is then mixed and diluted as it travels from the source (Kienast et al., submitted). The slightly lighter $\delta^{15}N$ values from San Pedro and Monterey Bays are a result of their distance from the ETNP and water column mixing (Altabet et al., 1999).

The $\delta^{15}N$ of Santa Barbara basin sediments during the last glacial period ranged from 5-8‰, whereas heavier values of 8 -9.5‰ are typical of the Holocene at Site 893 (Figure 13). Emmer and Thunell (1999) concluded that there was no correlation between $\delta^{15}N$ values and either opal MAR or organic carbon MAR in the SBB deposits. The SBB $\delta^{15}N$ signal was interpreted primarily as being affected by basin ventilation changes, not by local relative nutrient utilization or productivity fluctuations. But, the heavy $\delta^{15}N$ values are generally found in intervals with high Mo concentrations (Figure 13). Previous studies show no difference in the preservation of the nitrogen isotope record under oxic or anoxic sedimentary conditions (Pride et al., 1999). Variations in the sedimentary $\delta^{15}N$ records therefore can be interpreted as being independent of the oxygen content of the bottom waters and sediments, and more reflective of processes in the overlying surface and intermediate waters.

Previous work has suggested that the heavy $\delta^{15}N$ in the sediments of the region may be an imported signal of denitrification that takes place in the OMZ of the

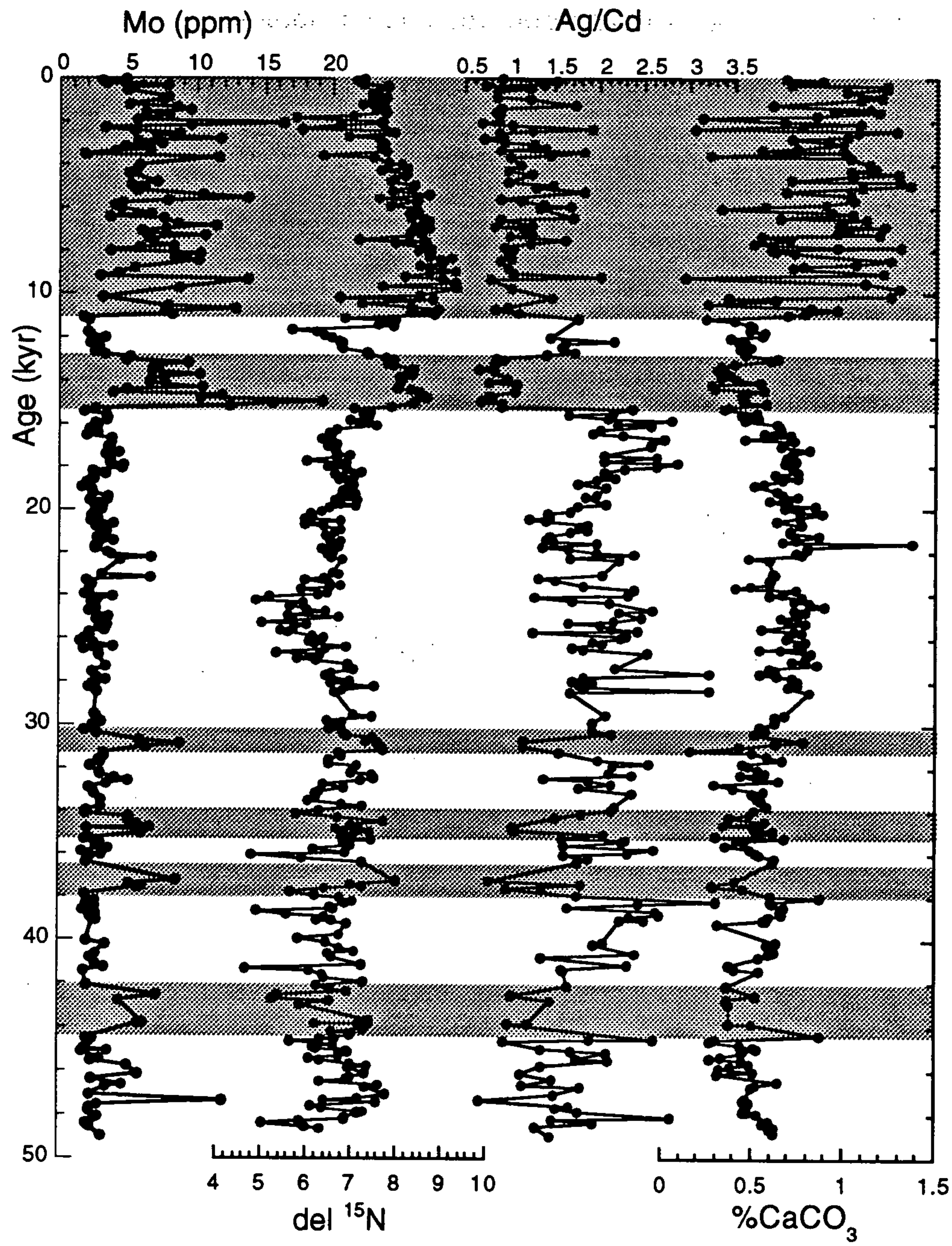

Figure 13. Mo (ppm) concentrations compared to proxies of primary productivity. $\delta^{15}N$ measurements are from Emmer and Thunell, 1999. Heavy $\delta^{15}N$ values suggest water column denitrification. The Ag/Cd ratio is thought to indicate the proportional input from silica producing organisms (Ag) and both silica and carbonate producing organisms (Cd). $\%CaCO_3$ is representative of the carbonate flux to the basin floor. The shaded areas indicate sections with laminated sediments.

eastern tropical North Pacific where waters are oxygen depleted (Emmer and Thunell, 2000). The transport of this heavy $\delta^{15}N$ into Santa Barbara Basin implies the importation of suboxic waters as well. Low $\delta^{15}N$ values in SBB (5-6 ‰) reflecting the open ocean value are found where there is no accumulation of authigenic Mo in the sediment. Such $\delta^{15}N$ values suggest relatively oxic waters entered the basin at these times when the organic matter flux to the basin floor alone did not cause accumulation of H_2S to the extent that allows the sequestration of Mo. However the high organic flux at this site during the Holocene, in addition to a reduction in water column oxygen concentrations, reflected in the heavy $\delta^{15}N$, does impact the sediments causing severe oxidant demand, increased pore water H_2S concentrations and Mo enrichment.

4.4.3. Trace Metals

The significant problems associated with variable preservation of biogenic opal and carbonate in various depositional environments have spurred researchers to look for alternative proxies of paleoproductivity. Trace metals are being explored for this role in the expectation that they may reveal previously hidden information (Friedl et al., submitted). As noted earlier, silver (Ag) is associated with the structural components of diatom frustules (Fisher and Wente, 1993; Lee and Fisher, 1994) and is sequestered in marine sediments as insoluble Ag_2S in the presence of H_2S (Section 3.5.). Similarly, Cd precipitates as CdS when trace amounts of sulphide are detectable in the pore waters. However, Cd is incorporated into the tissues of both silica secreting (diatoms), and carbonate producing (coccolithophores) phytoplankton. Therefore, authigenic sedimentary Ag may be indicative of the supply of silver to the sediment-water interface by the settling diatom shells while the Cd record in the sediments might be affected by both diatom and coccolithophorid vectoring of Cd to the seafloor (Friedl et al., submitted).

The effectiveness of these trace metals as paleoproductivity proxies depends on other factors that may confuse the sedimentary signal. Sulphide is necessary for both these elements to be enriched in the sediments. Changes in productivity will not be recorded by these two metals if the sediments are not reasonably reducing. As well, variations in the redox chemistry of the sediment can cause remobilization and/or oxidative burndown of both Ag and Cd, removing the biological signal after deposition. In order to interpret the paleoproductivity record provided by Ag and Cd, variations in the oxygen content of the sediments and bottom waters must be known.

In Figure 13 molybdenum is used as an indicator of anoxic sediments. As discussed above, the Holocene sediments are typically anaerobic. Though bioturbation occurred prior to 15 ka, the sedimentary redox boundary remained shallow throughout the time-span represented by the sampled section (section 4.3.3). The Ag/Cd ratio potentially indicates the proportional input to the sediments from diatoms and coccolithophores. Friedl et al (submitted), found that the ratio of Ag/Cd increased in diatomaceous oozes from the Gulf of Alaska, reflecting the larger flux of bound Ag with diatom frustules. Similar observations have been made very recently in ODP Hole 1017E raised from the slope west-northwest of the SBB (I. Hendy, pers. comm.). In SBB, both Cd and Ag are highly enriched in the Holocene sediments (Figure 6a). Prior to 12 ka the Ag concentrations, though variable, drop to

~120 ppb, only slightly above the background concentration expected in oxic sediment. The Cd profile similarly drops to background levels but does increase significantly during the Bølling-Ållerød (13-15.5 kya) (Figure 6a).

The requirement for anoxic sediments, or the presence of H_2S, essentially restricts application of the Ag/Cd proxy prior to the Holocene, with the exception of the Bølling-Ållerød. Large fluctuations are seen before 15 ka reflecting the noise in the Ag profile and the lack of both Ag and Cd retention in the deposits due to the absence of H_2S. Though the preservation of biogenic opal is poor in the pre-Holocene bioturbated sediments, opal Mass Accumulation Rate (MAR) values calculated for this site have been interpreted as indicating a high diatom flux between 30-46 kya that decreased during the LGM, 24-26 kya (Hemphill-Haley and Fourtanier, 1995). This decline is not reflected in the Ag/Cd ratio, for potential increases in the individual elements are not preserved in the suboxic sediments that dominate throughout that period.

Within the past 10,000 years, however, sediments in SBB have been reducing enough to sequester both Ag and Cd consistently. Therefore, the variation in the Ag/Cd seen throughout the Holocene probably reflects the changing proportion of diatoms and calcareous phytoplankton. In the Holocene, there is a dramatic increase in the carbonate and organic contents of the sediments, reflecting delivery of proportionally more Cd to the sediments. Cadmium concentrations averaged 0.77 ppm during the last glacial interval, and increased to 1.85 ppm during the Holocene. Although biogenic opal is not well preserved in SBB, an increase in diatom production during the past 10,000 years is suggested by the increases in Ag concentrations from 125 to 175 ppb across this interval (Figure 6b).

The Bølling-Ållerød in the SBB is characterized by anoxic sediments (section 4.3). Although Cd is enriched in the deposits at this time, no corresponding increase in the Ag concentration is evident, nor in % $CaCO_3$ or in the % organic carbon. Therefore, it is postulated that there was no increase in the organic flux, neither diatoms nor coccoliths, to the sediment. During this interval the Ag/Cd ratio is probably reflecting the difference in the water column concentrations of Cd and Ag, with Cd being passively sequestered by the reducing sediments in the absence of a significant delivery system for Ag to the deep basin.

Although the Ag/Cd ratio may be an effective proxy in different environmental conditions, variations in redox intensity and periodic instantaneous depositional events at Site 893 overshadow the information that can be gleaned from variations in this ratio in SBB. However, individually, both Ag and Cd distributions are geochemically consistent with Holocene increases in productivity.

5. Regional and Local Implications

The California margin has been the focus of several studies, particularly with regards to evolution of the North Pacific climate and the development of the California Current system. In 1996 during Leg 167, the Ocean Drilling Program drilled 13 sites from northern Baja California to the southern border of Oregon, the objective being to understand the sensitivity of the northeastern Pacific to global climate fluctuations. Two of these sites will be used here in comparison with Hole 893A in the Santa Barbara Basin, to determine local and regional trends within the broader area. Hole 1017E, located just north of Santa Barbara Basin, 50 km west of the California coastline (34°32.099′N, 12°16.430′ W), comprised 25 m of sediment and was raised from a water depth of 955 m. A 10 m core (Hole 1019A) was recovered from Site 1019, near the border of California and Oregon (41°40.963′N, 124°55.979′W) from a water depth of 977 m, and will serve as the second comparative site.

Site 1017 lies in an area of modern coastal upwelling, and is situated within the present day oxygen minimum zone (Kennett et al., 2000). The sedimentation rate at this site averages 18 cm/ky and the accumulation reflects input of both large amounts of terrestrial material and a high flux of marine organic matter. Sediments throughout the core are bioturbated, and a continuous record of planktonic and benthic forams has been preserved. The chronology of this core is based on eight ^{14}C dates between 9,412 and 32,958 ka. Thirteen "unambiguous paleoclimatic events" identified in Hole 1017E were correlated with the SPECMAP, a standard deep-sea oxygen isotope chronology (Martinson et al., 1987), and provide the timescale between 59 and 130 ka. (Kennett et al., 2000). Linear interpolation between each pair of events was employed to provide a continuous age model of the entire core. T.F. Pedersen and I. Hendy supplied trace metal and nitrogen isotope ratio measurements for Site 1017.

The chronology of 1019A is based on radiocarbon dating of a single terrestrial organic matter sample from 40 cm depth (6,800 ^{14}C y B.P.) and ten benthic-planktonic foram pairs that ranged in ^{14}C age between 10,100 and 24,000 ky (Mix et al., 1999). Linear interpolation between the dated horizons has provided ages for the samples used in this study (Figure 14). Error analysis appears in Mix *et al.* (1999). Site 1019 was specifically located to monitor the wind driven position of the boundary between the subtropical and subpolar Pacific gyres. As well, by being situated at ~1000 m water depth this core has potentially recorded variations in the character of the intermediate water mass that has bathed this area over time.

Water flowing toward the equator in the eastern expression of the Pacific Subtropical gyre links these three sites. As well, variations in the intermediate water mass adjacent to the North American coastline may affect these sites collectively. Productivity has significantly influenced the existence of sediment laminations at the Site1019 to the north (Lyle et al., 2000). Within the Santa Barbara Basin, however, variations in the oxygen content of the bottom waters have been explained as a function of changing basin ventilation (Behl and Kennett, 1996; Emmer and Thunell, 2000; Hendy and Kennett, 2000; Kennett et al., 2000). In contrast, the relationship between anoxic bottom water and surface productivity at Site 1017 appears to be

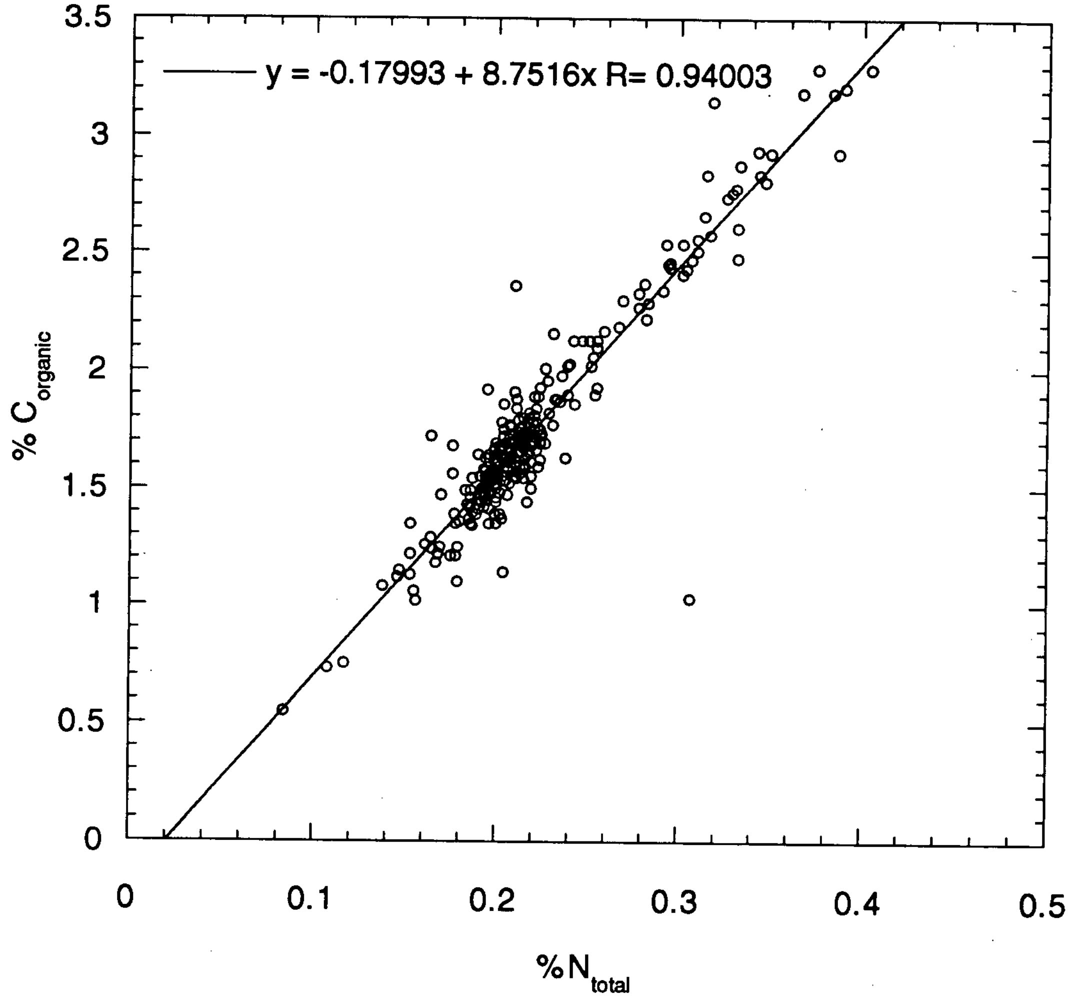

Figure 14. Age model for site 1019a. AMS dates are from Mix et al, 1999.

stronger during the Holocene than prior to the LGM (Irino and Pedersen, 2000) but is complicated by bottom currents and slope depositional processes (Tada et al., 2000). It is clear that the association between the organic flux and sedimentary oxygenation state is affected by the local setting. What is interesting however, is the interplay between the local and regional signals owing to variations in upwelling, nutrient utilization, source waters and basin isolation. Within a geographic region, such as the California margin, the strength of the current system connects sites with varying local identities. How then can local signals be differentiated from the regional signal?

5.1. Regional Trends

Identification of local and regional trends is accomplished here by using trace metal data from the three sites to indicate variations in the local oxygen content of the sediment pore waters along with $\delta^{15}N$, which shows water column variations in denitrification and nutrient utilization (Figure 15). There are obvious similarities in the larger trends of both the Mo and $\delta^{15}N$ records of all three locations. These can be distinguished despite the relatively poor age control of Hole 1017E during the very Late Pleistocene and Holocene. The Holocene is consistently a period of high productivity along the California margin. Although maximum values at individual sites may vary, the organic flux to the sediments overall during the last 10,000 years has been higher than during the last glacial (Gardner and Dartnell, 1995; Irino and Pedersen, 2000; Mix et al., 1999; Stein and Rack, 1995; Tada et al., 2000).

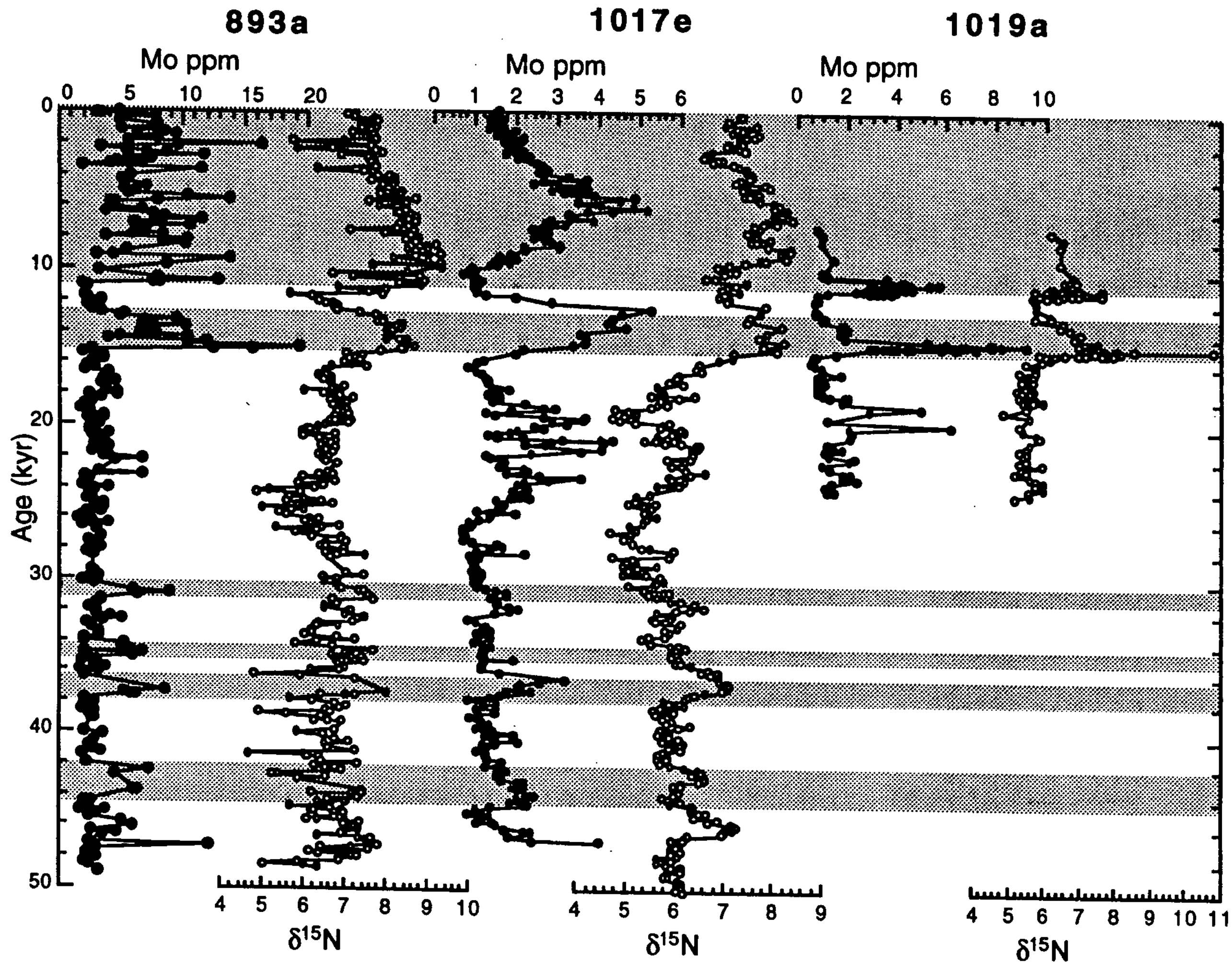

Figure 15. Mo (ppm) and $\delta^{15}N$ (‰) data from Santa Barbara Basin (893a), the nearby California margin (1017e), and the northern California margin (1019a). $\delta^{15}N$ data for 893a are from Emmer and Thunnell, 1999. Mo and $\delta^{15}N$ data from 1017e were supplied by T.F. Pedersen. The shaded areas indicate sections of laminated sediments from Site 893A and are extended for comparative purposes only.

Similarly, during the Holocene sedimentary anoxia and water column denitrification appear to be more intense, as elaborated below.

The extreme sedimentary anoxia of the Bølling (~14 -14.7 kya), indicated by high Mo concentrations is shared throughout the region, and is temporally associated with a heavy nitrogen isotope signal. During this period, nitrogen isotope values peak at approximately 8.4‰ at all sites. This suggests that either a change in the characteristics of the water-mass occurred in this region or that the local organic settling flux was consuming NO_3^- in the water column relative to supply at approximately the same rates at these locations. The northern California (1019) and the mid-coastal (1017) sites both have large peaks in the organic carbon flux associated with the anoxic sediments that were deposited at this time (Irino and Pedersen, 2000; Mix et al., 1999) implying enhanced export production and associated oxygen consumption in the underlying waters. However, no increase in production has been identified in Santa Barbara Basin during the Bølling.

Investigation of the $\delta^{15}N$ glacial and interglacial variations within the California Current system suggest the heavy $\delta^{15}N$ values generated in the denitrifying waters of the Eastern Tropical North Pacific during warm periods (Ganeshram et al., 2000), are transferred as far north as the Oregon coast (Kienast et al., submitted). The northward flow of the California Undercurrent, at a depth of 100-300 m, facilitates this propagation.

Heavy $\delta^{15}N$ values have also been suggested as an upwelling signal owing to increased productivity intensifying the oxygen demand of the subsurface waters (Altabet et al., 1999). The resulting denitrification signal is welled up and incorporated into phytoplankton, which is then relayed to the sediments where it is preserved. Within the California Current System, although apparent synchronicity exists in the $\delta^{15}N$ signal, productivity increases are not consistent (Dean and Gardner, 1998; Gardner et al., 1997; Kienast et al., submitted). Therefore the glacial interglacial variations in $\delta^{15}N$ values appear to be influenced more distinctly by regional hydrography than local productivity.

The northern California (1019) and the mid-coastal (1017) sites both have large peaks in the organic carbon flux associated with the anoxic sediments that were deposited at this time (Irino and Pedersen, 2000; Mix et al., 1999). However, during the Bølling, an increase in %TOC within Santa Barbara basin has not been identified. There is however a discernible response of planktonic foraminifera, namely an increase in *Globigerina bulloides*, representative of upwelling conditions, during the Ållerød as well as during previous interstadials (Hendy and Kennett, 2000).

The sedimentary Mo concentrations are not as areally consistent. Maxima off southern California range from 20 ppm in the SBB to 5.5 ppm on the nearby shelf, while the northern California site has a corresponding Mo maximum of 9 ppm. If the local settling fluxes and bottom water oxygen concentrations were equivalent, the effect on the oxygen content at these various sites must have been different. The varying sedimentation rates and the depths of the specific cores may explain these differences. Both 1019A and 1017E are approximately 400 m deeper than 893A and have lower sedimentation rates.

Two additional sites north of 1017 have been studied and Mo concentrations during the Bølling of 6 and 11 ppm at 760 m and 803 m water depth, respectively, have been reported (Zheng et al., 2000b). Thus, within the depth range where modern intermediate water impacts the shelf, roughly equal increases in Mo concentrations occurred throughout this region from 14-14.7 ka. The SBB site, however, is removed from the adjacent intermediate water mass by the presence of two sills. Today, water enters the basin at 475 m, a depth that decreased to approximately 395 m during the LGM (Hendy and Kennett, 2000).

In addition, the isolation of SBB contributes to the intensity of the local oxygen demand by limiting contact with the coastal currents as deep basin waters are only replenished periodically (Reimers et al., 1990). It has been proposed that the regional sedimentary anoxia of the Bølling is a result of poorly ventilated NPIW or a northern extension of oxygen depleted waters from the ETNP reaching the California margin and entering Santa Barbara Basin (Behl and Kennett, 1996; Hendy et al., 1999; Hendy and Kennett, 2000; Kennett and Ingram, 1995). If this is the case, the effects on the bottom waters of SBB, without a preserved signal of local increase in productivity, were far more severe than on the nearby coastal regions that did experience an increased organic flux.

In contrast to the Bølling, it appears that the Younger-Dryas (YD) is defined on the California margin as a period of less severe bottom water oxygen demand and negligible water column denitrification. Again, sites 1019 and 1017 experienced a corresponding change in productivity – the organic flux to the sea floor appears to have decreased (Irino and Pedersen, 2000; Mix et al., 1999) – but the SBB again does not conform to this pattern (Gardner and Dartnell, 1995; Stein and Rack, 1995). Mo decreases dramatically all three sites, however, although concentrations fall most in the SBB. This difference can be explained as a consequence of the geochemical behaviour of Mo (section 3.1). The requirement of a threshold level of H_2S for the precipitation of authigenic Mo dictates that although bottom waters may be suboxic, if sulphide is too low Mo will not be enriched in the sediment. It appears that in SBB during the YD, though not associated with a drop in %TOC, H_2S was not maintained at high enough concentrations in the pore waters to facilitate the sequestering of Mo.

Within SBB, prior to 15 ka, the Mo concentrations drop to background levels and $\delta^{15}N$ reverts to lighter values more characteristic of areas where denitrification is absent. Periodic oxygen-depletion events are mirrored by increases in $\delta^{15}N$ but these events are relatively short-lived and record conditions less severe than those in the Holocene.

5.2. Local Trends

During the Holocene, both the trace metal and $\delta^{15}N$ measurements from the Santa Barbara Basin reflect the episodic flood deposits identified as "grey beds" (section 4.4). These organic-poor terrestrial deposits are defined in the sedimentary record by low Mo concentrations and light $\delta^{15}N$ values. These local runoff events are limited to the SSB and are not reflected in the sediments of the nearby slope Site 1017E or 1019A from the northern California margin. Light $\delta^{15}N$ values of the LGM and glacial termination are not matched in the Mo profile. The general suboxic, but not anoxic, conditions prior to 10,000 ya, excluding the Bølling-Ållerød, do not allow the sequestration of molybdenum. Consequently the Mo record indicates low pore water H_2S concentrations during this period.

The absence of variation in the % TOC record from Santa Barbara Basin prior to the Holocene sets this site apart from those on the open shelf. Within SBB, the gradual increase in this productivity signal during the Holocene can be used to explain the presence of enriched sedimentary Mo. As the H_2S threshold allowing the sequestration of Mo imparts a "stepwise" control on the enrichment of this trace metal, a small increase in organic flux can trigger authigenic Mo formation. The lack of % organic carbon fluctuation in concert with the Mo signal prior to the Holocene suggests that the concentration of sedimentary H_2S is being affected by an imported low-oxygen signal.

6. Summary and Conclusions

The research conducted for this thesis was inspired by the desire to differentiate between the impacts of local variations in the settling flux of organic carbon and the regional variations in intermediate water ventilation on the oxygenation history of the Santa Barbara Basin. The three questions designed to direct the focus of this work are addressed below.

6.1. Have changes in the vertical flux of organic matter affect the bottom water oxygen content of SBB?

Measurements of %TOC within the Santa Barbara Basin sediments indicate a doubling of organic carbon flux to the basin floor in the Holocene relative to the last glacial interval. Laminated Holocene deposits from the deep basin exhibit a dramatic enrichment in Mo and Cd relative to older sediments, suggesting that the deposits have been severely anoxic during this same Recent period. In addition, periodic terrestrial runoff events inject low organic, oxic sediments to the basin floor, which are reflected as intervals of temporary relief from anoxia.

Therefore, there is evidence that the flux of organic carbon does indeed impact the oxygenation history of Santa Barbara Basin with the anoxic sediments of the Holocene being maintained by high primary production and the ensuing biological oxygen demand in the bottom waters and sediments.

6.2. Can changes in the ventilation of SBB be differentiated from changes in the vertical organic flux?

The oxygenation history of Santa Barbara Basin was determined through multiple proxy analysis. Major and minor elements were used in conjunction with the redox-sensitive trace metals Mo, Cd, Re, Ag and U to track variations in mineralogy and grain size with time and to identify changes from oxic through suboxic to anoxic sedimentary conditions. Organic proxies were investigated to determine the impact from overlying production and nitrogen isotope ratios were used to infer the intensity of denitrification indicating low oxygen concentrations in the source water region. In combination, these various proxies allow the impact of local organic flux upon the sediment to be differentiated from that of basin ventilation.

A comparison of the Santa Barbara Basin sediments with those from ODP sites 1017 and 1019 provides further evidence of the interplay between local and regional signals. SBB appears to be anomalous in this region, in that it lacks an indication of increased productivity during the Bølling-Ållerød. Similarly, though decreases in productivity are identified in the %TOC measurements from the nearby shelf and off Northern California during the Younger-Dryas, the sedimentary organic carbon concentrations remain constant in SBB throughout this period. Despite the low organic flux, SBB sediments still display similar trends to the additional sites: anoxic sediments are seen during the Ållerød and oxic-suboxic sediments during the Younger-Dryas. It has been noted that the %TOC from Site 1017 is affected by changes in grain size that have been attributed to variable bottom currents and slope depositional processes (Irino and Pedersen, 2000). Similar processes may be affecting the organic content at Site 1019, thus accentuating the variations in the sedimentary productivity signal at these coastal sites (I. Hendy, pers. Comm).

The similarity of the nitrogen isotope signal among sites suggests that the water column oxygen content of this area is impacted by a combination of denitrification in the ETNP and temporal variations in the strength of the California Undercurrent. The supply of poorly oxygenated water to the California Margin appears to impact the redox environment of the sediment at all three sites simultaneously. This is demonstrated by increases in Mo and Cd concentrations in conjunction with laminated sediments during the Holocene, the Ållerød, and in the "anoxic events" identified by Behl and Kennett (1996).

Periods of imported low oxygen water, identified by heavy $\delta^{15}N$, in SBB appear to be concurrent with a regional trend of low oxygen water bathing the California margin. During the last glacial interval these episodes may be associated with increased remote primary production but do not appear to be driven by local production. However, local productivity increases throughout the Holocene impact each site differently revealing the "signature" of local organic flux on the sediments of the individual sites. By analogy, local variations may have led to inter-site differences during the last glacial stage as they do today.

6.3. Can the organic flux to the sediment be used to explain the oxygenation history of SBB?

Santa Barbara Basin is a highly productive site within a region of intense seasonal upwelling. This basin is partially isolated from the California Current system by two sills that restrict free water flow to the deep sediments. Within the basin, measurements of sedimentary organic carbon content over the last 50,000 years indicate a gradual but steady increase from 1 % to 4 %. Today the deep basin contains anoxic sediments enriched in Mo, Cd, Re, Ag and U. Trace metal trends through time show variations in the concentrations of these elements, indicating that transitions from anoxic to suboxic conditions have occurred in the past. Trace metal enrichments correspond to periods of laminated sediments previously identified by Behl and Kennett (1996).

Although the high productivity in SBB today is undoubtedly increasing the biological oxygen demand and therefore affecting the oxygen content of the modern sediments, there is little evidence that anoxic episodes prior to the Holocene were triggered by increases in productivity in the SBB. Heavy $\delta^{15}N$ values are also recorded in the sediments during anoxic excursions, suggesting that the intrusion of poorly oxygenated waters from the ETNP onto the California shelf may have been primarily responsible for the periods of anoxia evident in the SBB sediments during the last glacial stage.

References

Adams, N.W.H. and Kramer, J.R., 1998. Reactivity of Ag^+ ion with thiol ligands in the presence of iron sulfide. Environmental Toxicology and Chemistry, 17(4): 625-629.

Adelson, J.M., Helz, G.R. and Miller, C.V., 2001. Reconstructing the rise of coastal anoxia; molybdenum in Chesapeake Bay sediments. Geochimica et Cosmochimica Acta, 65(2): 237-252.

Altabet, M., 2001. Nitrogen isotopic evidence for micronutrient control of fractional NO3- utilization in the equatorial Pacific. Limnology and Oceanography, 46(2): 368-380.

Altabet, M. et al., 1999. The nitrogen isotope biogeochemistry of sinking particles from the margin of the Eastern North Pacific. Deep-Sea Research1, 46(4): 655-679.

Altabet, M.A. and Francois, R., 1994. Sedimentary nitrogen isotopic ratio as a recorder for surface ocean nitrate utilization. Global Biogeochemical cycles, 8(1): 103-116.

Anderson, R.F., Fleisher, M.Q. and LeHuray, A.P., 1989. Concentration, oxidation state and particle flux of uranium in the Black Sea. Geochimica et Cosmochimica Acta, 53: 2215-2224.

Andren, A.W. and Armstrong, D.E., 1999. The environmental chemistry and toxicology of silver (editorial). Environmental Toxicology and Chemistry, 18(1): 1-2.

Archer, D., Lyle, M., Rodgers, K. and Froelich, P., 1993. What controls opal preservation in the tropical deep-sea sediments. Paleoceanography, 8(1): 7-21.

Beary, E.S. and Paulsen, P.J., 1993. Selective application of chemical separations to isotope dilution inductively coupled plasma spectrometric analyses of standard reference materials. Analytical Chemistry, 65: 1602-1608.

Behl, R.J., 1995. Sedimentary facies and sedimentation of the late Quaternary Santa Barbara Basin, site 893. In: J.P. Kennett, J.G. Baldauf and M. Lyle (Editors), Proceedings of the Ocean Drilling Program, Scientific Results.

Behl, R.J. and Kennett, J.P., 1996. Brief interstadial events in the Santa Barbara basin, NE Pacific, during the past 60 kyr. Nature, 379: 243-246.

Berger, W.H. and Soutar, A., 1975. Preservation of planktonic shells in an anaerobic basin off California. Geological Society of America Bulletin, 81: 275-282.

Berry, R.A., Cantwell, M.G., Edwards, P.A., Serbst, J.R. and Hansen, D.J., 1999. Predicting toxicity of sediments spiked with silver. Environmental Toxicology and Chemistry, 18(1): 40-48.

Bishop, J.K.B., 1988. The barite-opal-organic carbon association in oceanic particulate matter. Nature, 332: 341-343.

Boyle, E.A., 1988. Cadmium: Chemical Tracer of deepwater paleoceanography. Paleoceanography, 3(4): 471-489.

Brodie, I. and Kemp, A.E.S., 1994. Variations in biogenic and detrital fluxes and formation of laminae in late Quaternary sediments from the Peruvian coastal upwelling zone. Marine Geology, 116: 385-398.

Brumsack, H.J. and Geiskes, J.M., 1983. Interstitial water trace element chemistry of laminated sediments from the Gulf of California, Mexico. Marine Chemistry, 14: 89-106.

Burgess, B.K., 1990. The iron molybdenum cofactor of nitrogenase. Chemical Reviews, 90(8): 1377-1406.

Calvert, S.E., Bustin, R.M. and Pedersen, T.F., 1992. Lack of evidence for enhanced preservation of sedimentary organic matter in the oxygen minimum of the Gulf of California. Geology, 20(8): 757-760.

Calvert, S.E., Cousens, B.L. and Soon, M.Y.S., 1985. An X-ray fluorescence spectrometric method for the determination of major and minor elements in ferromanganese nodules. Chemical Geology, 51: 9-18.

Calvert, S.E. and Fontugne, M.R., 2001. On the late Pleistocene-Holocene sapropel record of climatic and oceanographic variability in the eastern Mediterranean. Paleoceanography, 16(1): 78-94.

Calvert, S.E. and Pedersen, T.F., 1993. Geochemistry of recent oxic and anoxic marine sediments: Implication for the geological record. Marine Geology, 113: 67-88.

Calvert, S.E. and Pedersen, T.F., 1996. Sedimentary geochemistry of manganese: Implications for the environment of formation of Manganiferous Black Shales. Economic Geology, 91(1): 36-47.

Cannariato, K.G. and Kennett, J.P., 1999a. Climatically related millennial-scale fluctuations in strength of the California margin oxygen-minimum zone during the past 60k.y. Geology, 27(11): 975-978.

Cannariato, K.G., Kennett, J.P. and Behl, R.J., 1999b. Biotic response to late Quaternary rapid climate switches in Santa Barbara Basin: Ecological and evolutionary implications. Geology, 27(1): 63-66.

Cochran, J.K., Carey, A.E., Sholkovitz, E.R. and Suprenant, L.D., 1986. The geochemistry of uranium and thorium in coastal sediments and sediment pore waters. Geochimica Cosmochimica Acta, 50: 663-680.

Collier, R.W., 1985. Molybdenum in the Northeast Pacific Ocean. Limnology and Oceanography, 30(6): 1341-1354.

Colodner, D., Edmond, J. and Boyle, E., 1995. Rhenium in the Black Sea: Comparison with molybdenum and uranium. Earth and Planetary Science Letters, 131: 1-15.

Colodner, D. et al., 1993. The geochemical cycle of rhenium: a reconnaissance. Earth and Planetary Science Letters, 117: 205-221.

Colodner, D.C., Boyle, E.A., Edmond, J.M. and Thomson, J., 1992. Post-depositional mobility of platinum, iridium and rhenium in marine sediments. Nature, 358: 402-404.

Crusius, J., Calvert, S.E., Pedersen, T.F. and Sage, D., 1996. Rhenium and molybdenum enrichments in sediments as indicators of oxic, suboxic and sulphidic conditions of deposition. Earth and Planetary Science Letters, 145: 65-78.

Crusius, J. and Thomson, J., 2000. Comparative behavior of authigenic Re, U, and Mo during reoxidation and subsequent long-term burial in marine sediments. Geochimica et Cosmochimica Acta, 64(13): 2233-2242.

Dean, W., Gardner, J.V. and Piper, D.Z., 1997. Inorganic geochemical indicators of glacial interglacial changes in productivity and anoxia on the California continental margin. Geochimica Cosmochimica Acta, 61(21): 4507-4518.

Dean, W.E. and Gardner, J.V., 1998. Pleistocene to Holocene contrasts in organic matter production and preservation on the California continental margin. Geological Society of America Bulletin, 110(7): 888-899.

Dymond, J. and Collier, R., 1996. Particulate barium fluxes and their relationships to biological productivity. Deep-Sea Research II, 43(4-6): 1283-1308.

Dymond, J., Suess, E. and Lyle, M., 1992. Barium in deep-sea sediment: A geochemical proxy for paleoproductivity. Paleoceanography, 7(2): 163-181.

Emerson, S. and Hedges, J.I., 1988. Processes controlling the organic carbon content of open ocean sediments. Paleoceanography, 3(5): 621-634.

Emmer, E. and Thunell, R., 2000. Nitrogen isotope variations in the Santa Barbara Basin during the last 50,000 years: Implications for Pacific intermediate water ventilation. Paleoceanography, 15(4): 377-387.

Erickson, B.E. and Helz, G.R., 2000. Molybdenum (VI) speciation in sulfidic waters: Stability and lability of thiomolybdates. Geochimica et Cosmochimica Acta, 64(7): 1149-1158.

Farrell, J.W., Pedersen, T.F., Calvert, S.E. and Neilsen, B., 1995. Glacial-interglacial changes in nutrient utilization in the equatorial Pacific Ocean. Nature, 377: 514-517.

Fisher, N. and Wente, M., 1993. The release of trace elements by dying marine phytoplankton. Deep-Sea Research 1, 40(4): 671-694.

Flegal, A.R., Sanudo-Wilhelmy, S.A. and Scelfo, G.M., 1995. Silver in the eastern Atlantic Ocean. Marine Chemistry, 49: 315-320.

Fleischer, P., 1972. Mineralogy and sedimentation history of Santa Barbara Basin, California. Journal of Sedimentary Petrology, 42(1): 49-58.

Francois, R., 1988. A study on the regulation of the concentrations of some trace metals (Rb, Sr, Zn, Pb, Cu, V, Cr, Ni, Mn, Mo) in Saanich Inlet sediments, BC, Canada. Marine Geology, 83: 285-308.

Friedl, G., Pedersen, T.F., Crusius, J. and McDonald, D.W., submitted. Enrichment of silver in marine sediments as an indicator of high paleoproductivity. Paleoceanography, submitted.

Ganeshram, R., Pedersen, T.F. and al., e., 2000. Glacial-interglacial variability in denitrification in the world's oceans: Causes and consequences. Paleoceanography, 15(4): 361-376.

Ganeshram, R.S., 1996. On the glacial-interglacial variability of upwelling, carbon burial and denitrification on the northwestern Mexican continental margin., University of British Columbia, Vancouver.

Ganeshram, R.S. and Pedersen, T.F., 1998. Glacial-interglacial variability in upwelling and bioproductivity off NW Mexico: Implications for Quaternary paleoclimate. Paleoceanography, 13(6): 634-645.

Ganeshram, R.S., Pedersen, T.F., Calvert, S.E. and Murray, J.W., 1995. Large changes in oceanic nutrient inventories from glacial to interglacial periods. Nature, 376: 755-758.

Gardner, J.V. and Dartnell, P., 1995. Centennial-scale late Quaternary stratigraphies of carbonate and organic carbon from Santa Barbara Basin, hole 893A, and their paleoceanographic significance. In: J.P. Kennett, J.G. Baldauf and M. Lyle (Editors), Proceedings of the Ocean Drilling Program, Scientific Results.

Gardner, J.V., Dean, W.E. and Dartnell, P., 1997. Biogenic sedimentation beneath the California Current System for the past 30 kyr and its paleoceanographic significance. paleoceanography, 12(2): 207-225.

Gendron, A., Silverberg, N., Sundby, B. and Lebel, J., 1986. Early Diagenesis of cadmium and cobalt in sediments of the Laurentian Trough. Geochimica et Cosmochimica Acta, 50: 741-747.

Gobeil, C., MacDonald, R.W. and Sundby, B., 1997. Diagenetic separation of cadmium and manganese in suboxic continental margin sediments. Geochimica et Cosmochimica Acta, 61(21): 4647-4654.

Gordon, K., 1997. Sedimentary Tracers of Sewage Inputs to the Southern Strait of Georgia. MSc. Thesis, University of British Columbia, Vancouver, 217 pp.

Grimm, K., Lange, C.B. and Gill, A.S., 1996. Biological forcing of hemipelagic sedimentary laminae: evidence from ODP site 893, Santa Barbara basin, California. Journal of Sedimentary Research, 66(3): 613-624.

Helz, G.R. et al., 1996. Mechanism of molybdenum removal from the sea and its concentration in black shales: EXAFS evidence. Geochimica et Cosmochimica Acta, 60(19): 3631-3642.

Hemphill-Haley, E. and Fourtanier, E., 1995. A diatom record spanning 114.000 years from site 893, Santa Barbara Basin. In: J.P. Kennett, J.G. Baldauf and M. Lyle (Editors), Proceeding of the Ocean Drilling Program, Scientific Results.

Hendershott, M.C. and Winant, C.D., 1996. Surface circulation in the Santa Barbara Channel. Oceanography, 9(2): 114-121.

Hendy, I.L. and Kennett, J.P., 1999. Latest Quaternary North Pacific surface-water responses imply atmosphere-driven climate instability. Geology, 27(4): 291-294.

Hendy, I.L. and Kennett, J.P., 2000. Dansgaard-Oeschger cycles in the California Current system: Planktonic foraminiferal response to rapid climate change in Santa Barbara Basin, Ocean Drilling Program hole 893A. Paleoceanography, 15(1): 30-42.

Heumann, K.G., 1988. Isotope Dilution Mass Spectrometry. In: F. Adams, R. Gijbels and R. Van Grieken (Editors), Inorganic Mass Spectrometry. Chemical Analysis: A series of monographs on Analytical Chemistry and its applications. John Wiley and Sons.

Heusser, L.E. and Sirocko, F., 1997. Millennial pulsing of environmental change in southern California from the past 24k.y.: A record of Indo-Pacific ENSO events. Geology, 25(3): 243-246.

Hulsemann, J. and Emery, K.O., 1961. Stratification in recent sediments of Santa Barbara basin as controlled by organisms and water character. Journal of Geology, 69(279-290).

Irino, T. and Pedersen, T.F., 2000. Geochemical character of glacial to interglacial sediments at site 1017, Southern Californian margin: minor and trace elements. In: M. Lyle, I. Kozumi, C. Richter and T.C.J. Moore (Editors), Proceeding of the Ocean Drilling Program, Scientific Results.

Kamatani, A. and Oku, O., 2000. Measuring biogenic silica in marine sediments. Marine Chemistry, 68(3): 219-229.

Karen, D.J. et al., 1999. Influence of water quality on silver toxicity to Rainbow trout (*Oncorhynchus mykiss*), Fathead minnows (*Pimephales promelas*) and water fleas (*Daphnia magna*). Environmental Toxicology and Chemistry, 18(1): 63-70.

Kennett, J.P. and Ingram, B.L., 1995. A 20,000-year record of ocean circulation and climate change from the Santa Barbara basin. Nature, 377: 510-514.

Kennett, J.P., Roark, E.B., Cannariato, K.G., Ingram, B.L. and Tada, R., 2000. Latest Quaternary paleoclimatic and radiocarbon chronology, hole 1017e, Southern California margin. In: M. Lyle, I. Koizumi, C. Richter and T.C. Moore (Editors), Proceedings of the Ocean Drilling Program, Scientific Results.

Kienast, S.S., Calvert, S.E., Collier, R.W. and Pedersen, T.F., submitted. Nitrogen isotope and productivity variations along the North East Pacific margin over the last 120 kyr: Surface and subsurface paleoceanography. Paleoceanography.

Kincaid, E. et al., 2000. Planktonic foraminiferal fluxes in the Santa Barbara Basin: Response to seasonal and interannual hydrographic changes. Deep-Sea Research II, 47: 1157-1176.

Klinkhammer, G.P. and Palmer, M.R., 1991. Uranium in the oceans: Where it goes and why. Geochimica et Cosmochimica Acta, 55: 1799-1806.

Koide, M. et al., 1986. Some comparative marine chemistries of rhenium, gold, silver and molybdenum. Applied Geochemistry, 1: 705-714.

Lee, B. and Fisher, N., 1994. Effects of sinking and zooplankton grazing on the release of elements from planktonic debris. Marine Ecology Progress Series, 110: 271-281.

Lyle, M., Koizumi, I., Delany, M. and Barron, J.A., 2000. Sedimentary record of the California current system, Middle Miocene to Holocene: A synthesis of leg 167 results. In: M. Lyle, I. Kozumi, C. Richter and T.C.J. Moore (Editors), Proceeding of the Ocean Drilling Program, Scientific Results.

Lynn, R.J. and Simpson, J.J., 1987. The California current system: The seasonal variability of its physical characteristics. Journal of Geophysical Research, 92(C12): 12,947-12,966.

Martin, J.H., Knauer, G.A. and Gordon, R.M., 1983. Silver distribution and fluxes in Northeast Pacific waters. Nature, 305: 306-309.

Martinson, D.G. et al., 1987. Age dating and the orbital theory of the ice ages: Development of a high-resolution 0 to 300,000-year chronostratigraphy. Quaternary Research, 27: 1-29.

McCorkle, D.C. and Klinkhammer, G.P., 1991. Porewater Cd geochemistry and the porewater Cd:13C relation. Geochimica et Cosmochimica Acta, 55(161-168).

McManus, J., Berelson, W.M., Klinkhammer, J.P., Kilgore, T.E. and Hammond, D.E., 1994. Remobilization of barium in continental margin sediments. Geochimica et Cosmochimica Acta, 58(22): 4899-4907.

McManus, J. et al., 1995. Early diagenesis of biogenic opal: Dissolution rates, kinetics, and paleoceanographic implications. Deep-Sea Research II, 42(2-3): 871-903.

Mix, A.C. et al., 1999. Rapid climate oscillations in the Northeast Pacific during the last deglaciation reflect Northern and Southern hemisphere sources. In: P.U. Clark, R.S. Webb and L.D. Keigwin (Editors), Mechanisms of Global Climate Change at Millennial Time Scales.

Montaser, A. (Editor), 1998. Inductively Coupled Plasma Mass Spectrometry. Wiley-VCH, New York.

Morford, J. and Emerson, S., 1999. The geochemistry of redox sensitive trace metals in sediments. Geochimica et Cosmochimica Acta, 63(11-12): 1735-1750.
Muller, P.J. and Suess, E., 1979. Productivity, sedimentation rate and sedimentary organic matter in the oceans-1. Organic carbon preservation. Deep-Sea Research, 26A(12): 1347-1362.

Nelson, D.M., Treguer, P., Brzezinski, M.A., Leynaert, A. and Queguiner, B., 1995. Production and dissolution of biogenic silica in the ocean: Revised global estimates, comparison with regional data and relationship to biogenic sediments. Global Biogeochemical Cycles, 9(3): 359-372.

Pedersen, T.F., Shimmield, G.B. and Price, N.B., 1992. Lack of preservation of organic matter in sediments under the oxygen minimum on the Oman margin. Geochimica et Cosmochimica Acta, 56(1): 545-551.

Pedersen, T.F., Waters, R.D. and MacDonald, R.W., 1989. On the natural enrichment of cadmium and molybdenum in the sediments of Ucluelet Inlet, British Columbia. The Science of the Total Environment, 79: 125-139.

Pike, J. and Kemp, A.E.S., 1999. Diatom mats in Gulf of California sediments: Implications for the paleoenvironmental interpretation of laminated sediments and silica burial. Geology, 27(4): 311-314.

Pilskaln, C. and Pike, J., 2001. Formation of Holocene sedimentary laminae in the Black sea and the role of the benthic flocculent layer. Paleoceanography, 16(1): 1-19.

Premuzic, E.T., Benkovitz, C.M., Gaffney, J.S. and Walsh, J.J., 1982. The nature and distribution of organic matter in the surface sediments of world oceans and seas. Organic Geochemistry, 4(1): 63-77.

Pride, C. et al., 1999. Nitrogen isotopic variation in the Gulf of California since the last deglaciation: Response to global climate change. Paleoceanography, 14(3): 397-409.

Rack, F.R., Heise, E.A. and Stein, R., 1995. Magnetic susceptibility and physical properties of sediment cores from site 893, Santa Barbara Basin: Records of sediment diagenesis or of paleoclimatic and paleoceanographic change? In: J.P. Kennett, J.G. Baldauf and M. Lyle (Editors), Proceedings of the Ocean Drilling Program, Scientific Results.

Ragueneau, O. et al., 2000. A review of the Si cycle in the modern ocean: recent progress and missing gaps in the application of biogenic opal as a paleoproductivity proxy. Global and Planetary Change, 26(4): 317-365.

Ratte, H.T., 1999. Bioaccumulation and toxicity of silver compounds: A review. Environmental Toxicology and Chemistry, 18(1): 89-108.

Reimers, C.E., Lange, C.B., Tabak, M. and Bernhard, J.M., 1990. Seasonal spillover and varve formation in the Santa Barbara Basin, California. Limnology and Oceanography, 35(7): 1577-1585.

Rivera-Duarte, I., Flegal, A.R., Sanudo-Wilhelmy, S.A. and Veron, A.J., 1999. Silver in the far North Atlantic Ocean. Deep-Sea Research II, 46: 979-990.

Rosenthal, Y., Lam, P., Boyle, E.A. and Thomson, J., 1995. Authigenic cadmium enrichments in suboxic sediments: Precipitation and postdepositional mobility. Earth and Planetary Science Letters, 132: 99-111.

Shimmield, G.B. and Price, N.B., 1986. The behavior of Molybdenum and Manganese during early sediment diagenesis-offshore Baja California, Mexico. Marine Chemistry, 19: 271-280.

Sholkovitz, E.R. and Geiskes, J.M., 1971. A physical-chemical study of the flushing of the Santa Barbara Basin. Limnology and Oceanography, 16(479-489).

Stein, R., 1995. Clay and bulk mineralogy of late Quaternary sediments at site 893, Santa Barbara Basin. Proceedings of the Ocean Drilling Program, Scientific Results, 146 (part 2).

Stein, R. and Rack, F.R., 1995. A 160,000-year high-resolution record of quantity and composition of organic carbon in the Santa Barbara Basin (site 893). In: J.P. Kennett, J.G. Baldauf and M. Lyle (Editors), Proceedings of the Ocean Drilling Program, Scientific Results.

Tada, R., Sato, S., Irino, T., Matsui, H. and Kennett, J.P., 2000. Millennial-scale compositional variations in late Quaternary sediments at sit 1017, Southern California. In: M. Lyle, I. Kozumi, C. Richter and T.C.J. Moore (Editors), Proceeding of the Ocean Drilling Program, Scientific Results.

Talley, L.D., 1993. Distribution and formation of the North Pacific Intermediate Water. Journal of Physical Oceanography, 23: 517-537.

Thomson, J., Jarvis, I., Green, D.R.H. and Clayton, T., 1998. Mobility and immobility of redox-sensitive elements in deep-sea turbidites during shallow burial. Geochimica et Cosmochimica Acta, 62(4): 643-656.

Thunell, R. et al., 2000. Organic carbon fluxes, degradation, and accumulation in an anoxic basin: Sediment trap results from the Cariaco Basin. Limnology and Oceanography, 45(2): 300-308.

Thunell, R.C., 1998. Particle fluxes in a coastal upwelling zone: Sediment traps results from Santa Barbara basin, California. Deep-Sea Research II, 45: 1893-1884.

Thunell, R.C., Tappa, E. and Anderson, D.M., 1995. Sediment fluxes and varve formation in Santa Barbara basin, offshore California. Geology, 23(12): 1083-1086.

Tuit, C.B., Ravizza, G.E., DeCarlo, E.H., Measures, C. and Vink, S., 2000. Non-conservative Molybdenum behavior in the Eastern Tropical North Pacific. EOS, Transactions, American Geophysical Union, 81 supplement(48): F614.

Tyson, R.V., 2001. Sedimentation rate, dilution, preservation and total organic carbon: some results of a modeling study. Organic Geochemistry, 32: 333-339.

van Geen, A., 1996. Cadmium in the California Current system: Tracer of past and present upwelling. Journal of Geophysical Research, 101(C2): 3489-3507.

van Geen, A., McCorkle, D.C. and Klinkhammer, G.P., 1995. Sensitivity of the phosphate-cadmium-carbon isotope relation in the ocean to cadmium removal by suboxic sediments. Paleoceanography, 10(2): 159-169.

Walton, H.F. (Editor), 1976. Ion Exchange Chromatography. Dowden, Hutchenson & Ross, Stroudsburg, PA.

Zhang, Y., Amakawa, H. and Nozaki, Y., 2001. Oceanic profiles of dissolved silver: Precise measurements in the basins of western North Pacific, Sea of Okhotsk, and the Japan Sea. Marine Chemistry, 75: 151-163.

Zheng, Y., 1999. The Marine Geochemistry of Germanium, Molybdenum and Uranium: the Sinks, Columbia University, New York, 336 pp.

Zheng, Y., Anderson, R.F., van Geen, A. and Kuwabara, J., 2000a. Authigenic molybdenum formation in marine sediments: A link to pore water sulfide in Santa Barbara Basin. Geochimica et Cosmochimica Acta, 64(24): 4165-4178.

Zheng, Y., van Geen, A., Anderson, R.F., Gardner, J.V. and Dean, W.E., 2000b. Intensification of the northeast Pacific oxygen-minimum zone during the Bølling-Ållerød ward period. Paleoceanography, 15(5): 528-536.

Appendix i

Trace Metal Data for ODP Site 893A

Depth (cm)	Age (kyr)	Mo (ppm)	U (ppm)	Re (ppb)	Cd (ppm)	Ag (ppb)
0.05	0.0	4.7	2.9	11.2	2.8	255.6
0.24	0.1	3.0	3.3	10.8	1.6	235.0
0.45	0.2	3.3	4.4	12.9	1.3	183.9
0.66	0.3	7.7	3.3	15.4	3.0	216.2
0.86	0.5	4.9	3.7	14.7	1.9	230.8
1.07	0.6	4.7	4.0	12.8	2.2	186.1
1.62	0.9	7.7	3.5	13.4	2.2	190.3
1.80	1.0	7.4	3.7	13.4	1.8	223.4
2.21	1.2	5.0	4.1	11.7	1.4	239.0
2.44	1.4	8.4	4.3	12.1	2.1	189.5
2.62	1.5	9.3	3.5	12.3	2.2	195.5
2.83	1.6	6.1	2.9	10.8	2.4	196.9
3.04	1.7	7.8	3.6	10.2	2.1	187.4
3.45	2.0	5.5	3.5	15.6	2.2	190.4
3.63	2.1	16.1	3.8	12.2	3.2	219.7
3.84	2.2	9.4	3.1	8.9	1.9	190.8
4.04	2.3	3.2	3.3	7.0	1.2	230.1
4.24	2.4	5.3	3.9	12.6	1.5	185.0
4.44	2.6	8.6	3.7	13.0	2.6	225.2
4.63	2.7	6.9	3.5	11.9	2.1	188.3
4.85	2.8	11.6	3.7	11.2	2.6	188.2
5.05	2.9	5.5	3.8	10.3	1.9	180.8
5.24	3.0	7.4	4.2	12.0	1.7	213.6
5.45	3.2	4.6	3.2	12.1	1.4	192.2
5.65	3.3	6.5	3.4	13.4	2.4	215.6
5.83	3.4	3.9	4.4	13.7	1.3	247.3
6.03	3.5	1.8	3.1	4.5	1.2	179.5
6.23	3.7	11.4	3.9	11.2	1.9	194.6
6.83	4.0	5.7	4.5	11.7	1.7	190.7
7.24	4.3	5.5	6.3	15.3	2.1	204.3
7.44	4.4	4.9	5.0	14.7	1.8	231.9
8.05	4.8	7.0	5.4	15.2	2.1	202.7
8.26	4.9	5.1	5.6	15.0	1.5	219.2
8.46	5.1	6.1	6.0	18.3	1.6	201.1
8.65	5.2	5.5	4.2	10.7	1.3	228.8
	5.4	10.3		19.9		193.8
8.99	5.5	13.6	5.0	13.3	2.1	185.9
9.41	5.7	7.8	6.1	15.6	1.8	198.7
9.58	5.8	4.5	4.2	10.0	1.4	195.6
9.74	5.9	4.0	3.9	12.1	1.1	179.8
9.98	6.0	4.5	3.8	6.6	1.4	186.5
10.37	6.3	6.6	5.1	17.2		197.0
10.57	6.4	3.6	3.9	12.1	1.2	198.8
10.73	6.5	7.5	4.9	13.5	2.3	202.8
11.09	6.7	8.5	4.7	11.9	1.9	240.8

Depth (cm)	Age (kyr)	Mo (ppm)	U (ppm)	Re (ppb)	Cd (ppm)	Ag (ppb)
11.25	6.8	11.3	5.5	15.8	2.3	193.1
11.44	7.0	7.6	5.1	20.2	1.8	210.9
11.62	7.1	5.9	4.7	16.3	1.6	198.1
11.77	7.2	6.1	4.5	11.5	1.7	209.2
11.98	7.3	10.5	3.8	10.5	2.1	208.7
12.15	7.4	6.4	3.9	8.6	1.2	201.5
12.31	7.7	6.8	3.6	10.1	1.6	190.0
12.50	7.8	8.2	4.6	16.8	1.8	169.4
12.82	7.9	5.8	4.2	15.0	1.6	164.9
13.01	8.0	3.7		6.8		131.6
13.19	8.1	10.2	3.6	10.9	1.7	166.1
13.37	8.3	8.2	3.9	10.1	1.3	133.6
13.54	8.4	10.1	4.3	13.3	1.8	165.7
13.72	8.7	7.3	3.6	10.6		149.8
14.27	8.8	5.4	4.0	12.8	1.7	168.2
14.67	9.1	4.3	4.6	9.5	1.4	140.4
14.85	9.2	2.9	3.0	5.3	0.9	186.5
15.06	9.3	13.6	3.4	8.0	2.1	170.2
15.66	9.7	8.6	3.8	11.4	1.7	176.5
16.35	10.2	3.1	3.0	7.1	1.4	201.6
16.92	10.5	7.8	3.5	9.1	1.7	166.2
17.12	10.7	12.7	3.4	7.5	1.9	154.3
17.32	10.8	7.6	3.7	9.7	1.3	139.7
17.52	10.9	8.1	4.0	8.9	1.4	
17.72	11.1	1.8	3.7	5.1	1.1	200.7
17.92	11.2	2.2	3.7	9.4	0.2	
18.72	11.7	2.1		8.3	0.8	119.6
18.92	11.9	2.2	4.1	10.0	0.6	
19.12	12.0	3.3	4.3	11.4	1.1	155.1
19.31	12.1	2.7	4.1	8.7	0.7	151.3
19.51	12.3	2.2	3.0	5.0	0.5	84.8
19.72	12.4	2.8	4.1	6.1	0.6	102.2
19.88	12.5	2.9	4.2	9.9	0.6	
20.07	12.6	2.6	3.8	8.6	0.7	116.6
20.27	12.8	3.3	3.9	13.3	1.0	136.9
20.46	12.9	5.1	3.7	13.5	1.5	130.4
20.66	13.0	4.8	3.6	6.7	1.6	146.1
20.86	13.2	9.3	3.1	8.1	1.4	118.7
21.06	13.3	6.8	3.2	4.4	1.3	106.1
21.26	13.4	7.1	2.9	6.9	1.6	104.0
21.46	13.6	6.7	3.6	5.9	1.6	134.5
21.66	13.7	10.1	3.1			
21.86	13.8	7.5	3.6	6.7	1.6	
22.00	13.9	6.6	3.5	5.3	1.5	144.8
22.20	14.1	6.5	3.1	5.9	1.5	113.3
22.38	14.2	7.7	3.1	6.3	1.3	139.7
22.54	14.3	10.3	3.7	9.8	1.1	
22.67	14.4	4.8	3.7	8.4	1.3	
22.87	14.5	3.9	2.9	5.7	1.1	113.2

Depth (cm)	Age (kyr)	Mo (ppm)	U (ppm)	Re (ppb)	Cd (ppm)	Ag (ppb)
23.07	14.7	11.7	3.8	6.0	1.7	133.0
23.26	14.8	10.2	3.6	7.7	1.7	138.8
23.48	14.9	19.0	3.8	6.6	2.0	138.2
23.61	15.0	15.4	3.8	7.3	1.9	173.6
23.81	15.1	12.3	3.6	5.9	2.0	183.1
24.01	15.3	2.6	3.0	5.9	0.7	163.0
24.21	15.4	1.8	3.6	9.4	0.6	137.9
24.41	15.6	3.4	4.0	10.3	0.8	138.3
24.61	15.7	3.5	4.1	8.8	0.7	145.5
24.80	15.8	3.4	3.4	7.8	0.5	141.7
25.00	16.0	2.6	4.1	7.8	0.6	137.5
25.20	16.1	2.8	3.9	6.4	0.6	142.2
25.40	16.2	2.2	4.1	7.6	0.6	115.8
25.65	16.4	2.8	4.1	9.0	0.7	145.4
25.85	16.5	2.0	4.4	10.9	0.9	198.5
26.05	16.7	3.8	3.5	6.8	0.7	180.8
26.42	16.9	3.7	4.0	7.1	0.6	157.8
26.62	17.0	3.5	4.0	8.0	0.5	135.7
27.03	17.3	4.3	4.0	8.2	0.5	
27.17	17.4	3.3	4.0	6.6	0.7	144.1
27.35	17.5			7.8	0.5	139.6
27.55	17.7	3.7	4.1	8.9	0.8	170.3
27.76	17.8	3.7	3.9	11.2	0.6	174.9
27.93	17.9	4.6	4.1	8.3	0.6	160.1
28.11	18.1	4.5	3.9	8.6	0.7	150.7
28.3	18.2	2.4	4.0	7.7	0.7	135.2
28.51	18.3	3.3	3.7	7.3	0.6	133.3
28.71	18.5	2.4	3.5	6.2	0.6	138.0
28.91	18.6	2.5	4.0	9.7	0.7	139.2
29.09	18.7	2.0	3.3	6.2	0.7	128.8
29.43	19.0	1.6	4.3	8.8	0.6	126.9
29.63	19.1	2.4	3.9	9.9	0.9	
29.84	19.2	2.4	3.8	10.6	0.7	146.3
30.04	19.4	3.5	4.7	12.1	0.7	134.6
30.25	19.5	3.5	4.2	10.0	0.7	
30.31	19.6	2.2		7.5	0.9	134.2
30.51	19.7	2.5	3.9	7.7	0.9	187.7
30.66	19.8	2.6	4.3	9.7	0.8	146.1
30.77	19.9	3.1	4.3	5.0	0.3	129.7
30.97	20.0	3.1	4.1	9.5	0.8	129.2
31.17	20.1	2.5	3.6	7.9	0.7	106.0
31.37	20.3	2.3	3.8	8.9	0.8	111.3
31.57	20.4	2.8	3.9	7.1	0.8	103.6
31.7	20.5	2.3	3.4	7.0	0.8	109.9
31.9	20.6	3.9	4.8	11.0	0.8	154.0
32.08	20.8	2.6	4.6	12.9	1.0	171.1
32.29	20.9	3.1	4.9	13.5	0.7	129.9
32.47	21.0	3.4	4.5	11.1	0.9	150.1
32.65	21.2	3.2	4.1	10.9	1.1	164.7

Depth (cm)	Age (kyr)	Mo (ppm)	U (ppm)	Re (ppb)	Cd (ppm)	Ag (ppb)
32.88	21.3	2.7	3.8	7.9	0.8	117.0
33.04	21.4	3.9	3.5	10.9	0.9	128.0
33.24	21.6	2.9	3.6	12.1	0.7	147.7
33.42	21.7	2.6	4.0	7.5	0.7	99.0
33.59	21.8	2.6	4.6	11.5	0.7	116.3
33.82	22.0	3.5	3.6	8.3	0.7	131.8
34	22.1	3.8	3.9	11.8	0.7	170.8
34.2	22.2	6.7	3.5	8.5	1.1	178.5
34.37	22.3	4.4	4.9	7.9	0.6	135.3
35.35	23.0	3.1	3.3	7.7	0.8	162.4
35.55	23.2	6.6	3.5	8.6	1.0	130.7
35.75	23.3	2.0	3.3	6.7	0.8	115.1
36.04	23.5	2.4	3.4	7.2	0.8	138.0
36.34	23.7	2.2	3.7	7.6	0.5	131.6
36.54	23.8	2.2	3.8	8.0	0.6	131.8
36.67	23.9	1.9	3.2	5.9	0.5	115.0
36.87	24.1	3.9	3.9	6.6	0.5	69.0
37.07	24.2	2.8	3.8	6.6	0.5	88.4
37.27	24.3	2.3	4.1	8.3	0.5	110.0
37.67	24.6	2.7	4.0	9.5	0.5	135.5
37.83	24.7	2.2	3.9	9.8	0.6	130.9
38.23	25.0	3.6	3.8	7.6	0.5	133.9
38.43	25.2	2.7	3.9	8.8	0.6	125.7
38.59	25.3	3.0	4.9	11.2	0.8	134.9
38.76	25.4	3.5	3.9	8.3	0.6	116.3
38.94	25.5	2.9	3.9	6.2	0.5	116.2
39.12	25.6	3.3	3.8	6.2	0.5	123.5
39.24	25.7	2.2	3.9	5.6	0.7	84.3
39.5	25.9	2.3	3.7	6.0	0.6	149.5
39.64	26.0	1.9	3.7	5.7	0.5	109.0
39.84	26.1	1.6	4.1	7.6	0.6	109.1
40	26.2	2.5	4.4	10.4	0.6	130.4
40.2	26.4	3.9	6.1	13.5	0.9	160.2
40.55	26.5	1.8	4.5	9.0	0.7	121.2
40.77	26.6	2.9	4.9	10.9	0.7	167.1
	26.8	2.9	4.9		0.7	
41.54	27.3	3.4	5.0	10.8	0.8	182.8
41.91	27.6	2.4	3.9	7.4	1.0	336.1
42.26	27.8	2.7	4.2	8.1	0.7	127.0
42.43	27.9	3.4	4.1	7.4	0.7	114.4
42.64	28.1	2.7	4.2	6.8	0.6	107.0
42.68	28.1	2.4	5.0	11.8	0.8	134.1
42.88	28.2	2.2	4.5	9.3	0.7	133.6
43.03	28.4	2.7	3.7	7.4	0.6	202.2
43.21	28.5	2.8	4.3	8.1	0.9	158.8
44.52	29.5	2.6	3.9	7.0	0.5	112.1
44.68	29.6	2.7		7.1	0.5	116.3
44.88	29.8	2.8		6.6	0.6	145.3
44.96	29.9	3.1	3.8	6.7	0.5	101.9

Depth (cm)	Age (kyr)	Mo (ppm)	U (ppm)	Re (ppb)	Cd (ppm)	Ag (ppb)
45.16	30.0	2.5	3.9	8.5	0.5	
45.28	30.1	2.5		7.0	0.7	98.2
45.41	30.2	1.8	4.2	7.4	0.6	120.2
45.61	30.4	2.7	4.6	10.6	0.6	123.7
46.02	30.7	5.9	4.0	9.9	1.2	139.5
46.22	30.9	8.7		6.6	1.0	113.3
46.42	31.0	6.3	3.6	7.7	1.0	118.0
46.76	31.3	3.3	3.8	6.3	0.6	101.4
46.95	31.4	3.3	4.1	7.3	0.6	
47.15	31.6	2.9	3.9	6.1	0.6	124.5
47.32	31.7	3.0	3.7	7.2	0.5	126.9
47.51	31.9	2.3	3.9	7.7	0.6	125.4
47.9	32.2	3.0	4.0	8.0	0.6	123.3
48	32.3	3.0	3.8	7.5	0.8	186.4
48.2	32.4	4.0	3.8	7.4	0.8	116.1
48.39	32.6	5.0	3.8	5.7	0.9	172.5
48.57	32.7	3.5	3.3	7.6	0.7	156.2
48.74	32.9	2.2	3.8	7.4	0.7	129.8
48.94	33.1	2.5		5.6	0.6	131.8
49.14	33.2	2.6	3.5	5.1	0.5	115.5
49.54	33.5	3.1	4.0	7.1	0.6	
49.72	33.7					
50.1	34.0	2.0	3.8	7.9	0.5	117.6
50.3	34.1	1.9	3.8	8.2	0.6	106.2
50.5	34.3	5.1	3.6	8.0	0.8	128.6
50.7	34.4	5.1	3.6	6.8		
50.9	34.6	5.7		5.1	1.0	111.6
51.1	34.8	6.6	3.9	5.7	1.1	112.4
51.18	34.8	2.1		4.5	0.5	112.9
51.28	34.9	5.7	3.7	6.7	1.2	129.8
51.48	35.1	6.0	3.5	5.5	1.0	199.4
51.73	35.3	2.3	3.6	6.8	0.7	111.1
51.79	35.3	1.9	3.3	4.9	0.6	145.5
51.95	35.4	3.0	3.3	4.8	0.5	113.4
52.15	35.6	2.7	3.3	5.5	1.1	173.1
52.35	35.8	3.6	3.5	6.2	0.4	109.6
52.53	35.9	1.7	3.1	5.3	0.5	114.8
52.73	36.1	3.2		4.3	0.5	75.9
52.94	36.2	2.3		5.6	0.6	110.0
53.14	36.4	2.0		5.4	0.6	102.9
54.2	37.2	8.5		5.4	1.4	112.6
54.4	37.4	5.2		4.9	0.7	131.9
54.54	37.5	6.0		5.5	1.1	143.9
54.6	37.6	5.6		5.9	1.3	123.9
55.3	37.9	2.0		5.1	0.6	104.0
55.67	38.2	2.7		5.2	0.5	164.2
55.81	38.3	2.1		5.0	0.5	115.9
55.98	38.4	2.7		5.5	0.6	98.4
56.21	38.6	1.8		5.6	0.4	104.1

Depth (cm)	Age (kyr)	Mo (ppm)	U (ppm)	Re (ppb)	Cd (ppm)	Ag (ppb)
56.38	38.8	2.7		6.4	0.5	124.4
56.58	38.9	2.3		6.4	0.5	114.4
56.78	39.1	2.8		5.3	0.4	112.9
56.78	39.1	2.6		5.1	0.5	121.5
58.01	40.1	2.1		7.3	0.5	107.8
58.21	40.2	3.4		6.7	0.6	125.1
59.76	40.7	2.7		6.1	0.5	115.6
59.96	40.8	2.4		7.6	0.9	126.4
60.36	41.1	2.7		6.4	0.6	133.8
60.54	41.3	3.4		7.4	0.8	128.7
60.74	41.4	1.9		8.2	0.8	136.0
61.54	42.1	2.1		6.4	0.7	114.0
62.11	42.5	7.1		5.0	1.2	127.6
62.46	42.8	4.4		5.9	0.9	131.7
63.7	43.8	6.2		5.2	1.0	123.9
63.9	43.8	5.8		5.4	1.2	115.6
65.37	44.5	2.1		7.1	0.5	138.5
65.44	44.5	2.6		5.6	0.8	158.7
65.64	44.7	2.3		4.5	2.0	192.2
65.97	44.9					134.2
66.12	45.0	1.9		5.6	0.9	120.5
66.3	45.1	3.6		5.8	0.6	102.8
66.35	45.1	1.7		6.0	0.6	133.8
66.69	45.4	3.0		5.4	0.7	121.0
66.87	45.5	2.4		6.6	0.6	136.6
67.22	45.7	5.0		5.2	0.9	122.2
67.77	46.1	5.8		5.5	1.0	117.7
68.17	46.4	2.5		7.1	0.8	115.6
68.54	46.6	4.7		6.7	1.1	126.1
68.73	46.7	3.5		7.7	0.9	154.8
68.93	47.1	2.4		7.7	0.8	122.1
69.68	47.3	12.0		6.8	1.9	131.6
70.04	47.5	2.9		6.6	0.6	99.5
70.22	47.7	2.3		8.1	0.7	106.8
70.42	47.8	2.3		7.0	0.7	125.8
70.88	48.1	2.9		6.7	0.6	181.8
71.08	48.1	2.7		6.4	0.6	87.9
71.35	48.4	2.1		6.6	0.6	112.0
71.57	48.5	2.3		6.6	1.0	126.0
	49.0	3.2		5.7	0.6	94.2

Appendix ii

Major Element Data for ODP Site 893A

Depth (cm)	Al wt %	Ca wt %	Fe wt %	K wt %
0.05	7.04	3.20	3.94	1.97
0.24	6.61	4.05	3.60	1.70
0.45	6.62	3.23	3.65	1.89
0.86	6.51	5.19	3.44	1.74
1.07	6.72	4.85	3.95	1.75
1.62	5.62	4.88	3.43	1.46
1.80	6.52	4.72	3.52	1.81
2.21	6.98	2.92	3.80	2.01
2.44	6.55	4.97	3.57	1.78
2.62	6.00	4.13	3.46	1.67
2.83	6.54	4.70	3.35	1.74
3.04	7.06	4.39	3.52	1.71
3.45	7.43	3.41	3.77	1.99
3.63	6.33	4.78	3.36	1.53
3.84	6.46	3.71	4.18	1.86
4.04	8.63	1.57	4.49	2.40
4.24	6.55	5.29	3.87	1.84
4.44	6.26	4.56	3.28	1.61
4.63	6.80	4.65	3.83	1.93
4.85	6.37	3.92	5.01	1.80
5.05	6.72	4.15	4.14	1.89
5.24	6.64	4.56	4.06	1.87
5.45	6.77	3.57	3.78	1.97
5.65	6.82	4.82	3.66	1.81
5.83	7.19	4.35	3.99	1.72
6.03	9.03	1.54	4.10	2.52
6.23	6.66	4.83	4.27	1.71
6.83	7.22	4.75	4.27	1.83
7.24	7.12	4.30	4.07	1.75
7.44	6.54	5.19	3.94	1.83
7.63	7.03	4.35	4.22	1.81
7.85	6.76	3.50	4.62	1.85
8.05	7.24	5.26	4.17	1.87
8.26	7.25	5.31	3.87	1.85
8.46	7.31	4.72	3.98	1.90
8.65	7.66	3.24	4.20	2.13
	6.76	4.49	3.83	1.96
8.99	5.72	4.53	4.04	1.78
9.41	7.45	4.75	4.07	1.87
9.58	7.22	3.81	4.27	2.08
9.98	7.48	2.13	4.46	2.17
10.17	7.04	4.05	4.35	1.95
10.37	7.39	4.54	3.92	1.98
10.57	7.44	3.10	4.35	2.15

Appendix ii

Major Element Data for ODP Site 893A

Depth (cm)	Mg wt %	Na wt %	Si wt %	Ti wt %	P wt %
0.05	1.83	7.15	23.89	0.39	0.11
0.24	1.86	7.80	22.60	0.36	0.12
0.45	1.72	5.07	22.82	0.36	0.11
0.86	1.74	4.50	22.09	0.35	0.12
1.07	1.86	6.96	21.71	0.36	0.12
1.62	1.81	5.04	22.58	0.33	0.10
1.80	1.86	2.74	22.61	0.36	0.11
2.21	1.77	4.35	23.43	0.38	0.10
2.44	1.83	4.51	22.77	0.36	0.12
2.62	1.77	4.39	22.89	0.33	0.10
2.83	1.71	4.90	22.24	0.34	0.11
3.04	1.86	6.72	23.06	0.36	0.12
3.45	1.80	5.29	24.56	0.40	0.12
3.63	1.64	4.13	22.46	0.33	0.11
3.84	1.70	3.79	22.24	0.36	0.10
4.04	1.97	3.87	23.47	0.46	0.10
4.24	1.74	4.27	21.26	0.36	0.11
4.44	1.74	4.01	22.51	0.35	0.11
4.63	1.79	4.76	23.03	0.37	0.11
4.85	1.71	4.16	21.37	0.35	0.11
5.05	1.80	3.65	21.94	0.37	0.11
5.24	1.75	3.61	21.23	0.36	0.10
5.45	1.71	4.15	23.33	0.38	0.10
5.65	1.75	3.61	22.80	0.37	0.12
5.83	1.81	3.94	21.57	0.37	0.10
6.03	1.98	3.89	25.72	0.49	0.10
6.23	1.74	3.93	22.62	0.35	0.11
6.83	1.85	3.88	22.91	0.38	0.12
7.24	1.78	3.99	22.07	0.38	0.10
7.44	1.70	3.92	21.73	0.37	0.11
7.63	1.81	3.90	21.98	0.38	0.10
7.85	1.68	3.50	22.61	0.38	0.09
8.05	1.82	4.24	22.47	0.38	0.11
8.26	1.80	5.72	22.82	0.39	0.12
8.46	1.85	4.53	23.06	0.39	0.11
8.65	1.85	3.41	23.54	0.40	0.10
	1.77	3.85	21.82	0.38	0.10
8.99	1.51	3.81	19.52	0.35	0.09
9.41	1.90	3.58	22.91	0.39	0.11
9.58	1.80	3.75	22.42	0.41	0.10
9.98	1.95	2.63	23.07	0.43	0.10
10.17	1.82	3.46	22.07	0.38	0.10
10.37	1.80	3.87	22.08	0.38	0.10
10.57	1.85	4.32	22.89	0.41	0.10

Depth (cm)	Al wt %	Ca wt %	Fe wt %	K wt %
10.73	6.92	4.75	4.08	1.86
10.91	6.93	4.25	4.19	2.01
11.09	7.01	4.35	4.04	1.88
11.25	6.72	5.13	3.93	1.91
11.44	6.73	4.43	4.13	1.88
11.62	6.76	4.28	3.99	1.84
11.77	7.13	5.03	4.01	1.70
11.98	7.28	2.93	4.48	2.10
12.15	7.63	3.37	4.20	1.96
12.50	6.88	4.47	4.22	1.93
12.70	6.58	5.32	4.19	1.91
12.82	7.52	3.09	4.15	1.88
13.01	7.24	3.35	3.38	2.13
13.19	6.65	4.34	3.99	1.97
13.37	6.83	4.51	4.00	1.95
13.54	6.54	5.21	3.79	1.85
13.72	6.78	4.66	3.65	1.94
13.88	6.50	5.03	3.80	1.83
14.07	7.26	3.69	4.11	1.83
14.27	7.28	4.18	4.02	1.86
14.47	6.58	4.62	3.80	1.79
14.67	6.59	5.17	3.65	1.84
14.85	8.83	1.57	4.10	2.53
15.06	7.12	4.35	4.87	1.79
15.26	6.49	4.71	3.73	1.93
15.66	6.76	5.26	3.70	1.83
16.15	6.78	5.03	3.86	1.95
16.35	8.13	1.94	4.02	2.46
16.52	6.90	3.78	4.80	1.89
16.92	6.99	3.92	4.43	2.04
17.12	6.54	4.90	4.16	1.86
17.32	7.14	3.95	4.15	1.77
17.72	8.35	1.70	3.89	2.51
17.92	7.67	2.12	4.28	2.26
18.12	7.49	2.44	4.36	2.21
18.32	7.54	2.38	4.28	2.17
18.72	7.42	2.56	4.25	2.19
18.92	7.82	2.69	4.19	2.11
19.12	7.16	2.04	4.15	2.04
19.51	8.06	2.36	4.22	2.05
19.88	8.08	2.19	4.25	2.11
20.07	7.33	2.17	4.41	2.18
20.27	7.52	2.64	4.40	2.14
20.46	8.11	2.99	4.51	2.13
20.66	7.54	3.23	4.28	2.06
20.86	7.33	2.80	4.50	1.92
21.06	7.28	2.61	4.82	2.07
21.26	7.25	2.72	4.57	2.03

Depth (cm)	Mg wt %	Na wt %	Si wt %	Ti wt %	P wt %
10.73	1.75	3.13	21.46	0.38	0.09
10.91	1.79	3.66	22.18	0.38	0.10
11.09	1.82	3.69	22.09	0.39	0.10
11.25	1.76	3.66	21.29	0.37	0.10
11.44	1.75	4.00	22.30	0.38	0.11
11.62	1.80	3.48	22.15	0.38	0.11
11.77	1.76	5.67	21.81	0.37	0.11
11.98	1.88	3.95	22.83	0.40	0.10
12.15	1.93	4.02	22.86	0.41	0.11
12.50	1.78	4.30	21.92	0.38	0.11
12.70	1.74	4.08	21.48	0.36	0.11
12.82	1.89	3.82	22.88	0.39	0.11
13.01	1.46	3.63	25.81	0.39	0.10
13.19	1.71	5.36	21.94	0.36	0.11
13.37	1.75	3.65	22.36	0.38	0.11
13.54	1.72	3.83	21.99	0.36	0.11
13.72	1.80	3.83	22.39	0.36	0.12
13.88	1.72	3.38	21.75	0.35	0.10
14.07	1.83	3.42	22.71	0.39	0.11
14.27	1.80	3.61	22.46	0.38	0.11
14.47	1.74	3.84	21.76	0.35	0.11
14.67	1.77	3.37	21.88	0.36	0.11
14.85	2.00	4.47	23.79	0.46	0.09
15.06	1.85	3.34	23.11	0.38	0.11
15.26	1.74	4.58	22.40	0.36	0.11
15.66	1.75	3.75	22.12	0.36	0.12
16.15	1.44	3.45	23.41	0.35	0.12
16.35	1.79	3.61	25.18	0.45	0.13
16.52	1.75	2.97	21.53	0.37	0.12
16.92	1.80	4.04	21.87	0.38	0.12
17.12	1.69	4.67	21.33	0.35	0.11
17.32	1.72	3.78	22.83	0.38	0.12
17.72	1.91	3.61	25.09	0.45	0.12
17.92	1.83	3.98	24.57	0.41	0.11
18.12	1.78	3.68	24.29	0.39	0.11
18.32	1.80	3.66	24.18	0.40	0.11
18.72	1.78	3.79	24.19	0.40	0.11
18.92	1.86	3.29	25.00	0.40	0.12
19.12	1.81	3.14	24.76	0.40	0.11
19.51	1.88	3.90	25.51	0.42	0.12
19.88	1.95	3.92	25.62	0.42	0.12
20.07	1.82	7.89	24.11	0.40	0.11
20.27	1.82	4.10	23.91	0.39	0.11
20.46	1.87	4.78	24.89	0.42	0.12
20.66	1.82	3.75	23.13	0.39	0.11
20.86	1.81	3.75	23.30	0.38	0.10
21.06	1.80	3.41	23.08	0.39	0.10
21.26	1.83	3.31	23.10	0.38	0.10

Depth (cm)	Al wt %	Ca wt %	Fe wt %	K wt %
21.66	7.41	2.82	4.43	2.08
21.86	7.13	2.70	4.48	2.07
22.00	7.98	2.58	4.78	2.06
22.20	7.60	2.69	4.33	1.95
22.38	7.47	2.76	4.60	1.81
22.54	7.47	2.39	4.21	2.17
22.67	7.80	3.17	4.41	2.07
22.87	7.50	2.70	4.22	1.93
23.07	7.05	3.15	4.37	1.97
23.26	7.29	3.16	4.45	2.08
23.48	6.83	3.12	4.39	2.03
23.61	6.99	3.33	4.25	2.02
23.81	7.07	2.92	4.29	1.98
24.01	7.54	2.21	4.11	1.94
24.21	7.51	2.75	4.13	2.17
24.41	7.46	2.39	4.21	2.17
24.61	7.48	2.59	4.11	1.95
24.80	7.18	2.39	3.55	2.18
25.00	7.24	2.72	3.97	2.13
25.20	7.44	2.68	4.12	1.93
25.40	7.33	2.69	4.07	2.09
25.65	7.68	2.62	4.22	2.19
25.85	7.58	2.88	4.13	2.06
26.05	7.33	2.49	3.73	1.93
26.22	7.07	2.99	4.19	2.17
26.42	7.47	2.67	4.18	1.95
26.62	7.33	2.80	4.05	2.18
27.03	7.16	2.88	4.08	2.12
27.17	7.43	2.93	4.28	2.05
27.35	7.22	3.03	4.13	2.13
27.55	7.33	3.01	4.21	2.07
27.76	7.09	3.24	4.22	2.04
27.93	7.35	3.08	4.14	1.93
28.11	7.37	3.04	4.16	2.03
28.30	7.45	2.92	3.98	1.93
28.51	7.14	2.97	4.04	2.14
28.71	7.25	3.03	4.06	2.15
28.91	7.29	3.02	4.34	2.12
29.27	7.32	2.69	4.48	2.16
29.43	7.34	3.07	4.06	2.15
29.63	7.07	2.84	4.21	2.05
29.84	7.39	2.81	4.16	1.94
30.04	7.44	3.18	4.25	2.13
30.25	7.30	2.96	4.41	2.14
30.31	7.46	2.74	4.13	2.20
30.51	7.49	3.00	3.97	2.17
30.66	7.34	3.35	3.92	1.97
30.77	7.27	3.57	4.09	1.88

Depth (cm)	Mg wt %	Na wt %	Si wt %	Ti wt %	P wt %
21.66	1.81	3.38	23.07	0.39	0.11
21.86	1.79	4.16	22.97	0.38	0.10
22.00	1.89	4.62	24.70	0.40	0.12
22.20	1.89	3.09	25.22	0.40	0.12
22.38	1.77	3.37	23.04	0.38	0.10
22.54	1.84	4.15	24.44	0.40	0.11
22.67	1.90	5.00	24.13	0.40	0.12
22.87	1.83	2.92	23.70	0.39	0.11
23.07	1.77	3.59	23.16	0.38	0.11
23.26	1.78	4.23	22.85	0.38	0.11
23.48	1.75	8.35	22.53	0.37	0.11
23.61	1.78	3.92	22.85	0.37	0.12
23.81	1.71	3.63	23.47	0.37	0.11
24.01	1.78	3.83	24.95	0.40	0.11
24.21	1.81	3.51	24.22	0.39	0.11
24.41	1.80	3.74	24.21	0.40	0.11
24.61	1.78	3.69	24.56	0.39	0.11
24.80	1.41	4.14	26.80	0.36	0.12
25.00	1.81	3.58	24.52	0.39	0.12
25.20	1.82	3.97	24.58	0.39	0.12
25.40	1.82	3.99	24.46	0.38	0.12
25.65	1.84	3.87	24.44	0.40	0.12
25.85	1.85	4.62	24.48	0.40	0.12
26.05	1.60	4.25	25.59	0.38	0.12
26.22	1.78	3.76	24.28	0.39	0.12
26.42	1.85	3.71	24.71	0.39	0.12
26.62	1.83	3.82	24.46	0.39	0.12
27.03	1.87	3.51	24.21	0.39	0.12
27.17	1.82	4.04	24.15	0.39	0.12
27.35	1.80	3.78	24.12	0.39	0.12
27.55	1.85	3.28	24.24	0.39	0.12
27.76	1.84	3.46	23.77	0.39	0.11
27.93	1.81	4.96	24.06	0.39	0.11
28.11	1.83	4.37	23.96	0.39	0.12
28.30	1.84	4.37	24.48	0.39	0.12
28.51	1.70	3.81	24.37	0.38	0.11
28.71	1.80	4.84	24.18	0.38	0.11
28.91	1.78	4.04	23.95	0.39	0.11
29.27	1.78	3.86	23.88	0.39	0.11
29.43	1.82	3.64	24.29	0.40	0.11
29.63	1.77	3.16	24.27	0.39	0.11
29.84	1.82	3.88	24.12	0.39	0.11
30.04	1.85	4.07	23.90	0.39	0.11
30.25	1.80	4.07	23.90	0.39	0.12
30.31	1.80	3.78	24.29	0.40	0.11
30.51	1.83	4.30	24.16	0.39	0.11
30.66	1.80	4.74	23.75	0.39	0.11
30.77	1.76	3.69	23.79	0.38	0.11

Depth (cm)	Al wt %	Ca wt %	Fe wt %	K wt %
30.97	7.19	3.21	4.11	2.02
	7.19	3.27	4.06	2.08
31.17	7.11	3.43	4.22	2.10
31.37	7.34	3.67	4.05	1.88
31.57	7.45	3.11	4.11	2.17
31.70	7.68	2.84	4.13	2.23
31.90	7.32	3.29	4.10	2.15
32.08	7.69	3.01	4.11	2.02
32.29	7.25	3.11	4.11	2.11
32.47	7.26	3.09	4.13	2.06
32.65	7.61	3.67	4.04	2.06
32.88	7.09	3.28	3.93	2.04
33.24	6.70	5.10	3.58	1.98
33.42	7.22	3.43	4.16	2.13
33.59	7.32	3.52	4.03	2.17
33.82	7.26	3.37	3.82	1.93
34.00	7.05	3.40	4.27	2.08
34.20	6.80	2.89	4.42	1.97
	7.06	2.94	4.53	1.94
34.37	7.21	3.29	4.19	1.93
35.15	6.87	2.92	4.13	2.03
35.35	6.78	2.98	3.99	1.98
35.55	7.22	2.96	4.25	1.92
35.75	7.65	2.70	4.10	1.98
35.95	7.48	2.90	4.04	1.95
36.04	7.39	2.92	3.94	2.14
36.21	6.80	2.72	4.41	2.01
36.34	6.71	3.14	4.08	1.81
36.54	7.43	3.08	4.02	2.14
36.67	7.15	2.80	3.41	2.18
36.87	7.30	3.19	3.97	2.13
37.07	7.59	3.03	4.03	1.98
37.27	7.23	3.34	3.92	2.15
37.47	7.16	3.54	3.93	2.11
37.67	7.16	3.15	4.20	2.12
37.83	7.46	3.18	4.10	1.93
38.03	7.40	3.12	4.01	2.13
38.23	7.52	2.92	4.20	1.98
38.43	7.46	3.16	3.92	1.95
38.59	7.53	3.25	4.31	2.14
38.76	7.34	2.85	4.37	2.08
38.94	8.15	2.63	4.66	2.37
39.12	7.53	2.96	4.18	2.01
39.24	7.34	3.05	3.95	2.09
39.50	6.79	3.14	4.08	2.06
39.64	7.22	3.00	4.13	2.11
39.84	7.59	3.17	4.02	1.95
40.00	7.50	3.21	4.17	1.96

Depth (cm)	Mg wt %	Na wt %	Si wt %	Ti wt %	P wt %
30.97	1.76	3.69	23.39	0.38	0.11
	1.74	4.38	23.81	0.39	0.10
31.17	1.78	3.78	23.58	0.38	0.11
31.37	1.75	3.79	23.70	0.38	0.11
31.57	1.78	3.92	24.09	0.40	0.11
31.70	1.80	3.61	24.34	0.40	0.11
31.90	1.80	3.78	23.78	0.39	0.11
32.08	1.91	2.49	25.19	0.40	0.12
32.29	1.79	3.64	23.92	0.39	0.11
32.47	1.72	3.64	24.22	0.39	0.11
32.65	1.77	2.94	24.94	0.39	0.12
32.88	1.72	3.53	23.99	0.38	0.11
33.24	1.62	5.60	23.60	0.36	0.11
33.42	1.75	3.72	23.57	0.39	0.11
33.59	1.79	3.69	23.78	0.39	0.11
33.82	1.55	3.87	24.92	0.37	0.11
34.00	1.72	3.77	23.42	0.38	0.11
34.20	1.62	4.19	23.32	0.36	0.10
	1.66	4.24	23.95	0.37	0.10
34.37	1.74	3.61	23.41	0.37	0.11
35.15	1.73	2.91	24.08	0.38	0.10
35.35	1.74	2.60	24.22	0.38	0.10
35.55	1.69	4.28	24.07	0.38	0.11
35.75	1.79	4.56	24.33	0.40	0.11
35.95	1.69	6.04	24.13	0.39	0.11
36.04	1.75	3.77	24.26	0.39	0.10
36.21	1.68	3.77	23.68	0.36	0.10
36.34	1.49	8.16	21.42	0.38	0.10
36.54	1.72	4.15	24.26	0.38	0.11
36.67	1.46	4.18	26.19	0.36	0.11
36.87	1.77	4.01	24.11	0.39	0.12
37.07	1.79	3.74	24.26	0.39	0.12
37.27	1.74	4.97	24.03	0.39	0.11
37.47	1.78	3.92	23.77	0.38	0.11
37.67	1.75	3.87	23.79	0.39	0.11
37.83	1.72	3.58	24.45	0.39	0.11
38.03	1.73	3.29	24.39	0.39	0.10
38.23	1.76	3.89	24.29	0.40	0.11
38.43	1.71	3.62	24.47	0.39	0.11
38.59	1.76	3.47	24.16	0.39	0.11
38.76	1.78	3.60	24.04	0.39	0.11
38.94	1.86	3.63	25.90	0.42	0.12
39.12	1.78	3.88	24.30	0.40	0.11
39.24	1.80	5.68	24.36	0.39	0.11
39.50	1.65	4.64	23.09	0.39	0.11
39.64	1.80	3.20	24.37	0.40	0.11
39.84	1.77	3.68	24.05	0.40	0.11
40.00	1.78	3.88	24.06	0.40	0.11

Depth (cm)	Al wt %	Ca wt %	Fe wt %	K wt %
40.20	7.21	3.30	4.17	2.10
40.38	7.27	3.11	4.18	2.11
40.55	7.57	2.92	3.99	2.19
40.77	7.23	3.42	4.01	2.13
40.94	7.35	3.28	4.06	1.90
41.14	7.40	3.22	4.23	2.22
41.34	6.96	3.77	4.22	2.00
41.54	7.39	2.83	3.97	2.16
41.74	6.95	3.41	4.20	1.83
41.91	7.43	2.95	3.94	2.25
42.14	7.18	2.94	4.06	2.14
42.26	7.50	3.23	4.10	2.13
42.43	7.30	3.28	4.08	1.90
42.64	7.23	3.11	4.13	2.12
42.68	7.19	3.16	4.00	2.11
42.88	7.51	3.11	3.99	2.15
43.03	7.12	3.12	4.04	2.13
43.21	8.17	3.34	3.97	2.17
44.52	7.44	2.92	4.08	2.18
44.68	7.40	2.85	4.01	2.19
44.88	7.55	2.79	4.06	2.20
44.96	7.15	2.66	4.16	2.15
45.16	7.67	2.55	4.11	2.19
45.28	7.61	2.52	4.10	2.28
45.41	7.42	2.56	4.20	2.17
45.61	7.40	2.38	4.17	2.12
46.02	7.86	3.38	4.32	2.13
46.42	8.06	2.71	4.48	2.20
46.58	8.21	1.80	4.25	2.44
46.76	7.60	2.55	4.68	1.94
46.95	7.13	2.77	4.24	2.04
47.32	7.31	2.55	4.21	2.21
47.51	7.55	2.52	3.94	2.15
47.70	7.46	2.43	4.00	2.19
47.90	7.45	2.54	4.05	2.20
48.00	7.44	2.29	4.13	1.93
48.20	7.30	2.77	3.97	2.14
48.39	7.48	3.09	4.08	2.14
48.74	7.93	3.04	4.01	2.15
48.94	7.32	2.60	4.15	2.17
49.14	6.95	2.47	3.67	2.18
49.34	7.24	2.79	3.96	2.13
49.54	7.31	2.50	4.25	2.13
49.90	7.47	2.47	4.13	2.17
50.10	7.28	2.39	4.07	2.08
50.50	7.12	2.24	4.33	1.80
50.70	7.49	2.89	4.15	2.21
50.90	7.70	2.65	4.15	2.25

Depth (cm)	Mg wt %	Na wt %	Si wt %	Ti wt %	P wt %
40.20	1.79	3.32	23.87	0.39	0.10
40.38	1.72	3.72	23.97	0.39	0.11
40.55	1.77	3.84	24.48	0.40	0.11
40.77	1.74	4.01	23.80	0.39	0.11
40.94	1.75	3.46	24.00	0.39	0.11
41.14	1.75	4.81	24.38	0.40	0.11
41.34	1.68	3.67	23.49	0.38	0.11
41.54	1.74	3.69	24.36	0.39	0.11
41.74	1.61	4.12	23.60	0.36	0.10
41.91	1.70	3.66	24.26	0.39	0.11
42.14	1.74	4.08	24.25	0.40	0.11
42.26	1.77	3.32	24.04	0.39	0.11
42.43	1.76	3.58	24.12	0.39	0.11
42.64	1.75	3.84	24.18	0.39	0.11
42.68	1.75	3.93	23.97	0.39	0.10
42.88	1.78	3.65	24.20	0.39	0.11
43.03	1.67	5.11	24.36	0.39	0.11
43.21	1.83	4.49	25.50	0.42	0.11
44.52	1.77	3.58	24.37	0.40	0.11
44.68	1.72	3.81	24.55	0.40	0.11
44.88	1.72	4.35	24.70	0.40	0.11
44.96	1.73	6.18	23.91	0.40	0.11
45.16	1.78	4.37	24.60	0.40	0.11
45.28	1.78	3.81	24.55	0.40	0.11
45.41	1.80	3.38	24.60	0.40	0.10
45.61	1.80	5.57	24.53	0.40	0.11
46.02	1.75	6.79	24.75	0.40	0.12
46.42	1.74	5.16	25.07	0.41	0.11
46.58	1.83	3.56	24.38	0.45	0.10
46.76	1.86	0.04	24.48	0.40	0.11
46.95	1.74	3.69	24.20	0.39	0.11
47.32	1.72	3.84	24.47	0.39	0.11
47.51	1.77	4.15	24.68	0.40	0.10
47.70	1.73	3.78	24.86	0.40	0.10
47.90	1.71	6.63	24.82	0.40	0.11
48.00	1.68	4.29	25.11	0.39	0.11
48.20	1.70	4.15	24.58	0.39	0.11
48.39	1.73	4.61	23.88	0.40	0.10
48.74	1.77	4.10	24.77	0.40	0.11
48.94	1.68	3.78	24.86	0.39	0.11
49.14	1.57	3.69	25.81	0.36	0.10
49.34	1.69	8.36	24.62	0.39	0.11
49.54	1.72	5.15	24.57	0.39	0.11
49.90	1.75	5.14	24.54	0.40	0.11
50.10	1.78	5.22	24.83	0.40	0.11
50.50	1.70	3.35	24.59	0.38	0.10
50.70	1.72	4.25	24.00	0.39	0.10
50.90	1.71	4.04	24.26	0.40	0.10

Depth (cm)	Al wt %	Ca wt %	Fe wt %	K wt %
51.10	7.15	2.77	4.51	2.10
51.18	7.65	2.32	4.20	2.24
51.28	7.94	3.04	4.46	2.08
51.38	7.88	2.25	4.43	1.88
51.58	7.69	2.40	4.17	2.21
51.63	7.86	2.46	4.25	2.27
51.73	7.55	2.36	4.56	2.16
51.79	7.75	2.41	4.39	2.28
52.15	8.44	1.73	4.25	2.18
52.53	7.55	2.39	4.14	2.20
52.73	7.75	2.49	4.25	1.96
52.94	7.74	2.31	4.46	2.21
53.14	7.68	2.34	4.47	2.19
54.20	7.41	2.56	4.26	2.03
54.40	8.05	2.24	4.34	2.09
54.54	7.64	2.45	4.25	2.18
54.60	7.69	2.94	4.21	1.97
55.30	7.63	2.83	4.03	2.18
55.50	7.50	2.44	4.09	2.17
55.67	7.55	2.49	4.11	2.23
55.81	7.49	2.62	4.22	2.18
55.98	7.91	2.72	4.16	2.15
56.21	7.37	2.83	3.90	2.10
56.38	7.57	2.67	4.08	2.15
56.58	7.50	2.62	4.04	2.24
56.78	7.51	2.36	4.10	2.01
56.98	6.88	2.18	2.50	2.25
	6.88	2.15	2.49	2.02
58.01	7.55	2.53	3.93	2.17
58.21	7.43	2.47	4.10	2.17
59.56	7.53	2.70	4.08	2.15
59.76	7.32	2.69	4.06	2.13
59.96	7.81	2.49	3.94	1.99
60.36	7.34	2.14	3.71	2.22
60.54	7.38	2.37	3.54	2.22
60.74	7.76	2.32	4.12	2.25
61.54	7.60	2.18	3.83	2.27
62.31	7.50	2.30	4.11	2.20
62.66	7.01	2.44	2.91	2.27
63.70	7.52	2.71	4.18	2.11
63.90	7.10	2.75	3.77	2.12
65.19	7.05	3.38	4.19	2.10
65.37	7.35	2.06	3.90	2.27
65.44	8.16	1.71	3.90	2.35
65.64	8.16	1.66	4.11	2.40
65.85	7.28	2.18	4.89	2.24
65.97	7.74	2.21	4.18	2.22
66.12	7.64	2.29	4.18	2.25

Depth (cm)	Mg wt %	Na wt %	Si wt %	Ti wt %	P wt %
51.10	1.73	6.09	23.74	0.40	0.10
51.18	1.78	3.69	24.77	0.41	0.10
51.28	1.81	0.42	24.53	0.40	0.11
51.38	1.88	3.49	24.48	0.42	0.10
51.58	1.78	3.70	24.73	0.41	0.10
51.63	1.72	3.93	23.93	0.42	0.10
51.73	1.87	4.01	24.44	0.41	0.10
51.79	1.73	4.53	23.99	0.42	0.10
52.15	1.83	3.72	24.77	0.44	0.10
52.53	1.76	5.25	24.83	0.41	0.11
52.73	1.75	3.98	24.61	0.41	0.10
52.94	1.86	3.53	24.61	0.42	0.10
53.14	1.88	3.16	24.47	0.42	0.10
54.20	1.56	5.76	23.86	0.39	0.10
54.40	1.68	3.89	24.60	0.43	0.10
54.54	1.64	3.65	24.46	0.40	0.10
54.60	1.69	3.86	23.66	0.40	0.10
55.30	1.77	3.36	24.54	0.40	0.09
55.50	1.75	3.79	24.64	0.40	0.11
55.67	1.77	4.82	24.74	0.40	0.10
55.81	1.74	3.78	24.60	0.40	0.10
55.98	1.71	4.06	24.56	0.40	0.10
56.21	1.72	3.31	24.82	0.39	0.10
56.38	1.76	3.75	24.82	0.39	0.11
56.58	1.71	3.72	25.00	0.39	0.10
56.78	1.74	4.06	24.98	0.39	0.11
56.98	0.94	3.58	29.98	0.30	0.10
	0.92	3.52	29.95	0.29	0.11
58.01	1.80	3.74	25.04	0.40	0.10
58.21	1.77	5.07	24.67	0.39	0.10
59.56	1.81	4.10	24.43	0.40	0.10
59.76	1.78	3.84	24.50	0.39	0.11
59.96	1.77	4.63	24.69	0.40	0.11
60.36	1.47	4.81	26.70	0.38	0.10
60.54	1.47	5.22	26.27	0.36	0.10
60.74	1.77	3.64	25.26	0.41	0.11
61.54	1.68	5.07	25.10	0.40	0.10
62.31	1.70	3.30	25.02	0.42	0.10
62.66	1.09	3.66	28.41	0.32	0.10
63.70	1.70	3.31	24.14	0.40	0.09
63.90	1.48	8.26	23.79	0.38	0.09
65.19	1.75	5.13	23.98	0.39	0.13
65.37	1.50	4.23	26.29	0.39	0.11
65.44	1.83	3.51	25.39	0.44	0.11
65.64	1.87	3.29	24.94	0.45	0.11
65.85	1.72	3.84	24.48	0.39	0.10
65.97	1.78	3.71	25.19	0.41	0.11
66.12	1.79	5.57	24.82	0.41	0.10

Depth (cm)	Al wt %	Ca wt %	Fe wt %	K wt %
66.30	8.16	2.21	4.20	1.98
66.35	7.85	2.11	4.23	2.21
66.40	6.94	1.89	3.96	2.00
66.69	8.58	2.22	4.69	2.34
67.02	7.58	2.44	4.05	1.93
67.22	7.61	2.62	4.33	2.16
67.37	7.62	2.42	4.43	2.14
67.77	7.20	2.82	4.68	2.09
67.97	7.99	2.02	2.97	2.46
68.17	7.81	2.11	4.14	2.26
68.54	7.65	3.05	4.20	2.20
68.73	7.66	2.94	4.20	1.91
68.93	7.96	2.19	4.07	2.30
69.68	7.05	3.27	4.27	2.09
69.88	7.26	2.95	3.78	2.16
70.04	7.51	2.61	3.97	2.20
70.22	7.19	2.53	4.15	2.12
70.42	7.76	2.62	4.21	1.76
70.62	7.06	2.42	3.99	2.15
70.68	7.63	2.27	4.09	1.90
70.88	7.56	2.58	4.29	1.95
71.08	7.56	2.43	4.11	2.17
71.35	7.50	2.67	4.16	2.17
71.57	7.65	2.54	4.25	2.08
71.96	7.47	2.64	4.27	2.15

Depth (cm)	Mg wt %	Na wt %	Si wt %	Ti wt %	P wt %
66.30	1.81	3.61	25.05	0.42	0.11
66.35	1.85	3.65	24.87	0.42	0.11
66.40	1.71	2.98	23.08	0.36	0.10
66.69	1.95	4.02	28.42	0.45	0.12
67.02	1.74	3.84	24.54	0.39	0.10
67.22	1.74	3.33	23.93	0.40	0.10
67.37	1.79	3.72	24.04	0.41	0.10
67.77	1.68	3.45	23.94	0.39	0.10
67.97	1.44	3.87	27.52	0.42	0.10
68.17	1.77	5.42	24.99	0.43	0.10
68.54	1.80	3.67	23.70	0.40	0.10
68.73	1.80	3.13	23.83	0.40	0.10
68.93	1.84	3.87	24.87	0.43	0.11
69.68	1.60	3.87	23.62	0.38	0.09
69.88	1.54	3.78	24.86	0.39	0.10
70.04	1.70	4.53	24.81	0.40	0.10
70.22	1.75	5.82	24.46	0.40	0.10
70.42	1.76	3.82	24.31	0.39	0.11
70.62	1.60	3.76	24.93	0.38	0.10
70.68	1.77	3.96	25.13	0.39	0.10
70.88	1.75	3.71	24.38	0.40	0.10
71.08	1.69	3.72	24.85	0.40	0.10
71.35	1.76	3.95	24.68	0.40	0.10
71.57	1.76	3.60	24.88	0.40	0.11
71.96	1.72	3.51	25.00	0.40	0.10

Appendix iii

Minor Element Data for ODP Site 893A

Depth	V ppm	Cr ppm	Mn ppm	Co ppm	Ni ppm	Cu ppm	Zn ppm	Rb ppm
0.45	186.7	129.1	353.2	16.4	51.0	31.9	112.5	136.7
0.66	212.4	119.9	312.1	14.2	51.0	30.8	100.7	123.1
2.21	191.1	128.6	359.9	16.9	50.7	32.5	116.2	135.9
2.62	213.7	124.0	313.6	14.4	54.1	30.4	104.9	120.9
2.83	210.2	131.7	336.8	14.2	54.6	30.3	107.1	122.7
3.63	223.9	172.8	380.4	14.5	53.8	31.7	112.6	118.3
3.84	216.4	123.7	367.6	19.7	50.9	33.5	113.7	129.4
4.04	186.1	144.6	412.5	17.5	49.6	30.3	112.4	138.6
4.44	224.6	129.0	385.4	14.5	51.9	30.9	107.9	121.9
4.63	228.0	129.2	376.2	16.4	52.6	32.4	113.9	126.7
4.85	213.0	125.2	360.8	23.8	53.1	32.2	116.8	124.9
5.24	220.3	123.1	386.6	18.5	51.1	34.7	115.6	130.7
5.45	187.7	129.9	401.5	16.7	51.4	29.9	113.1	129.9
5.83	219.4	131.7	380.1	18.0	51.9	33.0	117.5	132.1
7.04	215.8	130.8	389.6	17.8	54.4	33.2	129.6	130.7
7.44	211.6	124.0	357.6	17.1	56.2	32.2	114.1	125.7
7.63	230.9	133.1	376.9	19.3	58.2	35.1	120.6	131.5
7.85	200.3	122.4	400.4	20.9	52.3	33.7	113.0	130.2
8.65	206.4	143.9	398.5	19.1	62.4	35.5	127.0	143.0
	214.6	139.1	382.6	16.8	56.2	31.6	114.1	128.0
8.99	227.6	136.9	378.1	18.2	56.0	33.3	122.0	124.8
9.21	244.5	150.0	428.7	19.4	59.3	42.1	146.5	159.0
9.58	220.7	132.1	390.3	19.0	53.5	35.6	121.6	137.8
9.74	217.4	133.5	413.0	20.2	49.9	35.5	140.0	143.3
10.17	206.8	133.4	400.9	19.6	52.9	33.4	117.0	131.5
10.37	220.7	133.3	385.2	17.6	54.8	34.1	147.0	129.4
10.57	219.3	131.5	408.5	19.9	51.4	34.9	125.6	140.4
10.73	224.0	133.6	384.5	17.7	54.3	34.1	115.1	125.3
10.91	228.3	143.3	397.9	18.9	55.7	34.7	119.4	132.1
11.09	231.1	139.6	389.6	17.9	55.2	34.3	117.7	131.0
11.25	233.1	140.0	372.6	17.6	56.8	33.2	113.6	124.1
11.62	212.4	140.2	369.4	17.7	54.3	33.0	113.7	125.2
11.77	217.5	137.1	369.5	17.2	53.0	31.3	110.7	120.4
11.98	239.3	144.4	403.4	20.8	58.4	37.0	128.1	140.2
12.15	225.2	146.9	407.9	19.5	61.3	36.3	129.0	140.8
12.31	231.1	139.5	413.9	21.7	54.5	37.4	131.8	143.4
12.50	224.5	139.4	399.8	19.0	55.0	34.1	116.9	128.8
12.70	220.7	141.2	385.7	18.6	54.3	32.0	111.3	121.5
12.82	220.6	140.1	414.8	19.1	54.9	32.6	122.4	142.5
13.01	153.3	124.9	385.1	13.9	43.0	22.8	92.0	117.3
13.19	216.4	137.9	395.9	18.1	53.8	31.0	114.9	125.6
13.37	210.2	136.1	389.4	17.5	53.7	29.9	109.7	123.4
13.54	219.1	139.7	385.0	16.9	55.0	30.6	106.9	118.8
13.72	206.6	138.1	377.3	15.9	52.3	29.9	106.7	120.9

Appendix iii

Minor Element Data for ODP Site 893A

Depth	Sr ppm	Y ppm	Zr ppm	Ba ppm	Pb ppm	Nb ppm	I ppm	Br ppm
0.45	292.0	23.5	105.6	513.2	29.6	15.3	254.1	60.3
0.66	374.0	19.6	100.6	558.9	27.3	14.4	305.3	56.8
2.21	275.3	24.7	97.6	536.5	29.7	16.3	166.8	10.7
2.62	322.8	21.6	94.7	474.7	26.9	14.9	221.6	
2.83	359.5	22.1	106.8	505.7	23.5	15.1	227.4	13.3
3.63	371.9	21.7	109.5	517.7	24.8	15.1	220.0	29.4
3.84	325.6	28.7	106.5	533.2	31.0	15.1	187.5	11.9
4.04	274.8	27.7	121.8	560.9	23.3	15.6	74.4	
4.44	358.6	23.0	110.8	526.3	23.4	15.3	210.2	33.2
4.63	350.8	24.1	104.2	524.2	24.8	15.6	190.3	30.5
4.85	315.6	25.6	100.2	499.2	35.6	13.9	184.0	13.3
5.24	349.1	23.4	97.2	518.1	25.7	15.6	208.0	47.4
5.45	307.4	25.0	116.1	524.7	25.7	15.4	177.6	23.8
5.83	337.1	23.8	95.9	505.5	26.6	16.2	211.1	31.7
7.04	365.6	24.1	107.1	532.3	48.3	15.8	198.0	48.4
7.44	377.4	23.6	110.7	516.3	30.7	15.5	196.8	39.1
7.63	335.7	26.1	100.5	513.9	28.0	15.7	175.1	20.5
7.85	300.4	27.0	109.3	541.4	34.2	14.5	150.6	5.4
8.65	273.9	30.1	106.8	550.8	34.1	15.6	114.4	5.4
	334.5	24.3	103.4	512.3	27.7	15.4	160.6	13.3
8.99	353.2	24.3	102.0	505.5	27.6	14.8		
9.21	213.6	31.4	91.7	559.6	40.1	16.1	83.7	
9.58	302.8	26.9	98.2	518.0	26.5	15.8	140.5	9.4
9.74	256.9	27.9	97.0	534.9	31.0	15.4	111.4	5.2
10.17	309.6	26.5	99.3	520.2	31.3	15.0	143.8	5.7
10.37	335.3	26.2	101.0	514.8	28.1	15.5	151.3	16.2
10.57	275.3	27.5	102.7	542.5	32.2	15.5	118.6	1.7
10.73	349.1	26.3	102.3	533.4	29.0	15.5	137.8	8.3
10.91	328.1	27.4	109.3	534.3	29.6	15.1	147.3	2.1
11.09	326.1	27.3	102.4	537.1	31.2	15.8	136.4	5.3
11.25	365.1	25.2	99.2	523.5	33.2	15.4	148.7	0.3
11.62	321.3	25.8	99.9	515.2	29.1	15.0	133.1	4.9
11.77	347.6	25.2	101.9	506.7	25.9	14.6	132.4	7.1
11.98	263.3	28.5	94.4	511.5	31.3	14.8	111.7	
12.15	281.6	28.8	96.5	526.8	29.4	16.0	110.6	4.5
12.31	245.9	29.3	91.8	518.3	30.1	14.7	93.1	
12.50	335.0	26.8	101.0	536.5	34.7	15.5	125.1	
12.70	379.8	25.5	103.0	521.9	31.2	15.2	135.6	
12.82	262.7	26.4	88.9	515.8	30.1	14.7	126.5	
13.01	310.4	27.3	169.8	613.2	27.0	15.3	80.4	2.9
13.19	306.3	25.3	96.0	518.4	30.9	15.1	148.6	89.6
13.37	341.1	25.8	102.1	526.5	28.0	15.7	111.1	
13.54	369.3	24.1	102.3	529.8	26.1	15.3	132.9	12.1
13.72	342.1	25.1	103.7	514.4	19.7	15.5	129.9	

Depth	V ppm	Cr ppm	Mn ppm	Co ppm	Ni ppm	Cu ppm	Zn ppm	Rb ppm
13.88	219.9	143.5	382.2	16.7	54.2	31.9	108.4	120.7
14.07	220.0	138.9	399.8	18.6	54.0	33.4	119.1	132.5
14.27	213.9	140.5	406.4	18.2	53.3	32.9	116.1	130.8
14.47	221.9	144.0	404.7	18.0	55.6	33.0	113.8	125.8
14.67	209.9	139.0	384.0	15.7	53.0	29.8	106.6	121.3
14.85	245.2	143.9	438.8	20.2	54.7	43.8	146.5	167.6
15.26	210.9	141.8	404.8	16.5	52.3	29.1	107.7	124.2
15.66	217.7	138.1	369.1	16.1	53.3	29.9	105.6	119.4
16.15	170.5	116.6	359.7	16.6	44.7	26.2	96.5	114.2
16.35	213.9	143.9	511.9	18.7	62.8	38.8	129.3	145.2
16.52	221.9	137.4	454.8	23.8	52.4	34.1	119.8	133.8
16.92	229.8	146.8	464.9	20.7	57.7	34.2	116.5	133.6
17.12	219.3	135.9	421.8	19.8	52.5	30.5	109.2	122.2
17.32	221.6	154.8	405.2	19.2	53.5	30.8	109.0	126.5
17.72	222.3	154.4	416.2	18.1	65.2	37.8	133.3	157.0
17.92	195.4	135.3	411.4	19.7	50.0	30.7	116.7	140.3
18.12	199.2	141.4	423.5	20.5	50.3	31.1	117.2	141.3
18.32	193.5	133.4	406.7	19.6	50.1	30.6	115.9	140.4
18.52	191.1	135.3	407.9	18.3	49.7	30.1	115.0	139.5
18.72	186.6	132.0	396.3	18.8	49.3	29.0	111.5	136.0
19.12	186.1	136.8	391.3	18.6	50.5	28.8	111.5	134.6
19.72	192.5	139.3	400.6	19.2	51.2	30.1	119.3	137.6
20.27	193.8	140.5	408.6	20.0	51.2	29.4	112.5	134.7
20.66	215.6	137.2	432.8	18.9	50.5	32.6	113.0	133.8
20.86	203.9	126.5	416.1	21.8	48.7	30.9	113.5	131.8
21.06	211.7	126.9	428.2	22.8	47.0	32.1	115.1	135.1
21.26	214.1	135.6	434.7	22.3	50.9	33.2	115.8	135.1
21.46	216.1	136.6	423.7	20.9	52.1	33.6	116.5	135.9
21.66	216.6	135.3	431.8	20.7	49.6	33.6	116.0	134.6
21.86	212.6	127.9	407.1	21.6	49.3	33.0	113.7	135.5
22.20	211.1	126.5	426.8	20.8	47.3	32.8	123.2	135.9
22.38	210.3	125.6	414.7	22.2	47.8	33.1	120.0	135.6
22.87	213.2	140.8	430.8	18.6	48.4	31.8	121.1	135.9
23.07	205.4	139.0	417.3	20.4	50.3	31.7	114.8	130.5
23.26	217.4	139.9	422.1	20.9	51.2	33.0	113.6	133.2
23.48	207.6	136.5	405.8	20.9	52.2	32.9	121.8	131.4
23.61	205.6	139.5	409.8	19.6	51.6	32.2	117.4	129.0
23.81	199.3	133.3	411.4	19.9	50.2	32.0	112.1	127.0
24.01	187.3	140.4	422.7	18.2	47.3	29.7	112.9	130.2
24.21	189.9	133.0	422.8	18.6	47.2	30.6	110.9	136.1
24.41	192.9	133.9	425.2	18.8	47.4	30.3	114.9	137.0
24.61	190.0	139.5	425.6	18.2	46.7	28.9	110.9	131.0
24.80	161.5	134.5	381.2	15.2	41.4	23.7	90.0	119.2
25.00	187.1	140.6	400.9	17.6	50.5	29.1	108.5	132.0
25.20	186.9	138.5	404.4	18.4	49.9	29.6	108.8	132.0
25.40	186.8	146.7	408.1	17.9	49.7	29.7	105.9	131.8
25.7	197.6	141.7	428.4	18.8	50.5	30.7	113.9	135.0
25.9	188.6	133.6	420.4	18.1	46.5	30.7	110.2	133.3

Depth	Sr ppm	Y ppm	Zr ppm	Ba ppm	Pb ppm	Nb ppm	I ppm	Br ppm
13.88	353.8	24.6	101.4	538.6	26.1	15.3	135.2	13.0
14.07	298.8	26.9	97.9	523.5	30.5	15.7	118.0	
14.27	314.5	27.1	100.4	531.8	27.7	15.6	109.6	
14.47	334.8	25.4	97.9	521.7	26.6	14.6	137.2	18.3
14.67	360.8	24.6	99.4	526.3	24.0	15.7	128.1	5.4
14.85	183.1	29.9	87.6	597.3	25.2	16.6	79.9	
15.26	357.8	25.1	103.6	545.5	28.3	15.1	131.8	
15.66	381.1	24.5	98.9	522.4	26.3	15.7	133.1	2.7
16.15	352.2	25.9	153.7	549.5	36.5	14.3	81.4	14.4
16.35	220.6	33.3	110.8	631.4	24.9	16.7	65.9	
16.52	301.8	27.2	92.0	525.0	58.0	15.0	123.3	1.1
16.92	315.1	26.4	94.6	503.5	30.1	14.9	129.2	
17.12	360.8	25.6	97.7	532.7	33.1	15.8	122.9	
17.32	316.0	25.4	103.1	512.9	34.1	14.7	132.7	8.0
17.72	201.4	31.0	101.0	585.2	22.9	16.1	70.4	
17.92	229.0	27.6	109.8	520.1	32.2	15.1	109.8	16.5
18.12	251.9	27.6	116.8	558.2	32.4	15.3	113.8	31.0
18.32	242.1	28.3	105.7	523.9	35.6	15.4	112.9	19.3
18.52	240.0	26.6	107.5	525.0	32.2	15.0	115.5	23.8
18.72	251.5	26.0	110.9	508.6	26.2	15.0	113.9	22.7
19.12	218.7	25.2	104.3	505.4	29.1	14.6	120.3	18.4
19.72	232.4	26.9	104.3	502.6	26.1	14.8	115.5	13.9
20.27	235.6	26.7	107.3	506.1	29.0	14.5	164.5	30.4
20.66	274.8	28.1	103.3	542.9	29.8	15.2		
20.86	269.0	26.3	98.0	481.1	33.1	14.4	122.0	9.2
21.06	251.3	27.0	98.9	508.1	34.4	14.9	123.5	8.7
21.26	247.8	27.0	97.2	508.1	31.7	15.0	126.2	4.2
21.46	277.6	27.6	97.3	524.1	32.0	15.2	122.3	7.8
21.66	270.0	27.9	101.0	521.6	28.1	15.7	121.3	11.2
21.86	254.7	28.0	99.5	493.1	32.7	15.1	111.4	
22.20	289.0	27.3	102.2	546.0	33.6	15.8	105.5	0.9
22.38	255.8	26.3	97.3	519.5	32.6	14.6	116.8	8.7
22.87	266.9	26.9	99.8	546.3	26.2	14.7	107.8	7.2
23.07	275.5	26.4	101.0	521.4	32.1	14.5		
23.26	282.6	27.1	99.7	518.4	29.2	15.0	113.1	8.1
23.48	295.7	26.5	103.7	545.6	32.2	14.9	121.5	9.4
23.61	300.7	25.6	101.9	542.1	30.9	14.5	120.3	3.7
23.81	270.2	25.8	100.4	505.7	28.5	13.9	118.6	0.0
24.01	246.4	27.2	112.8	549.2	30.1	15.3	96.6	9.5
24.21	261.4	27.0	110.0	540.9	26.1	16.0	114.6	22.6
24.41	243.6	27.4	106.2	541.1	30.4	15.2	102.3	24.8
24.61	249.7	26.3	105.4	543.2	27.0	14.8	106.6	35.9
24.80	269.5	26.1	138.8	605.1	29.0	13.9	80.9	18.5
25.00	259.3	26.3	111.4	523.7	30.2	14.7	118.0	39.6
25.20	252.5	26.7	112.0	518.6	25.4	14.5	120.2	39.4
25.40	252.3	26.1	106.3	524.0	25.7	14.3	128.3	49.9
25.7	244.8	27.4	107.1	532.4	30.4	14.6		
25.9	265.0	28.6	110.5	541.5	24.9	15.2	112.5	31.0

Depth	V ppm	Cr ppm	Mn ppm	Co ppm	Ni ppm	Cu ppm	Zn ppm	Rb ppm
26.1	173.6	137.1	405.3	15.8	45.6	27.0	96.7	123.6
26.2	188.3	140.8	430.4	18.4	49.7	31.0	111.6	134.9
26.4	187.5	132.1	405.6	18.8	48.1	30.3	109.6	133.3
26.6	197.5	144.3	430.7	18.5	50.4	31.9	113.7	137.4
27.0	193.9	144.1	413.4	18.4	49.7	29.6	110.0	131.9
27.2	185.3	136.6	409.2	19.0	48.1	30.9	110.7	134.1
27.4	192.7	147.9	438.7	18.9	48.9	31.5	111.7	135.1
27.6	186.3	139.4	411.3	18.9	49.4	31.1	109.5	132.9
27.8	191.4	136.1	404.7	19.3	49.9	31.2	110.8	131.8
27.9	190.5	139.5	409.0	18.9	50.5	30.2	113.3	132.1
28.1	192.2	137.8	396.7	18.9	52.0	30.8	111.7	134.0
28.3	191.4	141.8	401.2	17.9	51.0	29.9	111.7	133.3
28.5	181.0	140.9	403.9	18.2	48.5	29.6	105.9	132.4
28.7	178.9	135.9	404.4	17.9	49.9	29.5	106.5	131.6
28.9	182.0	138.2	408.1	19.2	49.4	30.0	108.7	131.7
29.1	189.1	143.3	421.9	19.1	50.3	31.0	112.2	137.2
29.3	187.1	138.0	413.6	19.5	51.1	30.9	111.3	139.7
29.4	181.1	136.5	405.8	17.6	50.6	31.3	110.1	136.4
29.6	185.2	148.2	419.6	19.1	50.5	31.7	112.2	134.5
29.8	179.1	139.5	399.5	18.6	50.4	31.4	110.4	135.9
30.0	187.2	140.5	409.5	18.6	53.8	31.0	113.6	136.9
30.3	185.3	144.1	408.7	19.1	51.3	31.0	112.6	135.7
30.3	186.6	141.6	404.8	18.7	52.2	31.5	113.5	138.6
30.5	191.0	145.0	413.1	17.5	51.2	31.5	111.3	136.7
30.7	184.7	139.2	407.7	17.2	48.1	30.9	108.2	134.3
30.8	179.4	133.7	396.1	17.4	49.2	30.2	105.5	130.2
31.0	180.5	139.7	413.2	17.8	49.1	31.5	108.5	133.0
31.2	180.0	140.0	408.6	18.3	50.0	30.9	112.8	133.7
31.4	182.4	140.5	406.2	17.9	48.7	30.8	111.3	133.2
31.6	182.1	140.0	397.7	18.2	50.8	30.6	111.1	135.3
31.7	194.0	145.0	420.0	18.0	50.4	31.0	115.1	138.5
31.9	189.4	142.5	399.5	18.1	52.2	31.7	111.2	135.5
32.3	184.3	144.1	406.9	17.5	50.7	31.6	111.8	136.7
32.5	177.1	140.2	391.6	18.1	50.4	30.6	110.3	131.8
32.9	180.9	139.4	399.3	17.0	46.7	29.8	108.0	131.7
33.0	180.5	139.8	398.5	18.5	48.3	32.1	109.5	132.8
33.2	168.7	132.2	368.8	15.0	46.5	27.4	95.0	119.0
33.4	187.7	136.5	409.8	18.2	47.4	30.2	108.4	133.2
33.6	185.1	136.9	403.7	17.2	49.3	30.8	110.3	135.8
33.8	172.1	141.6	395.4	16.7	46.3	27.9	98.7	126.5
34.0	183.3	137.2	394.4	18.3	49.3	31.3	109.7	132.3
34.2	177.1	134.9	385.8	20.2	49.2	32.4	109.1	130.4
34.4	183.3	139.8	390.4	18.9	49.9	32.9	110.0	133.3
35.2	183.3	142.9	412.7	18.1	49.8	30.9	154.3	137.0
35.4	180.2	135.3	399.8	17.4	48.5	30.3	110.7	135.2
35.6	183.4	135.0	404.9	19.4	49.4	31.9	119.1	134.7
35.8	185.0	140.1	421.7	17.8	47.5	31.0	113.9	140.6
36.0	178.9	145.6	426.8	18.2	49.5	31.5	111.0	139.9

Depth	Sr ppm	Y ppm	Zr ppm	Ba ppm	Pb ppm	Nb ppm	I ppm	Br ppm
26.1	261.6	26.3	128.0	572.7	29.3	14.6	98.8	23.3
26.2	276.6	27.1	113.1	556.1	26.3	15.1	121.9	32.0
26.4	251.7	26.6	108.8	527.4	30.7	14.9	116.7	21.4
26.6	267.6	28.0	115.5	555.5	27.2	15.3	112.8	30.9
27.0	262.2	26.6	106.1	525.7	25.3	15.1	116.6	25.2
27.2	266.9	27.2	109.9	525.5	24.8	15.2	111.3	24.4
27.4	275.9	27.6	113.9	558.2	25.9	15.3	120.7	36.3
27.6	273.6	26.5	108.1	523.6	30.2	15.2	123.2	33.1
27.8	274.3	26.7	105.5	528.7	28.6	14.8	117.4	13.9
27.9	271.8	26.6	107.4	521.4	29.1	15.3	124.5	24.2
28.1	267.4	26.8	106.4	522.4	26.2	15.5	121.0	19.1
28.3	262.6	25.9	107.0	529.5	27.4	15.0	111.0	34.5
28.5	278.6	26.8	123.5	545.3	26.4	14.8	115.0	28.2
28.7	273.3	26.4	111.5	531.9	27.2	15.2	121.1	26.9
28.9	267.9	26.5	110.2	532.2	30.0	15.2	118.1	20.0
29.1	243.3	28.1	115.7	530.7	26.3	14.9	124.6	11.9
29.3	252.3	27.3	114.3	539.3	31.6	14.9	131.1	29.2
29.4	276.5	26.7	114.6	526.1	28.2	15.7	118.8	21.6
29.6	269.7	26.8	117.8	558.6	31.7	14.8	119.9	44.5
29.8	256.7	26.7	110.2	509.4	31.2	15.1	123.4	24.5
30.0	282.7	27.3	106.7	525.9	30.6	15.1	120.2	12.6
30.3	268.0	26.9	109.0	525.0	30.7	14.5	115.8	22.8
30.3	259.0	27.9	121.2	522.8	29.0	15.2	124.5	21.6
30.5	267.4	26.7	110.8	526.5	30.9	15.2	126.0	18.2
30.7	292.4	26.6	115.1	540.0	29.3	15.3	126.4	20.9
30.8	299.5	26.1	113.1	526.3	26.1	15.3	121.6	21.7
31.0	287.4	26.7	116.0	543.9	28.0	15.3	121.1	22.0
31.2	293.1	26.7	111.4	533.4	26.6	15.2	128.9	29.3
31.4	294.0	26.7	114.2	539.3	24.2	15.3	119.0	22.5
31.6	278.4	26.7	111.9	528.2	29.4	15.6	120.2	23.7
31.7	261.6	27.6	111.0	548.1	27.3	15.2	116.0	30.4
31.9	294.2	27.1	114.5	525.7	29.7	15.0	121.2	18.8
32.3	276.2	26.5	111.8	516.9	29.6	15.4	115.8	20.9
32.5	275.3	25.8	112.4	521.2	30.3	14.7	124.7	22.5
32.9	285.5	26.2	112.0	538.0	28.0	15.0	115.9	17.3
33.0	261.7	26.1	108.2	509.2	34.2	15.1	122.1	16.4
33.2	411.3	25.3	122.7	551.8	28.4	16.1	110.8	25.9
33.4	299.2	26.2	117.2	548.3	26.3	15.3	117.7	23.5
33.6	304.4	27.0	114.6	545.8	30.3	15.8	117.9	26.0
33.8	315.7	26.2	131.4	579.6	27.1	14.9	104.2	25.1
34.0	287.9	26.4	111.3	535.3	30.5	14.9	133.3	19.9
34.2	268.9	26.2	101.6	517.6	33.3	14.6	121.5	23.2
34.4	276.4	26.1	112.0	537.3	26.1	15.1	126.4	35.2
35.2	263.6	26.7	113.5	533.3	33.9	15.6	131.3	21.8
35.4	255.8	25.8	106.5	529.0	28.8	14.4	140.5	21.3
35.6	266.0	27.3	107.2	539.8	32.6	15.0	130.1	26.7
35.8	261.0	27.6	111.7	538.3	24.5	15.1	122.4	15.2
36.0	268.6	27.5	119.2	571.7	30.5	15.7	132.6	11.7

Depth	V ppm	Cr ppm	Mn ppm	Co ppm	Ni ppm	Cu ppm	Zn ppm	Rb ppm
36.0	183.8	143.4	417.1	17.3	47.7	30.7	111.9	138.5
36.2	195.3	139.6	412.7	21.5	51.2	34.0	109.1	136.0
36.3	182.5	135.9	413.5	18.1	48.6	31.0	111.3	135.5
36.5	183.2	137.8	406.7	17.5	48.4	29.8	108.4	135.6
36.7	155.7	137.0	377.3	14.3	43.0	25.2	92.3	124.9
36.9	182.7	136.8	405.2	17.7	48.4	34.6	109.7	135.6
37.1	187.1	137.5	406.4	18.2	49.4	30.1	110.3	138.3
37.3	182.0	134.9	403.1	17.5	47.6	28.8	105.9	134.1
37.5	182.7	140.6	412.6	17.3	49.4	30.4	108.8	136.1
37.7	184.3	135.1	418.7	17.7	48.6	32.0	109.2	138.2
37.8	177.3	129.8	409.8	17.7	47.7	28.8	106.5	135.0
38.0	173.5	132.4	399.0	17.0	46.7	29.5	113.1	134.7
38.2	180.8	132.0	400.9	18.5	49.0	30.2	109.7	137.7
38.4	182.7	137.5	408.8	17.3	48.5	29.7	108.0	135.9
38.6	179.1	130.3	396.0	19.3	48.3	30.4	114.9	136.9
38.8	186.8	134.2	403.0	19.3	50.0	31.1	113.9	141.0
38.9	188.0	139.9	415.9	18.8	49.4	30.5	111.5	140.7
39.1	181.9	136.9	396.6	18.6	49.8	30.8	110.4	138.9
39.2	187.4	136.6	413.4	17.5	46.6	29.1	109.4	135.8
39.5	184.3	137.7	411.5	17.9	47.6	29.1	109.6	136.3
39.6	186.6	138.3	410.4	17.0	46.7	29.8	119.3	135.8
39.8	188.6	140.8	408.6	18.4	49.3	30.7	112.0	137.5
40.0	178.3	141.1	398.1	18.2	50.0	31.1	111.0	135.2
40.2	186.8	145.2	411.4	19.5	48.9	30.6	111.4	137.2
40.6	183.6	142.6	406.9	17.3	49.0	29.9	110.9	136.7
40.8	179.6	143.1	400.8	17.4	49.4	29.7	108.7	135.2
40.9	186.0	144.1	412.8	18.1	48.6	31.5	109.5	136.4
41.1	194.1	147.3	425.9	18.1	49.5	31.3	111.2	137.1
41.3	188.1	142.1	402.1	18.0	51.3	32.0	108.1	132.1
41.5	187.3	144.8	421.3	17.4	50.8	30.1	112.5	134.3
41.7	193.7	136.5	405.2	19.9	50.3	31.9	104.9	128.3
41.9	240.2	136.4	418.7	20.8	53.5	45.1	145.8	158.3
42.1	183.0	133.7	414.7	18.3	48.5	30.7	109.2	136.5
42.3	176.5	135.5	402.1	17.9	49.1	30.7	107.6	135.5
42.4	176.4	139.1	396.8	17.3	50.6	31.3	109.0	135.3
42.6	182.1	143.1	412.9	17.9	50.3	29.8	108.2	134.5
42.7	183.3	137.9	405.1	17.1	49.0	30.6	109.3	135.5
42.9	186.1	137.8	408.5	17.2	49.9	30.1	109.8	135.5
44.5	182.4	131.3	412.6	18.5	48.1	29.5	108.4	135.0
44.7	190.9	127.7	396.6	19.7	48.5	31.5	103.8	128.6
44.9	182.6	136.7	406.9	17.8	47.7	29.2	108.2	134.8
45.0	180.6	134.2	412.9	19.4	47.9	30.2	109.3	137.8
45.2	190.0	138.9	420.3	18.9	48.7	31.1	110.2	138.9
45.3	188.9	137.0	415.0	18.8	50.3	30.8	111.6	138.4
45.4	188.9	138.6	418.3	18.7	49.5	30.4	111.3	138.3
45.6	192.2	146.3	423.1	18.4	52.0	31.4	113.5	141.0
46.6	188.4	133.5	408.8	17.6	48.6	29.8	108.3	136.3
46.8	215.4	141.9	453.8	20.1	58.2	39.3	129.0	153.2

Depth	Sr ppm	Y ppm	Zr ppm	Ba ppm	Pb ppm	Nb ppm	I ppm	Br ppm
36.0	257.4	27.4	113.0	535.4	24.5	15.0	128.7	29.2
36.2	262.2	27.0	108.0	532.5	31.5	14.5	138.5	13.7
36.3	288.3	26.8	115.0	555.7	24.0	14.9	126.9	35.8
36.5	277.1	26.5	121.2	562.0	24.6	14.5	135.2	42.8
36.7	287.8	26.4	151.5	592.0	26.2	14.7	106.3	29.8
36.9	286.8	26.8	116.5	556.2	27.9	15.3	121.5	34.5
37.1	277.9	27.5	116.8	553.8	24.1	15.5	128.7	39.5
37.3	302.0	26.5	120.4	572.0	26.2	15.5	120.8	35.3
37.5	315.3	27.4	118.6	566.6	26.4	15.8	133.5	36.3
37.7	258.5	27.1	123.4	552.2	27.6	15.5	124.3	37.9
37.8	294.4	27.7	122.9	557.9	32.3	14.8	115.6	27.1
38.0	284.8	27.2	115.9	544.3	24.8	15.6	122.0	42.8
38.2	276.0	26.8	120.3	535.0	30.0	15.3	131.8	41.5
38.4	292.4	26.4	135.2	571.1	30.6	15.8	130.2	39.8
38.6	299.9	27.5	129.2	548.4	28.4	15.2	121.1	29.1
38.8	273.7	27.2	114.9	551.5	28.2	15.7	121.0	30.0
38.9	248.8	28.1	118.9	558.5	26.0	15.2	116.6	50.4
39.1	279.5	28.0	119.0	528.3	26.3	15.8	128.2	30.2
39.2	288.0	27.5	118.7	562.6	23.1	15.8	113.6	37.1
39.5	285.3	27.3	121.3	559.2	25.2	14.6	113.5	41.3
39.6	295.4	27.2	120.1	559.7	20.7	15.7	121.1	29.9
39.8	294.1	26.5	117.0	556.7	29.1	15.5	121.9	42.1
40.0	300.6	27.2	117.9	543.2	32.7	15.0	131.7	37.4
40.2	280.4	27.0	120.8	566.5	25.1	14.8	122.0	32.3
40.6	274.0	27.3	120.1	553.3	23.0	15.4	121.2	44.6
40.8	298.5	26.1	117.4	544.1	35.8	15.3	130.7	36.4
40.9	295.6	25.8	118.8	561.5	31.0	15.6	134.3	35.1
41.1	288.0	27.1	122.0	572.0	27.6	15.6	128.9	36.7
41.3	312.2	26.0	120.9	554.7	32.5	15.4	131.2	34.1
41.5	263.0	26.3	112.2	546.4	26.7	15.8	118.6	29.4
41.7	304.9	26.3	116.1	542.1	31.7	14.9	133.3	24.3
41.9	202.1	31.4	87.8	577.7	25.8	16.7	115.0	25.1
42.1	279.5	26.9	123.8	561.9	29.1	15.2	127.3	41.6
42.3	288.8	26.5	116.8	546.0	24.9	14.8	133.4	39.4
42.4	293.3	26.9	116.3	553.9	30.0	14.8	135.4	43.2
42.6	281.3	26.3	117.8	546.6	25.5	15.2	120.1	39.4
42.7	289.1	26.6	118.9	554.2	28.8	15.3	127.9	33.7
42.9	285.5	26.8	115.3	550.1	29.1	15.5	127.9	33.2
44.5	269.1	27.7	117.5	540.8	30.3	15.4	118.0	21.3
44.7	307.5	25.5	117.5	527.6	30.4	15.5	112.5	20.8
44.9	282.8	27.5	118.8	549.7	24.4	15.1	114.1	28.9
45.0	262.5	27.1	120.5	541.2	28.7	15.0	129.2	51.6
45.2	247.0	27.6	118.2	548.5	30.0	15.1	117.8	25.2
45.3	254.6	27.4	120.0	539.4	28.7	15.6	122.0	11.8
45.4	252.3	27.7	118.8	553.3	28.8	15.5	113.2	29.7
45.6	247.0	26.9	119.9	539.2	32.5	15.1	129.1	30.7
46.6	273.6	27.0	121.4	543.5	27.6	15.4	121.1	15.3
46.8	208.9	30.6	106.3	574.7	26.7	16.0		

Depth	V ppm	Cr ppm	Mn ppm	Co ppm	Ni ppm	Cu ppm	Zn ppm	Rb ppm
47.0	182.9	134.5	417.1	18.7	49.5	31.2	109.3	134.0
47.2	179.7	136.9	405.4	18.7	50.1	30.0	106.7	134.1
47.3	182.9	141.2	403.6	18.8	50.5	30.5	109.5	137.9
47.5	186.8	143.3	415.5	17.8	53.6	31.6	110.2	137.4
47.9	177.3	136.3	406.7	18.2	49.5	28.6	107.0	135.4
48.0	178.5	137.6	409.0	18.2	48.7	29.1	105.2	133.8
48.2	187.3	138.2	413.1	17.3	50.9	30.4	107.4	135.2
48.4	199.1	127.8	416.4	18.5	49.0	32.6	111.6	140.3
48.6	185.8	139.2	393.7	18.2	47.0	29.6	103.2	133.8
48.9	180.1	135.4	394.9	18.2	49.8	29.9	106.9	135.7
49.1	174.7	134.7	400.7	16.6	46.6	27.4	100.9	132.0
49.3	173.2	134.5	407.9	17.5	49.6	28.0	104.9	131.3
49.5	181.3	131.5	400.1	18.9	50.2	29.6	109.2	137.2
49.9	180.5	132.5	404.2	18.8	49.8	29.3	107.7	136.6
50.1	178.6	138.3	403.7	18.2	49.2	29.4	108.6	137.2
50.3	173.4	136.8	413.3	17.5	46.2	27.7	103.4	133.4
50.5	179.1	131.9	408.9	19.9	49.1	30.1	106.3	132.9
50.7	196.0	129.4	413.0	19.3	48.5	30.8	111.5	136.2
50.9	190.6	128.3	424.4	20.7	47.8	30.8	110.7	138.0
51.1	197.7	122.5	427.5	20.5	45.0	32.2	112.3	137.7
51.2	178.1	122.8	417.3	19.3	46.9	30.6	109.6	137.9
51.4	191.1	126.2	420.5	20.8	47.3	30.7	113.5	139.1
51.5	187.7	120.5	426.1	19.8	45.7	31.1	112.8	137.4
51.6	185.8	121.6	416.5	19.2	45.1	29.7	108.3	135.0
51.6	201.0	118.8	435.2	19.3	44.0	34.4	115.7	139.7
51.7	189.1	132.1	417.9	21.2	47.0	30.7	111.9	138.7
51.8	193.5	121.8	422.8	20.6	45.0	33.5	116.7	143.2
52.2	212.1	127.7	413.3	19.5	49.6	37.5	127.7	152.7
52.4	178.0	123.5	411.3	21.1	46.4	31.5	111.2	137.5
52.5	182.5	121.6	415.8	19.4	45.7	30.3	110.2	136.9
52.7	185.6	123.6	417.3	19.4	45.2	31.0	109.0	135.7
52.9	192.9	126.2	427.6	20.4	47.2	31.8	113.0	138.4
53.1	176.4	132.7	411.0	17.9	46.3	29.4	106.4	134.6
54.2	195.9	117.9	415.5	19.8	46.2	34.2	110.2	133.5
54.4	195.1	119.0	453.2	19.6	42.5	32.6	114.9	143.3
54.5	196.3	133.4	420.2	20.0	47.4	32.2	111.5	137.5
54.6	199.9	123.6	413.8	19.6	47.3	33.4	114.8	137.8
55.3	180.7	125.5	413.2	18.3	46.1	31.5	110.7	138.6
55.5	180.2	124.7	422.5	18.2	47.2	30.7	118.3	138.5
55.8	171.7	127.3	416.0	18.9	44.8	30.1	106.6	134.3
56.0	171.0	117.8	398.8	19.0	45.1	30.6	110.4	135.6
56.2	165.0	126.7	395.9	17.5	46.2	29.6	104.2	133.6
56.4	172.0	129.2	403.4	18.3	47.8	30.4	104.7	133.8
56.6	174.8	130.7	405.6	17.9	46.9	29.7	107.5	134.6
56.8	173.0	128.0	406.9	17.8	46.2	29.0	104.5	134.1
56.8	178.2	135.3	399.9	18.1	50.2	30.4	109.5	135.2
57.0	105.1	126.7	294.9	9.3	30.8	16.0	60.3	105.2
58.0	181.5	133.9	406.2	17.6	48.4	29.9	110.1	135.1

Depth	Sr ppm	Y ppm	Zr ppm	Ba ppm	Pb ppm	Nb ppm	I ppm	Br ppm
47.0	264.1	27.0	118.1	550.5	31.0	15.1	119.2	39.6
47.2	273.1	26.6	122.1	531.3	28.6	14.7	121.2	39.3
47.3	246.7	26.3	118.8	540.4	28.8	15.0	125.3	29.9
47.5	244.2	27.4	113.7	538.9	27.3	15.1	122.2	16.9
47.9	257.6	26.9	121.5	538.9	31.3	15.0	121.9	25.1
48.0	250.1	27.6	125.7	542.1	30.7	14.9	122.3	23.2
48.2	262.5	27.2	115.4	537.0	32.5	14.7	121.0	25.5
48.4	298.6	28.4	119.1	550.6	28.0	15.7	117.8	10.9
48.6	260.1	27.1	124.9	563.3	32.7	14.8	117.4	19.6
48.9	262.0	26.5	116.9	535.4	30.1	14.2	123.2	22.6
49.1	252.3	24.5	112.0	557.5	24.2	14.4	118.4	32.2
49.3	254.8	25.5	122.1	542.1	27.1	15.0	121.4	17.3
49.5	251.4	26.7	117.4	528.9	29.2	15.1	133.1	24.3
49.9	249.0	26.4	118.5	540.3	27.3	14.9	126.1	24.0
50.1	246.0	27.0	123.3	530.0	27.7	15.2	126.5	29.0
50.3	252.1	27.0	129.6	558.3	32.6	15.2	111.6	21.7
50.5	242.9	26.7	122.9	519.3	38.6	14.0	129.9	23.2
50.7	292.8	27.7	110.0	539.1	27.7	16.0	115.1	24.4
50.9	243.6	27.4	112.6	548.3	24.5	15.7	109.7	21.5
51.1	294.0	28.0	114.0	550.1	30.6	16.1	122.3	19.9
51.2	245.3	28.0	113.3	544.2	36.2	15.7	105.6	16.7
51.4	240.2	27.9	111.0	544.9	24.2	16.3	110.7	24.8
51.5	282.7	27.8	114.4	542.7	30.5	15.6	113.1	25.1
51.6	248.5	27.3	118.3	541.6	25.1	15.7	103.2	8.6
51.6	254.7	28.0	107.4	549.9	26.9	15.9	109.9	12.9
51.7	245.4	28.5	111.2	548.5	25.0	15.4	109.9	28.5
51.8	257.3	29.3	113.6	564.3	25.4	16.3	113.7	9.4
52.2	210.5	29.8	100.0	559.4	30.4	16.4	108.9	18.6
52.4	245.1	27.0	114.6	541.9	29.2	14.6	116.8	28.1
52.5	252.2	26.7	114.2	536.7	29.1	15.9	108.2	15.1
52.7	254.1	27.5	116.1	542.9	27.2	16.2	105.5	16.1
52.9	242.7	27.4	114.1	556.8	25.3	15.0	113.5	25.0
53.1	272.0	26.5	123.9	553.5	28.0	15.1	101.0	25.3
54.2	282.0	27.6	121.2	539.2	29.6	15.5	118.5	21.6
54.4	260.9	27.3	105.4	588.8	27.3	16.8	95.8	14.9
54.5	268.4	27.2	113.8	558.1	32.3	15.4	116.4	24.0
54.6	303.9	26.9	109.8	550.6	25.8	16.9	118.3	27.4
55.3	275.5	26.7	112.7	527.2	25.8	15.8	120.5	27.2
55.5	252.4	26.9	114.7	551.2	28.8	15.4	115.7	42.2
55.8	258.7	26.7	115.0	558.7	27.6	15.4	118.1	50.2
56.0	272.1	27.3	120.2	559.2	26.1	15.1	122.0	36.2
56.2	270.9	26.0	126.1	540.6	27.4	14.8	129.4	47.8
56.4	261.4	25.9	120.6	534.0	30.0	14.7	121.5	42.8
56.6	255.6	26.1	131.1	551.0	29.2	14.7	110.1	34.2
56.8	262.7	27.2	123.4	555.3	27.6	15.0	119.5	36.3
56.8	284.0	26.2	115.1	541.2	31.4	14.7	108.0	33.1
57.0	295.2	23.7	244.3	681.7	23.3	11.4	60.8	5.8
58.0	261.0	26.7	126.5	525.4	25.6	15.4	125.7	31.8

Depth	V ppm	Cr ppm	Mn ppm	Co ppm	Ni ppm	Cu ppm	Zn ppm	Rb ppm
58.2	178.0	132.9	402.3	18.0	48.2	30.2	106.0	134.3
59.6	193.5	126.7	416.2	18.2	48.6	31.5	111.8	136.9
59.8	180.0	142.3	408.1	18.1	49.4	29.8	111.7	134.1
60.0	196.0	122.5	427.1	18.8	46.5	31.9	110.3	136.8
60.4	153.2	123.0	376.6	15.8	40.8	24.8	92.3	125.7
60.5	162.2	121.5	366.8	15.2	42.1	24.8	89.7	123.8
60.7	178.3	134.1	412.4	18.5	46.9	30.5	110.2	137.5
61.5	184.2	134.4	411.4	17.4	48.9	30.1	110.6	138.4
62.1	177.9	138.9	403.0	17.7	50.1	29.4	108.6	136.4
62.3	187.4	131.4	413.9	17.9	46.3	29.6	107.8	135.2
62.5	187.4	133.2	426.2	18.8	47.8	31.6	111.6	139.7
62.7	119.7	99.3	331.1	10.8	33.9	19.6	71.9	111.2
63.7	201.2	128.2	407.9	19.5	47.7	33.5	113.7	140.0
63.9	194.3	129.2	408.4	16.9	47.9	31.5	105.4	132.2
65.2	171.9	127.9	417.8	18.7	45.8	29.3	104.9	129.7
65.4	174.3	133.2	397.5	17.0	46.3	26.6	104.8	130.1
65.4	229.6	152.6	399.1	18.1	61.3	36.0	131.5	148.0
65.6	199.6	130.8	404.2	18.1	47.9	30.7	106.0	130.9
65.9	176.2	123.5	399.2	21.0	46.5	31.5	112.3	136.3
66.0	188.2	131.8	418.0	18.9	48.7	29.8	113.1	136.8
66.1	192.4	133.4	418.7	18.9	48.3	30.6	118.7	135.5
66.3	196.5	135.0	414.0	19.4	50.4	31.9	114.9	138.7
66.4	193.4	129.5	406.9	19.4	49.3	31.2	113.3	140.7
66.4	183.6	134.6	410.4	19.2	48.8	30.8	114.8	139.0
	179.3	129.5	398.8	18.8	47.4	30.2	111.8	135.0
66.9	193.5	130.8	423.3	17.9	47.4	31.2	119.6	141.6
67.0	193.4	128.6	431.5	18.6	47.2	31.5	115.9	139.6
67.2	202.6	124.8	417.0	20.2	46.7	33.7	120.8	141.3
67.4	198.6	128.0	423.8	20.3	48.8	32.8	116.8	138.5
67.6	181.7	125.1	432.0	19.0	44.7	30.0	121.7	136.9
67.8	187.9	124.6	429.9	21.7	49.2	31.2	113.4	133.5
68.0	154.2	114.9	420.3	12.8	48.5	26.8	99.1	130.6
68.2	183.1	129.1	440.4	18.6	44.8	30.0	111.4	137.0
68.5	201.3	130.9	423.3	19.1	50.0	32.9	116.2	138.0
68.7	194.2	128.5	428.5	18.6	50.4	31.8	111.8	135.5
68.9	198.6	138.3	448.8	18.9	49.9	31.6	149.4	143.4
69.7	197.8	129.7	401.2	20.3	49.9	33.4	110.1	131.7
69.9	178.2	119.8	413.7	17.0	44.3	28.1	101.1	130.8
70.0	179.8	135.2	409.0	17.9	47.7	30.9	108.4	137.9
70.2	180.0	130.0	415.8	18.4	47.7	30.8	110.1	138.2
70.4	176.3	131.2	399.3	18.5	49.7	30.7	108.7	136.2
70.6	174.3	137.9	409.0	17.8	48.3	30.2	105.3	134.2
70.7	181.0	138.6	403.9	18.1	50.0	31.2	109.2	137.3
70.9	181.7	131.7	393.0	19.2	49.6	31.6	110.9	137.6
71.1	177.5	129.9	401.6	18.4	47.8	30.9	108.6	137.3
71.4	176.8	131.4	406.3	18.5	48.2	31.1	109.0	137.1
71.6	182.7	136.3	409.3	19.1	49.6	31.2	109.5	137.4
72.0	178.6	130.0	397.9	18.5	48.3	29.5	106.2	134.6

Depth	Sr ppm	Y ppm	Zr ppm	Ba ppm	Pb ppm	Nb ppm	I ppm	Br ppm
58.2	255.7	26.3	113.7	525.5	32.9	15.1	126.2	6.8
59.6	270.4	27.3	110.0	532.9	26.6	15.4	127.6	25.7
59.8	255.2	25.8	118.7	535.5	30.6	14.8	114.5	27.6
60.0	270.7	26.9	115.6	551.9	29.2	15.8	122.4	25.9
60.4	268.8	26.0	155.2	594.5	28.1	14.2	99.4	14.7
60.5	269.2	25.0	132.8	584.2	34.2	14.5	99.6	23.5
60.7	252.1	27.9	119.9	560.0	26.0	15.6	106.4	31.8
61.5	234.5	27.0	123.2	555.9	27.8	14.7	111.3	26.4
62.1	249.4	25.9	116.9	521.0	29.4	15.3	119.7	15.3
62.3	242.7	26.4	113.1	533.2	31.3	15.9	101.0	13.4
62.5	248.8	27.2	110.2	552.9	27.8	15.7	114.1	14.9
62.7	308.4	23.5	139.7	669.9	20.8	13.6	61.3	14.5
63.7	271.5	26.8	107.9	532.8	26.8	15.5	119.8	30.2
63.9	290.3	26.0	117.2	556.2	24.5	15.0	121.7	23.0
65.2	324.2	26.9	124.1	621.3	27.3	15.4	117.3	45.6
65.4	247.3	26.2	149.0	569.9	38.3	13.9	92.6	31.6
65.4	210.6	29.8	104.8	557.1	25.5	16.0	108.2	19.8
65.6	287.3	25.6	110.6	513.9	26.9	15.0	70.3	11.1
65.9	248.3	26.5	118.5	552.6	29.7	15.2	108.9	30.9
66.0	247.9	27.5	120.1	566.3	33.0	15.6	110.2	31.5
66.1	247.3	27.8	114.5	558.6	27.6	15.1	107.7	29.8
66.3	243.7	27.9	115.0	560.3	25.5	15.9	112.2	28.7
66.4	237.3	27.8	114.8	542.5	28.1	15.5	112.4	32.8
66.4	240.3	27.6	114.8	557.7	28.7	15.7	113.1	29.1
	232.8	25.6	108.7	527.5	29.0	14.5	112.8	56.9
66.9	216.9	26.2	107.4	559.9	28.9	15.3	130.2	33.8
67.0	264.6	26.4	108.0	556.8	29.4	15.2	127.6	19.0
67.2	268.0	27.0	102.2	540.3	28.8	15.3	119.1	20.2
67.4	255.5	27.7	101.3	536.0	27.9	15.4	97.5	10.2
67.6	249.0	26.4	107.7	584.5	28.9	15.7	124.7	13.2
67.8	291.5	26.7	111.1	528.2	30.7	15.3	53.5	
68.0	272.1	27.8	135.5	687.9	19.2	17.9	99.6	33.5
68.2	248.9	27.3	115.1	572.6	28.4	16.4		
68.5	292.6	26.5	103.3	534.0	27.9	15.9	120.7	39.5
68.7	276.2	26.8	107.2	552.9	26.1	16.2	115.8	20.4
68.9	242.6	28.2	112.5	570.8	29.6	15.7		
69.7	301.6	26.4	117.9	541.5	34.2	15.0	106.1	22.7
69.9	304.2	25.1	119.4	599.8	28.2	16.0	117.4	37.7
70.0	263.6	25.7	117.1	560.5	25.8	15.4	123.5	39.1
70.2	267.0	26.8	118.8	576.3	28.4	15.7	129.3	23.4
70.4	259.2	26.2	116.0	544.9	24.4	15.2	124.0	36.7
70.6	255.2	24.9	116.9	562.6	27.1	14.8	120.3	34.5
70.7	247.0	25.6	110.5	545.2	26.5	14.8	131.4	35.8
70.9	256.3	26.0	112.6	536.0	28.9	15.0	127.9	29.9
71.1	252.4	26.9	114.4	550.0	30.4	15.3		
71.4	261.9	26.6	119.4	556.5	27.6	14.7	113.4	16.5
71.6	256.6	26.5	120.3	566.1	30.8	15.1		
72.0	270.5	27.0	129.5	577.4	32.0	14.8	110.5	35.5